EXPERIMENTAL STUDY AND ANALYTICAL METHOD OF PARTIALLY CONCRETE-FILLED STEEL BRIDGE PIERS UNDER BI-DIRECTIONAL DYNAMIC LOADING

September, 2013

Huihui Yuan

ABSTRACT

From past large earthquake, it has been recognized that the highway steel bridge piers in urban areas play a very important role in the social lifeline system. The seismic design specification of steel bridge piers introduced in the current Japan allows independent, longitudinal, and transverse forces. To date the seismic performance of steel bridge piers has been widely studied through static cyclic loading tests, pseudo-dynamic loading tests, and numerical analysis in a single lateral direction under constant axial force. However, the actual seismic waves consist of three-directional components and the seismic response of bridge piers is simultaneously affected by the two horizontal components. It is difficult to properly evaluate the seismic performance of bi-directional horizontal seismic motions through single-directional loading tests because of the complex behavior of local buckling and inelastic behavior caused in the component plates of the pier at the ultimate state.

To clarify the seismic performance of partially concrete-filled steel bridge piers subjected to bi-directional seismic loading, the performance of partially concrete-filled steel bridge piers under actual earthquake conditions was investigated using 20 square section specimens through cyclic static loading tests and single- and bi- directional hybrid loading tests in this study. Three acceleration records of two horizontal NS and EW direction components in three different ground types, obtained during the 1995 Kobe Earthquake, were adopted during the dynamic tests. The experimental results clarified that the maximum displacement and residual displacement under actual earthquake conditions cannot be correctly estimated by conventional single-directional loading test results in medium and soft ground types, and the filled-in concrete can effectively improve the seismic resistance performance in sufficiently high

concrete filled steel bridge piers.

In this study, an analytical model consisting of a concentrated mass and a rigid bar with multiple springs located at the base was developed to simulate the hysteretic behavior of partially concrete-filled steel bridge piers subjected to single- or bi-directional ground motions. In order to describe the complicated nonlinear behavior of each spring element accurately, a series of approximate curves whose parameters were determined by results of single-directional static cyclic loading tests had been adopted. To examine the validity of the proposed model, the results due to the simulation were compared with those of static cyclic tests, single- and bi-directional hybrid tests. By comparison, it is demonstrated that the proposed multiple-spring model can predict well the hysteretic behavior of partially concrete-filled thin-walled steel bridge piers with square cross-section.

ACKNOWLEDGMENTS

This thesis is part of a larger study on the seismic behavior of steel bridge piers supported by Grant 21560508 from the Grants-in-Aid for Scientific Research with respect to highway structures. This report is gratefully acknowledged. Any opinions expressed in this report are those of the author and do not reflect the views of the sponsoring agency.

I wish to thank my profound and respectable academic advisor, Prof. Tetsuhiko Aoki, for his valuable instruction in the field of seismic performance study on structures and his great patience in the past three years. I'm also grateful to him for his suggestions and encouragement and all the efforts he has made to help me complete the paper. And I am also very grateful to the help of Prof. Moriaki Suzuki, who continues to guide my courses after Prof. Aoki's retirement so I can successfully get my PHD degree.

I would like to thank Researcher J. Dang of the Saitama University for fruitful discussions during the course of this study. My special thanks go to technician Mr. Hiroshi Suzuki of Seismic Research Center for providing me with the great help in the operation of experimental equipment, and all the students from Structural Laboratory, such as Yoshiyuki Shimaguchi, Takuya Ozawa, Hikari Kishita, Takahito Mizutani, and Hiroki Nagasaka, who have participated in my research for their invaluable contribution to my data collection.

Above all, I want to thank my parents, my wife, and my younger sister for their support and encouragement during the course of the accomplishment of this thesis.

TABLE OF CONTENTS

CHAPTER 1
INTRODUCTION

1.1 General

From past large earthquake, it has been recognized that the highway piers play a very important role in the social lifeline system. Highway steel piers are generally served in urban areas in Japan because of its tough strength and demand for narrow constructional site. The appropriate seismic design and keep the function of steel piers is significant for safe and serviceability in big cities especially in post-earthquake periods.

In the Seismic Design Specifications for Highway Bridges (JRA 2012), the performance- based design concept is described clearly on the necessary performance requirements and the verification policies. Table 1-1 shows the seismic performance matrix including the design ground motions and the Seismic Performance Level (SPL) provided in the Specifications.

Table 1-1. Seismic Performance Matrix

Type of Design Ground Motion		Type-A bridges	Type-B bridges
Level 1 Earthquake		SPL 1: Functional	
Level 2 Earthquake	Type-I	SPL 3: Prevent critical damage	SPL 2: Retain Limited damage
	Type-II		

The two level ground motion are instructed in the Seismic Design Specifications as the moderate ground motions induced in the earthquakes with high probability to occur (Level 1 Earthquake) and the extreme ground motions induced in the earthquakes with low probability to occur (Level 2 Earthquake). The Level 1 Earthquake provides the ground motions induced by the moderate earthquakes. For the Level 2 Earthquake, two types of ground motions are

considered. The first one is the ground motions induced in the inter-plate type earthquakes with the magnitude of around 8 (Type-I). The ground motion at Tokyo in the 1923 Kanto Earthquake is a typical target of Type-I ground motion. The second is the ground motion developed in earthquakes with magnitude of around 7 at very short distance (Type-II). The ground motion at Kobe during the Great Hanshin Earthquake is a typical target of this type of ground motion.

The bridges are categorized into two types depending on their importance: ordinary bridges (Type-A bridges) and important bridges (Type-B bridges). Depending on the importance of bridges, the Seismic Performance Level (SPL) is based on the viewpoints of "Safety," “Functionality," "Reparability" during and after the earthquakes. For the Level 1 Earthquake, both Type-A and Type-B bridges shall behave in an elastic manner without essential structural damage (SPL 1). For the Level 2 Earthquake, the Type-A bridges shall prevent critical failure (SPL 3), while the Type-B bridges shall perform with limited damage (SPL 2).

As mentioned in the above, the seismic performance is specified clearly. It is the fundamental policy of the verification of seismic performance that the response of the bridge structures against design earthquake ground motions does not exceed the determined limit states.

Fig.1-1 shows the seismic design flow for bridge structures introduced in the 2012 Specifications. In the seismic design of highway bridge structures, it is important to increase the strength and the ductility capacity to appropriately resist the intensive earthquakes. The verification methods are based on the static analysis and dynamic analysis. The static verification methods including the seismic coefficient method and the ultimate earthquake resistance method are applied for the bridges with simple behavior with predominant single mode during the earthquakes. The dynamic verification method is applied for the bridges with complicated behavior for the applicability of the static verification methods is restricted.

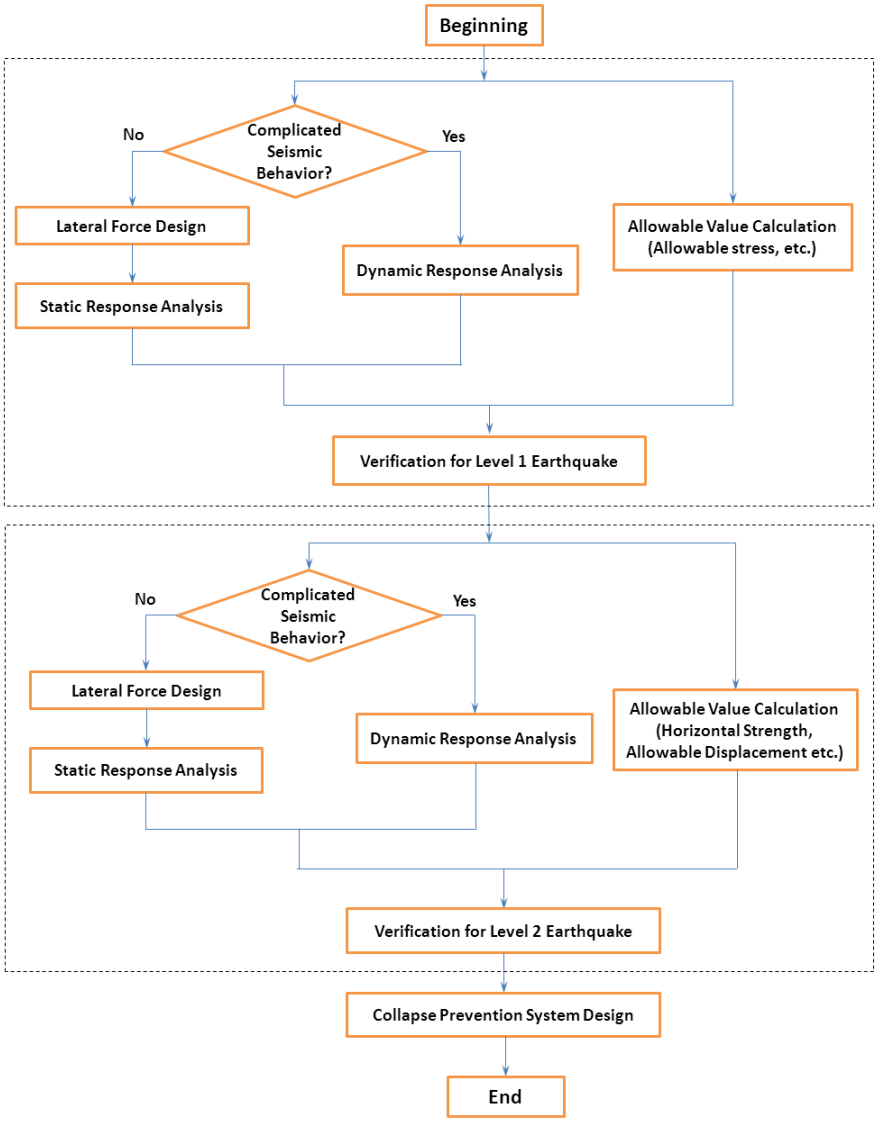

Fig. 1-1. Seismic design flow introduced in 2012 specifications

To date the seismic performance of steel bridge piers has been widely studied through static cyclic loading tests, pseudo-dynamic loading tests, and numerical analysis in a single lateral direction under constant axial force. Based on these research results, the seismic design verification method for steel bridge piers introduced in 2012 Specifications, suggests carrying out static analysis, dynamic analysis, and response verification in longitudinal and transverse direction independently which is leaded based on the consideration that two directional major

seismic forces occur simultaneously. The Specification consists of Static Specification Method for the SPL1 and Dynamic Specification Method for the SPL2 and SPL3 as shown in Table 1-2.

Table 1-2. Verification Methods for Steel Bridge Piers

Seismic Performance	Design Ground Motion	Verification Method	Main Verification Item
SPL 1	Level 1	Static	$\sigma < \sigma_a$
SPL 2	Level 2	Dynamic	$\delta_R < \delta_{Ra}$, $\delta_M < \delta_{Ma}$
SPL 3	Level 2	Dynamic	$\delta_M < \delta_{Ma}$

However, as is well understood that, the actual seismic waves consist of three-directional components in orthogonal directions and the seismic response of the structure is also influenced by more than one directional seismic excitation. It is difficult to properly evaluate the seismic performance of bi-directional horizontal seismic motions through merely single-directional loading tests. Therefore, it needs to study bi-directional loading effect on the steel bridge piers for establishing rational design procedure.

1.2 Literature Survey of Studies on Bi-directional Loading

A review of existing analytical and experimental studies relevant to the seismic response of bridge piers subjected to bi-directional loading is presented in the following. After the Kobe Earthquake occurred in 1995, which caused remarkable damages to the highway bridges, the necessity to know the precise spatial behavior of the bridge structures has arisen greatly in Japan. A concerned effort to clarify the inelastic response of these structures under actual strong earthquakes has been continued but still under way for several years. The current state of the art is summarized in this short survey.

1.2.1 Experimental Studies

In recent years, to clarify the seismic performance of columns subjected to bi-directional seismic loading, some bi-directional static cyclic loading tests have been conducted under various loading patterns such as rectangular, circular, and elliptical in the horizontal plane.

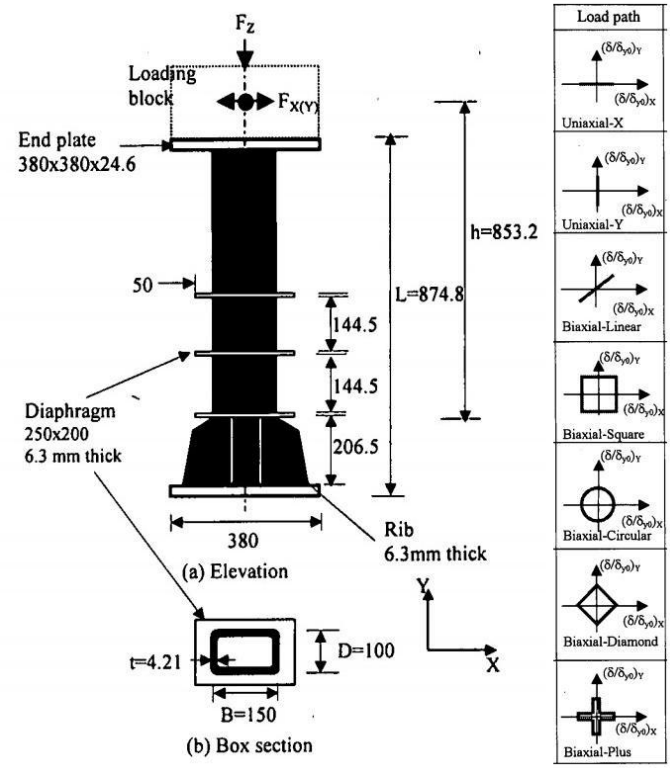

Fig. 1-2. Test specimen and load path used in Watanabe's study

Watanabe et al. (2000) experimentally investigated the effects of multi-directional load histories, such as biaxial-linear, -square, -circular, -diamond and -plus pattern as shown in Fig. 1-2, on the response of tubular columns with small electric-welding and cold formed box section. The main conclusion drawn from this experimental study is that biaxial displacement paths cause more extensive degradation of stiffness, strength and ductility of tubular columns in comparison with uni-axial displacement paths. From the test results, it is also clearly understood that the biaxial

effects were more prominent in the inelastic range.

In order to investigate the dynamic behavior of bridge piers subjected to strong ground motions in horizontal bi-directions, Nagata et al. (2004) conducted a hybrid loading test using the same box section steel piers as in Watanabe' study subjected to Japan Meteorological Agency(JMA) bi-directional ground motions, as shown in Fig. 1-3. It is found that the strength and ductility of steel pier subjected to bi-directional loading reduced and the response displacement tended to increase in comparison with those under single-directional loading.

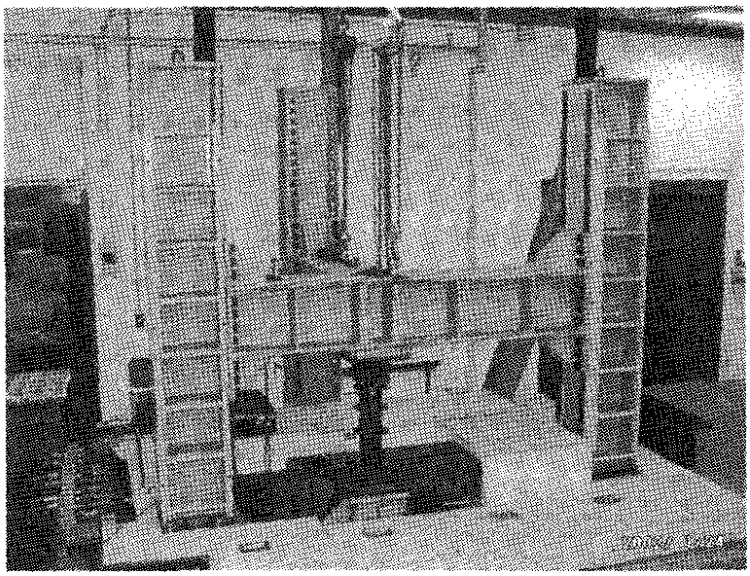

Fig. 1-3. 3D loading system setup by Nagata et al.

Aiming to clarify the flexural strength and ductility of reinforced concrete bridge piers under bilateral loadings, five RC test specimens subjected to bilateral loadings with four orbits, such as oblique direction to the strong axis, rectangular, circular and ellipse as illustrated in Fig. 1-4, were tested under a constant vertical load by Hayakawa et al. (2004). It was found that the deterioration of strength and ductility capacities of the piers resulted from the bilateral loadings was substantial.

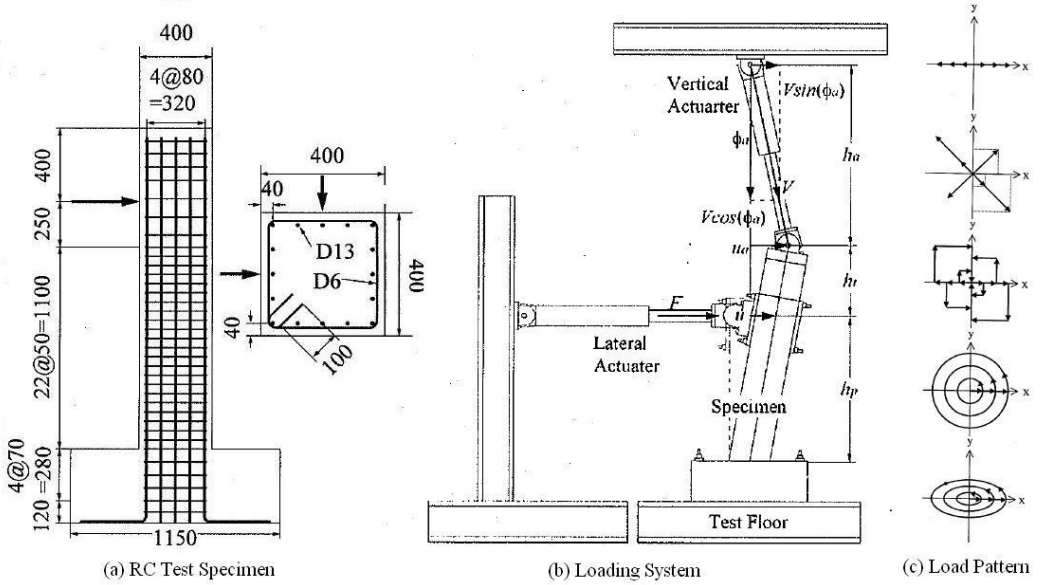

Fig. 1-4. Test specimen, test set-up and bilateral load pattern of Hayakawa's study

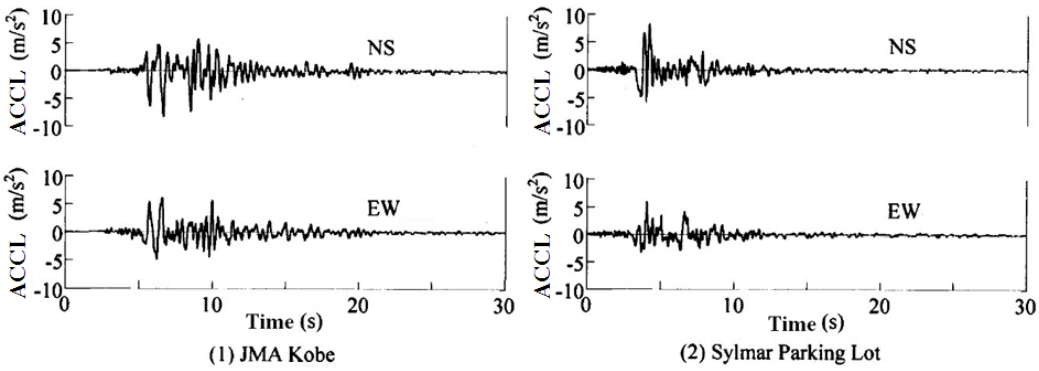

Fig.1-5. Input earthquake motions adopted in Ogimoto's hybrid loading test

Ogimoto et al. (2005) conducted a hybrid loading test on six reinforced bridge piers as the same as Hayakawa's research subjected to unilateral and bilateral excitations, which were 30% and 40% of original JMA ground motions obtained in Kobe Earthquake and 50% of Sylmar Parking Lot ground motions recorded in Northbridge Earthquake, as presented in Fig. 1-5. It can be observed from the test results that flexural strength and ductility capacity of RC bridge piers significantly deteriorate under the bilateral excitation than the unilateral excitation.

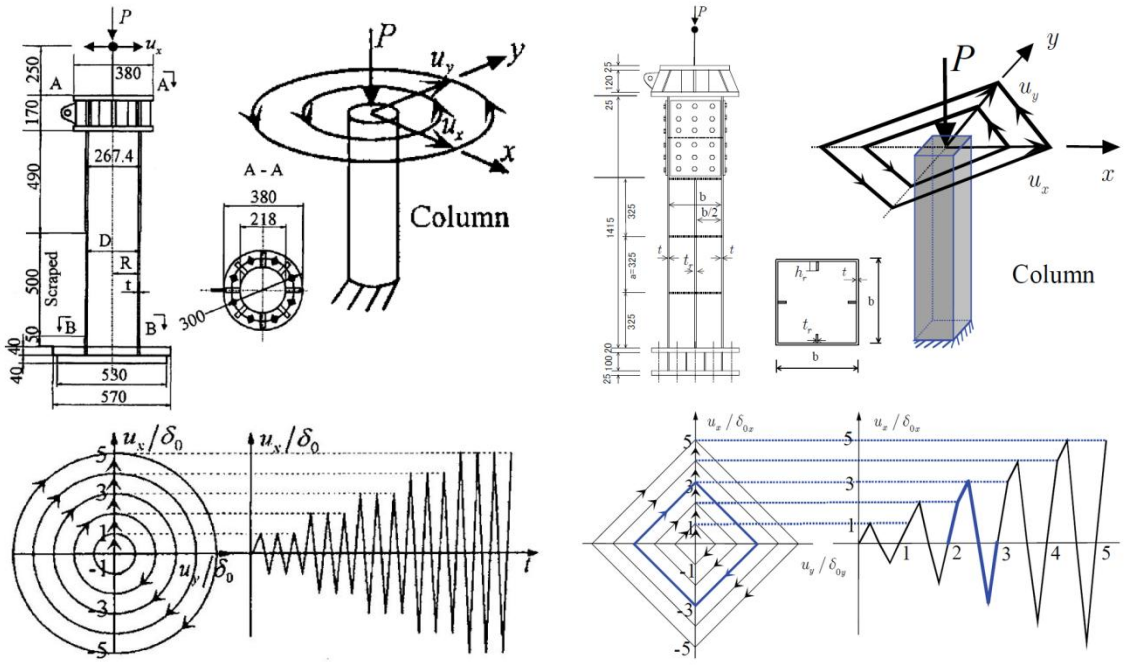

(a) Circular cyclic loading (b) Diamond cyclic loading

Fig.1-6. Bi-Directional Loading Experiments Conducted by Goto et al. (2006, 2007)

Goto et al. (2006, 2007) performed two kinds of bi-directional cyclic loading experiments, as shown in Fig. 1-6, to examine the ultimate seismic behavior of thin-walled steel columns of circular and rectangular section shapes, respectively, by using a spherical three-dimensional (3D) experimental system. The seismic performance of these piers, which have different cross section types, under cyclic bi-axial loading was extensively examined in comparison with that under in-plane cyclic loading. From the experimental results, it is observed that the strength and ductility of the columns decreased considerably under the cyclic bi-directional loads, compared with those under the conventional cyclic uni-axial loads. Goto et al. (2009) then made an investigation on how the coupling of bi-directional horizontal seismic excitations affects the ultimate behavior of thin-walled stiffened rectangular bridge piers. They also carried out a bi-directional pseudo-dynamic test by using the JMA ground motions.

In 2007, 8 steel piers with rectangular cross section subjected to bi-directional horizontal forces, which were idealized into several simple hysteretic loading patterns, such as linear, circle, oval, radial, square and octagon types as shown in Fig. 1-7, were tested by Aoki et al. (2007) to investigate the corresponding strength and ductility. They provided the basic information for establishing the rational design rules from the test results.

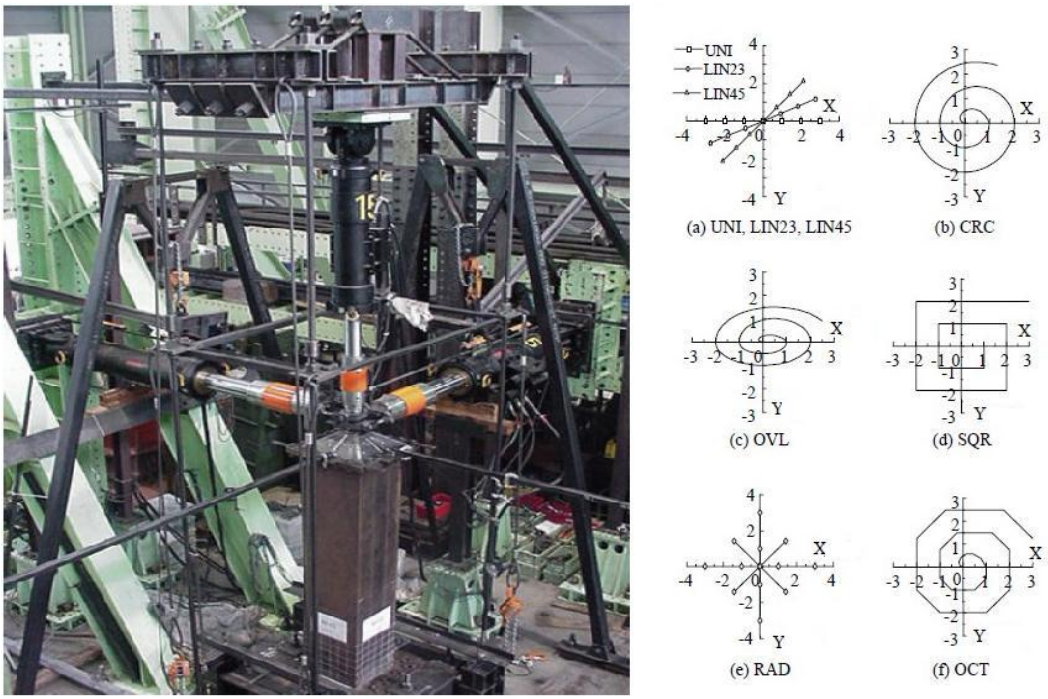

Fig. 1-7. Actual loading system and loading patterns used by Aoki et al. (2007)

As a consecutive research, Dang et al. (2010) performed a series of hybrid loading tests to examine the response behavior of square steel bridge piers subjected to 3 types of bi-directional ground motions named JMA, JRT, and PKB, respectively, which were obtained during the Great Hanshin Earthquake. It is found from the experiments that the bi-lateral excitation deteriorates the lateral force of the piers compared to unilateral excitation and the response displacement under actual earthquake conditions cannot be correctly estimated by conventional single-directional loading test results.

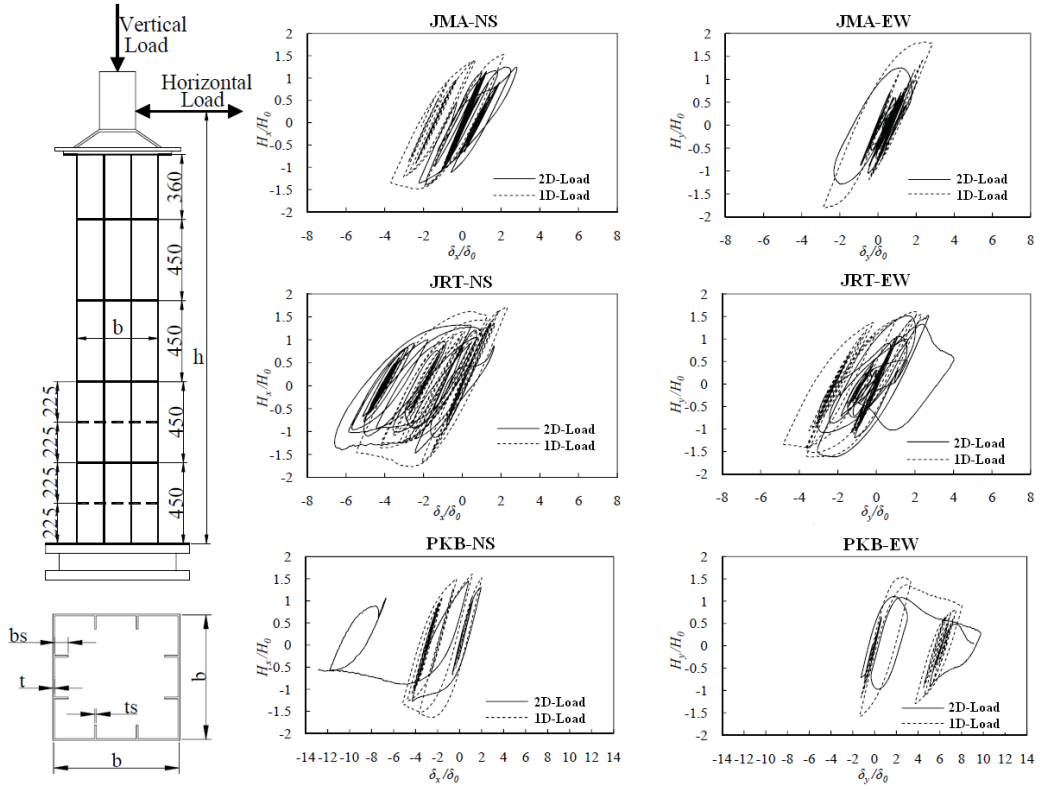

Fig.1-8. Test specimen and test results obtained in Dang's research

1.2.2 Analytical Studies

The seismic response of bridge piers to earthquake excitations depends on several factors, such as earthquake characteristics, ground conditions and structural properties. The determination of the structural properties of a pier is an essential step in the evaluation of its seismic response. As shown in Fig. 1-1, a complete assessment of the seismic design of bridge piers often requires a nonlinear dynamic analysis.

As stated in section 1.2.1, the dynamic characteristics of bridge piers subjected to bilateral seismic forces can be obtained by the static cyclic tests and hybrid loading tests. However, the loading system and test specimens of such tests require expenditure, especially for large scale models. Results from these tests are then used in the development and calibration of hysteretic

numerical models that permit the extrapolation for the limited test data of the dynamic response in other conditions. A concerned effort to model and analyze the nonlinear seismic response of bridge piers subjected to bi-directional loadings has been done in these several years but still under way.

Existing models for the nonlinear response analysis of bridge piers subjected to bi-directional loadings can be divided into two main categories in accordance with the increasing level of refinement and complexity: discrete finite element models and microscopic finite element models. A review of the relevant analytical studies is presented in the following.

(1) Microscopic finite element models

In this category of models, members and joints are subdivided into a large number of finite elements. Constitutive and geometric nonlinearity is typically described at the stress-strain level or averaged over a finite region.

As a constitutive model to express the cyclic plasticity of steel, the three-surface cyclic plasticity model, which includes a yield surface, a discontinuous surface, and a bounding surface as illustrated in Fig. 1-9. One of these models was developed by Goto et al. (1998) to analyze specifically the uni-directional cyclic behavior of thin-walled steel columns by the nonlinear FEM shell analysis. The three-surface cyclic plasticity model takes into account the important characteristics of cyclic steel plasticity such as existence of yield plateau, contraction or expansion of elastic range, and cyclic strain hardening.

The three-surface model stated earlier was slightly modified by Goto et al. (2006) to take into account the behavior under large equivalent plastic strains that is often encountered in the

bi-directional cyclic loading experiment. Then, the results obtained from a cyclic circular loading test for thin-walled circular steel piers (Goto et al. 2006), a cyclic diamond loading experiment (Goto et al. 2007) and a bi-directional pseudo-dynamic test (Goto et al. 2009) for thin-walled stiffened rectangular steel piers were used to confirm the validity of the proposed geometrically and materially nonlinear FEM shell analysis, as illustrated in Fig. 1-10.

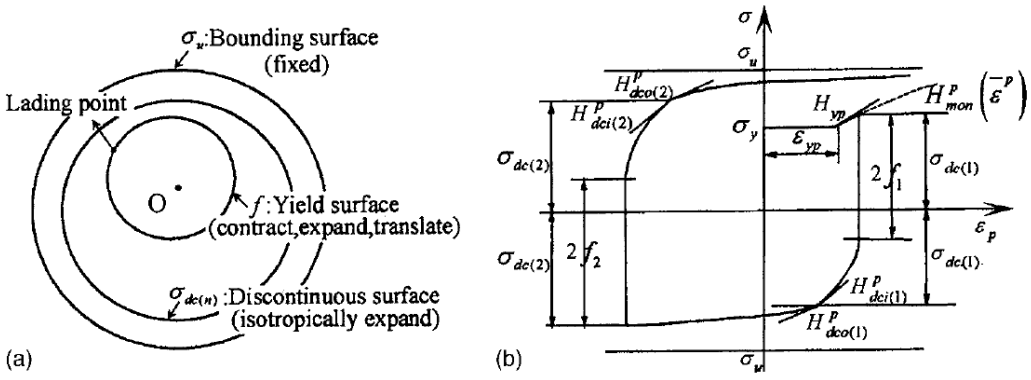

Fig.1-9. Three-surface model: (a) multi-axial stress space; (b) uni-axial stress-strain relation

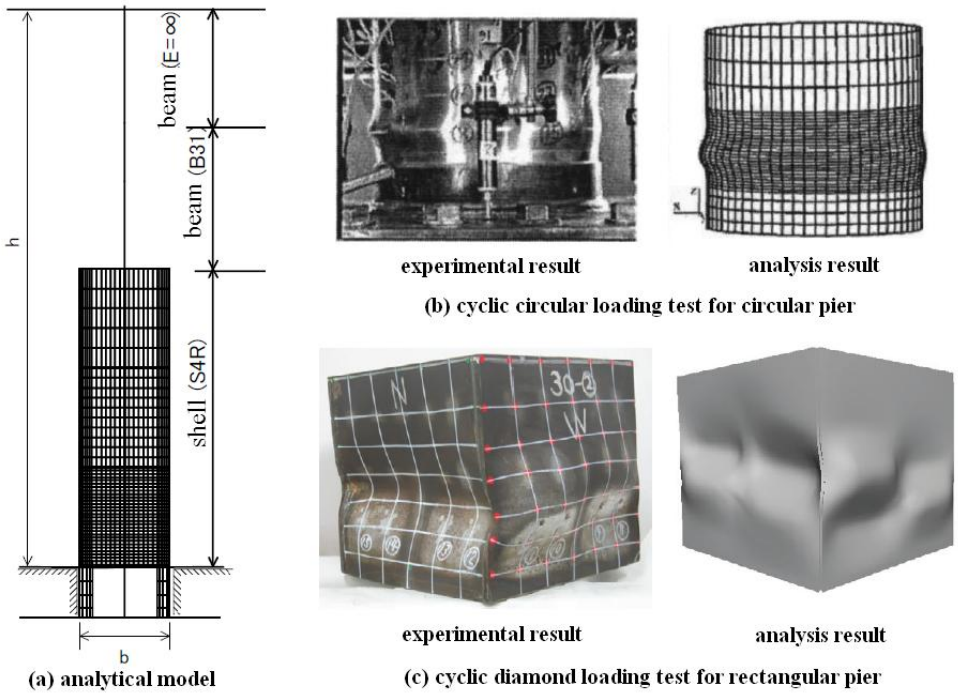

Fig. 1-10. Analytical models proposed by Goto et al. (2006 and 2007)

The elasto-plastic finite displacement analyses of box steel piers subjected to strong ground motions in horizontal 2 directions, which also adopted shell element as shown in Fig. 1-11, were carried out by Nagata et al. (2004). The influence of bi-directional cyclic loading on finite shell element models of thin-walled circular steel piers was evaluated by Kulkarni et al. (2009) as presented in Fig.1-12.

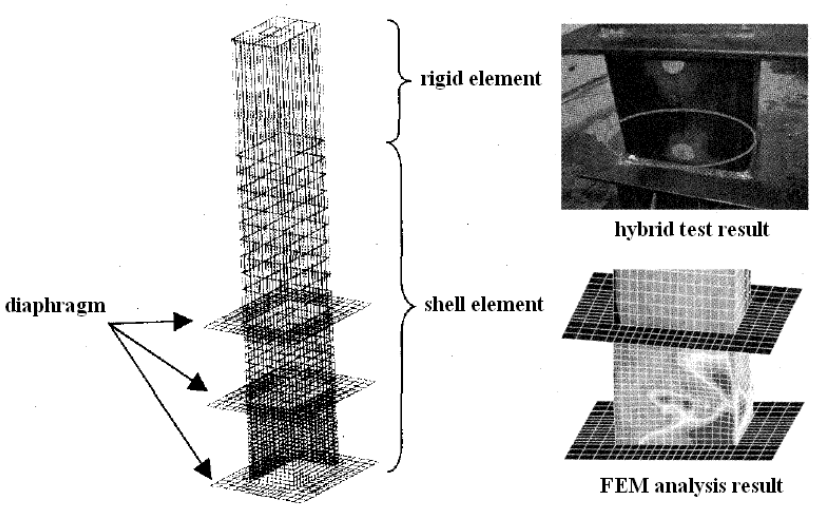

Fig.1-11. Elasto-plastic finite displacement analytical model (Nagata et al. 2004)

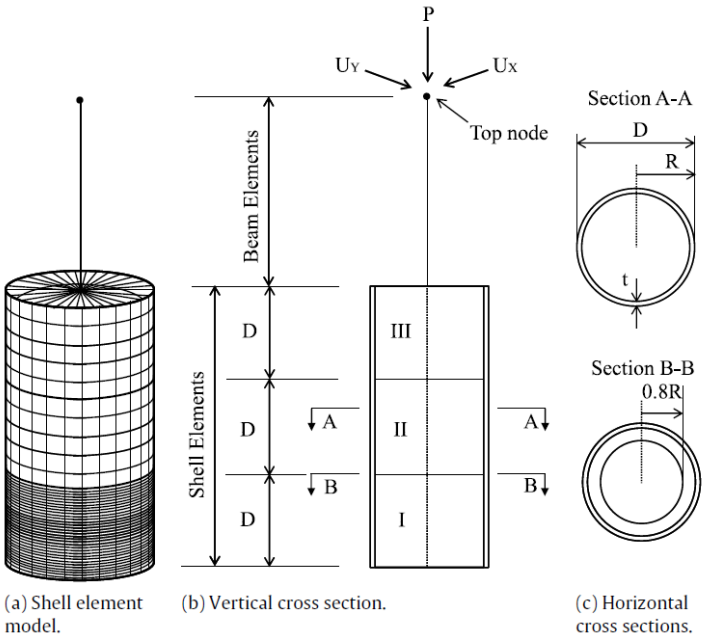

Fig. 1-12. Shell element model proposed by Kulkarni et al. (2009)

The most promising models for the nonlinear analysis of reinforced concrete (RC) bridge piers are flexibility-based fiber elements. In these models the element is subdivided into longitudinal fibers, as shown in Fig. 1-13. The constitutive relation of the section is not specified explicitly, but is derived by integration of the response of the fibers, which follow the uni-axial stress-strain relation of steel and concrete.

In comparison with the results of shaking table tests, the analytical method using fiber element model proposed by Nishida et al. (2004) could be simulated the experimental dynamic response results well until damage of the column such as peeling of the concrete and buckling of the longitudinal bar was occurred.

Using the same analytical model, the fiber element analyses were conducted to simulate the test results of RC bridge piers subjected to bilateral static cyclic loading and bi-directional ground motions by Hayakawa et al. (2004) and Ogimoto et al. (2005), respectively. It is also found that the fiber element analysis is effective to reproduce the hysteretic behavior of the columns under bi-lateral loadings.

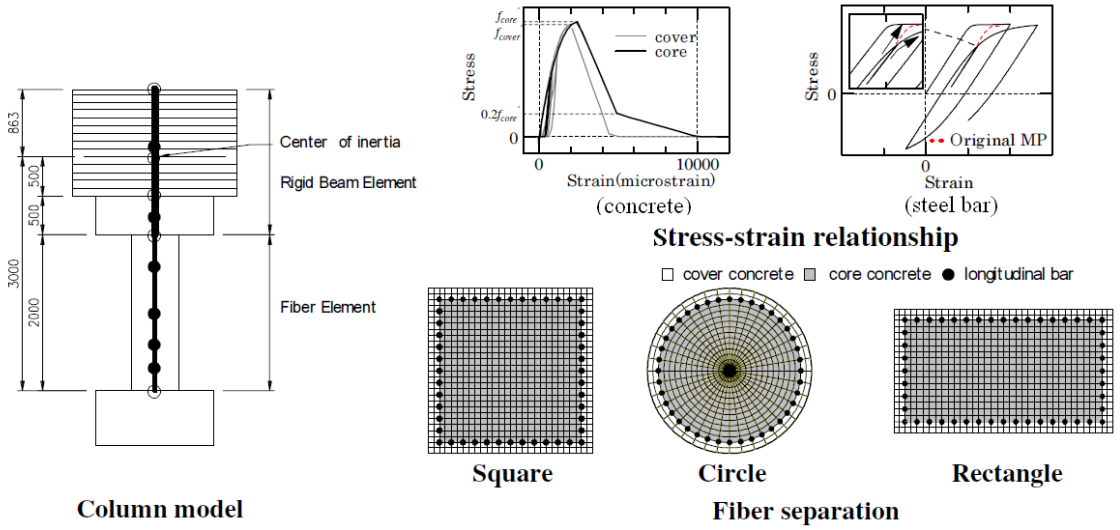

Fig. 1-13. Analytical model using fiber element (Nishida et al. 2004)

(2) Discrete finite element models

In this category of models, the piers are modeled as an assembly of interconnected elements that describe the hysteretic behavior of material members. Constitutive nonlinearity is either introduced at the element level in an average sense or at the section level.

An elasto-plastic dynamic response analysis method of beam-column elements, which took into account the yielding of pier section due to biaxial bending and torsional behavior, was formulated by Oide et al. (2000). As shown in Fig. 1-14, there are multiple axle springs (k_a), two shear springs (k_{sy}, k_{sz}), and torsional rotation spring (k_r) placed between the two rigid elements. These spring constants can be obtained by the equal relationship between strain energy stored in spring elements and rigid body. In comparison with behavior that subjected to one horizontal directional earthquake motion, a fundamental behavior of a steel bridge pier subjected to a set of two horizontal directional earthquake motions (JRT) recorded during Great Hansin Earthquake was investigated by employing above analysis method in the study.

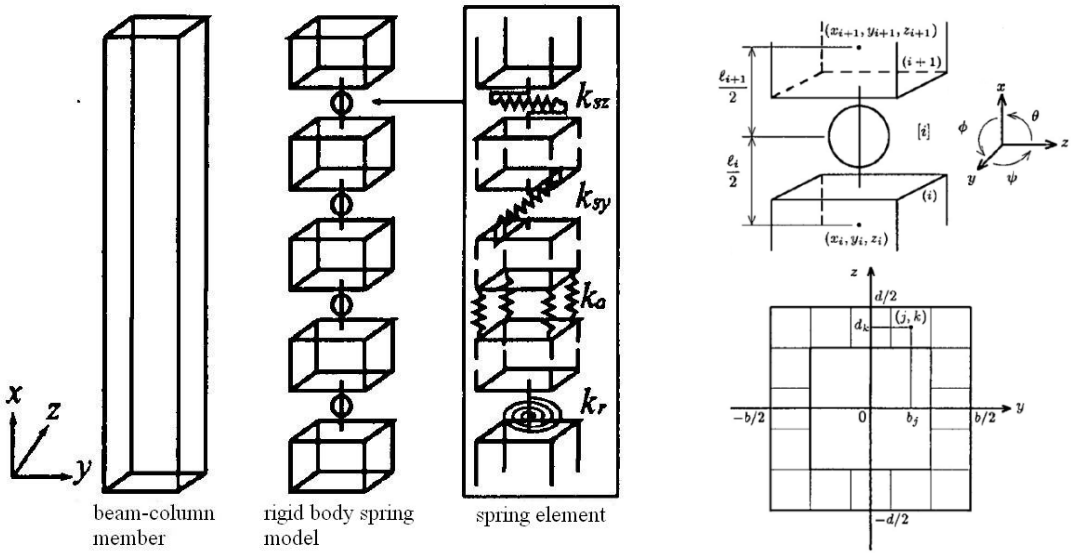

(a) Rigid body and spring element (b) Division of the cross-section

Fig. 1-14. Modeling of steel bridge pier (Oide et al. 2000)

In order to predict the ultimate seismic behavior of cantilever-type thin-walled circular steel piers, a hysteretic model consisting of a concentrated mass and a rigid bar with multiple nonlinear springs located at the pier base was proposed by Jiang et al. (2001) as shown in Fig. 1-15(a). These springs can represent not only the interaction between the axial force and the biaxial bending but also the local buckling effect. The validity of the proposed model was examined by comparing with the results of the 3D-earthquake response analysis carried out by using FEM shell models as illustrated in Fig. 1-15(b). The analysis results showed that the multiple-spring model can be an acceptable alternative to the costly FEM shell analysis. The computation time of the multiple-spring model was drastically reduced to 1/5000~1/6000 in comparison with that of the FEM shell model in the 3D dynamic response analyses.

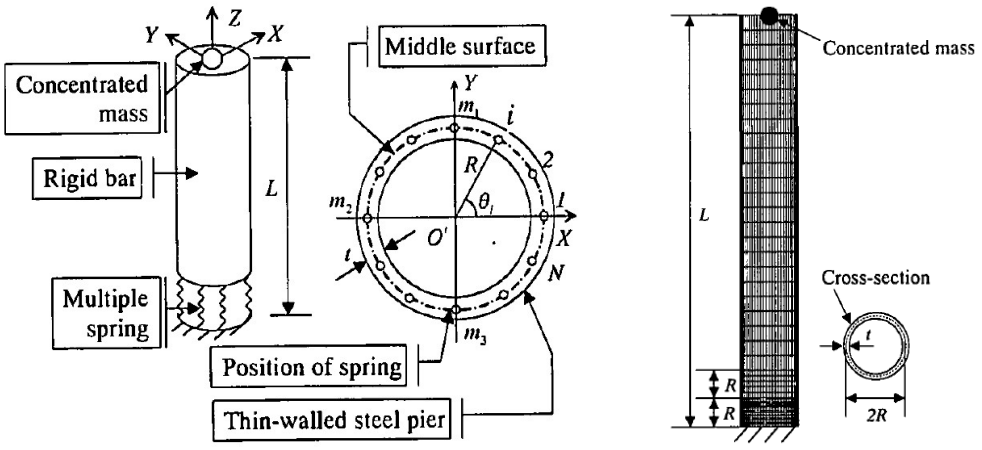

(a) Multiple-spring model (b) 3D FEM model

Fig. 1-15. Jiang's multiple-spring model in comparison with FEM shell model

To evaluate strength and ductility of the circular steel column, a shell element model proposed by Kulkarni et al. (2009) was statically analyzed with bi-directional horizontal displacement, as shown in Fig. 1-12. However, to understand the behavior of the pier during earthquake, a beam element model of column was generally used in practice as illustrated in Fig. 1.16. In this beam

element model, the modified two-surface constitutive law of steel was applied for all elements. During bi-directional dynamic analysis, the node displacement response on the top and average compressive strain were observed in effective failure height (L_e) at the base.

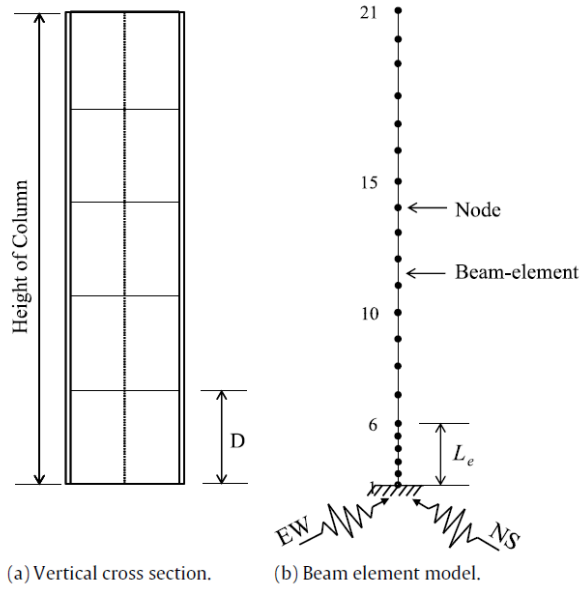

Fig. 1-16. Beam element model considered for dynamic analysis (Kulkarni et al. 2009)

The discrete finite element models are the best compromise between simplicity and accuracy in nonlinear seismic response studies and represent the simplest class of models that still allows significant insight into the seismic response of members and of the entire structure. The microscopic finite elements, on the other hand, should be limited to the study of critical regions, since these models are extremely computational expensive for large scale nonlinear dynamic analyses, where the model involves thousands of degrees of freedom.

1.3 Objectives and Scope

With the rapid development of urban highway and bridge constructions and with the effective

use of narrow city sites, the use of steel bridge piers has become increasingly popular in Japan. Steel bridge piers are normally designed as cantilever columns or planar rigid frames. The shapes of cross-section are mostly thin-walled box or pipe sections.

Since the steel bridge piers play a very important part for the total life-line system, the seismic design is required to ensure that the strength and deformation capacities of steel piers exceed the limit values specified for severe earthquakes with an adequate margin of safety. Accordingly, stiffness, strength, and ductility, defined as shown in Fig. 1-17, are three most important indices in the design of a pier.

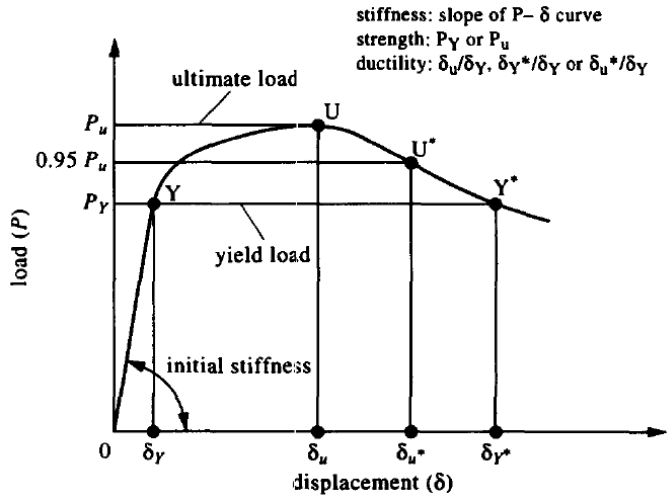

Fig. 1-17. Definition of stiffness, strength, and ductility (Kitada 1998)

The use of concrete-filled steel box sections have shown great improvement in the inelastic behavior of the steel piers, because the encased concrete not only provides stiffness and strength, but also prevents the buckling deflection of the component plates toward the inside of the cross section, as illustrated in Fig. 1-18 (Ge & Usami 1992). However, in many cases of the pratical designs, steel bridge piers were partially filled with the concrete, since it is need to be considered to reduce the dead weight of upper structure for designing foundations.

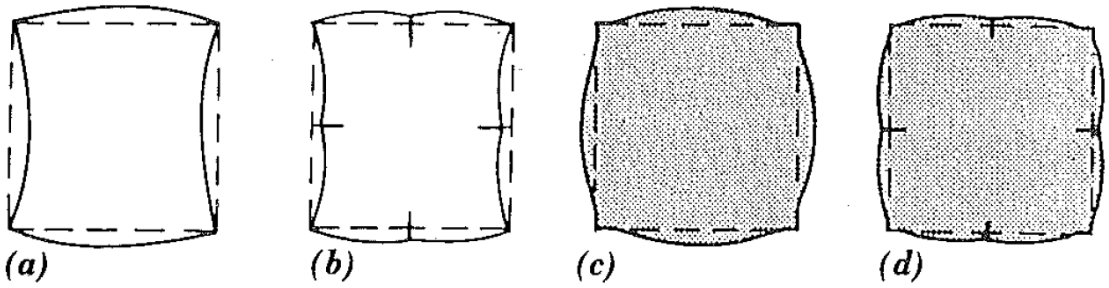

Fig.1-18. Failure modes of cross-sections: (a) steel column; (b) stiffened steel column; (c) concrete-filled steel column; (d) concrete-filled stiffened steel column

In the 1995 Kobe Earthquake, the partially concrete-filled steel bridge piers also demonstrated their excellent structural performance in the strong earthquake. Thus, a lot of experimental and analytical studies on the inelastic cyclic behavior of partially concrete-filled steel bridge piers have been conducted in order to develop a reliable earthquake-resistant design method in the last ten years (Usami et al. 1994, 1995a, 1995b, 1997; Ge et al. 1995, 1996, 2001, 2002, 2003; Saizuka et al. 1995, 1997; Kobayashi et al. 1997; Morishita et al. 2000; Maeno et al. 2002; Iura et al. 2002; Goto et al. 2009).

It is indicated from the tests and the subsequent analysis as stated earlier in the section 1.2 that the stiffness, strength, and ductility of the piers under bi-directional displacement patterns or bi-directional ground motions result in significant degradation in comparison with those of uni-lateral displacement paths or single-directional ground motion. However, the test data is still lack for the seismic behavior of partially concrete-filled steel piers under coupled ground motions in two horizontal directions. Therefore, further experimental investigations on the behavior of such piers under severe earthquakes are required to make a supplement to the current seismic design method.

The main objectives of this study are:

- to investigate the effect of filled-in concrete on seismic performance of partially concrete-filled steel bridge piers subjected to either single- or bi- directional loading;
- to discuss the characteristics of different input seismic excitations which may result in the obvious different seismic behavior of steel bridge piers in the earthquake;
- to present the differences of seismic performance parameters, such as the maximum displacement, residual displacement, maximum horizontal force, and cumulated energy absorption, between single- and bi- directional dynamic loadings;
- to propose some advices for the conventional seismic design which allows for the use of results obtained from single-directional loading tests or analyses, with emphasis on considering a more rational design treatment according to the differences between the results of single- and bi-directional loadings;
- to develop an analytical model which can accurately simulate the hysteretic behavior of partially concrete-filled steel bridge piers under single- or bi-directional ground motions.

Following the review of previous relevant studies in this chapter, Chapter 2 introduces the details of test specimens and test systems, and presents the experimental results of static cyclic loading tests. Chapter 3 discusses the differences of seismic behavior between single- and bi-directional dynamic loadings and gives some suggestions for a more rational design of partially concrete-filled steel bridge piers. Chapter 4 develops a multiple-spring model for simulating the inelastic behavior of such piers and the validity of the proposed model is then established by comparing the analytical results with the results from experimental studies. The conclusions of this study and directions for future research are presented in Chapter 5.

CHAPTER 2
BEHAVIOR OF PARTIALLY CONCRETE-FILLED STEEL BRIDGE PIERS UNDER STATIC CYCLIC LOADING TEST

2.1 General

The Seismic Design Specifications for Highway Bridges (JRA 2012) allows applying independent single-directional transverse forces in the design of bridge piers. To date the seismic performance of steel bridge piers has been widely studied through mainly static cyclic loading tests, some pseudo-dynamic loading tests, and numerical analysis. Most of them are tested in a single lateral direction. However, the actual seismic waves consist of three-directional components and the seismic response of bridge piers is affected by the two horizontal components simultaneously. Therefore, it is difficult to properly evaluate the seismic behavior due to bi-directional horizontal seismic motions through single-directional loading tests because the real complex behavior of local buckling and inelastic behavior in the component plates of the pier are caused by bi-directional loading at the ultimate state.

During the past decade, some efforts were concentrated on investigating basic characteristics of the seismic response of steel bridge piers through cyclic bi-directional loading tests. After Kobe Earthquake partially concrete-filled steel piers have been widely used in earthquake-prone regions in Japan for their excellent structural performance and properties such as high ductility, high strength, and large energy absorption capacity. However, there are still lacks of dynamic test results on partially concrete-filled steel columns under coupled ground motions in two horizontal directions.

To investigate the basic seismic performance of partially concrete-filled steel bridge piers under bi-directional loading, a series of static cyclic tests and single- and bi- directional pseudo-dynamic loading tests have been conducted in present study.

In this chapter, the details of test specimens with different cross sectional shapes and various concrete-filled ratios are introduced first, and the experimental results of test specimens subjected to the static cyclic loadings are presented prior to the single- and bi- directional pseudo-dynamic loading tests.

Numerous static cyclic loading tests on steel piers have been conducted after Kobe earthquake in Japan because the testing procedure is relatively simple. Although it is not able to obtain the response due to seismic acceleration data from this test, general fundamental characteristics of the piers under cyclic loading, such as yield horizontal strength, corresponding yield displacement, maximum horizontal strength, ductility, basic value of the energy absorption are acquired. These values will be applied as normal values to the test results of piers undergoing uni- and bi- directional pseudo- dynamic loading tests which described in following Chapter 3.

The load- displacement hysteretic curves obtained from the static cyclic loading will be utilized also in Chapter 4, where numerical analysis is developed to calculate response behavior instead of single- and bi- directional loading hybrid tests. The values of parameters of the numerical model are determined directly from the static cyclic loading test results.

2.2 Outline of Experiment

2.2.1 Test Specimen

In the static cyclic loading tests, 3 stiffened rectangular test specimens made of SM490 steel and

3 un-stiffened circular test specimens made of SS400 steel are designed. These test columns are cantilever-type with fixed conditions in the footing and free at the top as a common bridge piers. A schematic illustration of test specimens is shown in Fig. 2-1. The geometrical properties of the test specimens are listed in Table 2-1.

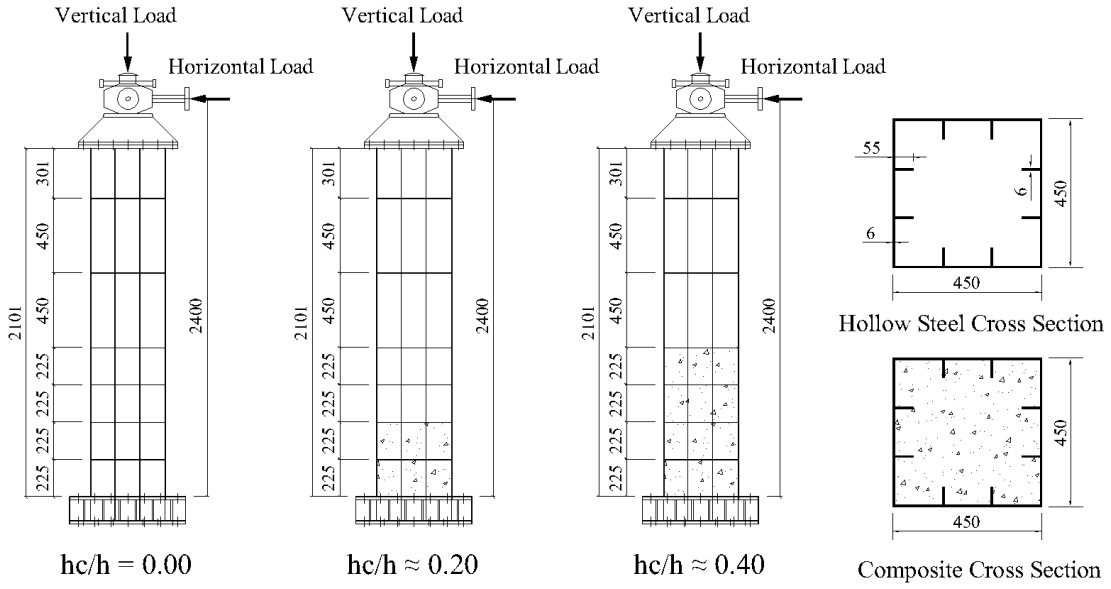

(a)

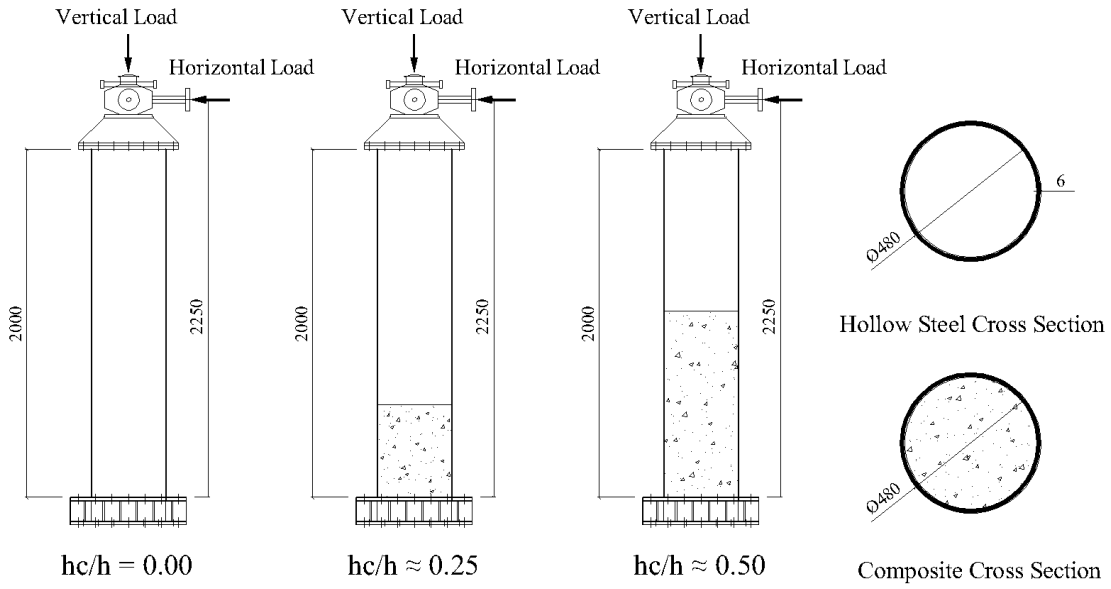

(b)

Fig. 2-1. Test specimens: (a) Stiffened rectangular piers; (b) Un-stiffened circular piers

In the case of stiffened rectangular piers, the entire test specimens with 2400 mm effective height have the same cross-sectional dimensions (450 × 450 × 6 mm) and each panel plate of cross section are welded by two vertical stiffeners (55 × 6 mm), as presented in the Fig. 2-1(a). To prevent cross-sectional distortions, the diaphragms are welded at intervals of 225 mm along the length of the specimens, and then at a distance of 450 mm in the upper region, i.e., from 900mm to top.

Table 2-1. Geometrical properties of the test specimens

Cross-sectional shape		Rectangular	Circular
Width or diameter of cross section	b (mm)	450	480
Plate thickness of cross section	t (mm)	6	6
Width of vertical stiffener	b_s (mm)	55	-
Thickness of vertical stiffener	t_s (mm)	6	-
Area of cross section	A (mm^2)	1.33×10^4	0.89×10^4
Moment inertia of cross section	I (mm^4)	4.12×10^8	2.51×10^8
Gyration radius of cross section	r (mm)	176	168
Effective height of specimen	h (mm)	2400	2250

Table 2-2. Parameters of the test specimens

Specimen	R_R	R_t	λ	hc
(a) Stiffened Rectangular Piers				
S-00	0.52	-	0.34	0.00h
S-20	0.52	-	0.34	0.20h
S-40	0.52	-	0.34	0.40h
(b) Un-stiffened Circular Piers				
U-00	-	0.076	0.29	0.00h
U-25	-	0.076	0.29	0.25h
U-50	-	0.076	0.29	0.50h

Actual circular piers have generally neither diaphragms nor vertical stiffeners because the carved plate is hard to occur local buckling. So, circular test piers in this study have no diaphragms or vertical stiffeners, as shown in Fig. 2-1(b). Test piers are made of 6mm thick SS400 steel grade and the outside diameter of cross section is 480mm, then radius-thickness ratio parameter (R_t) value becomes 0.076 by Eq. 2.2. The effective height is 2250mm. It is specified in the seismic design code (Japan Road Association 2012) that thin-walled circular columns should be designed such that $R_t \leq 0.08$ in order to prevent the decrease in strength and ductility due to local buckling.

The values of various parameters of the test specimens are listed in Table 2-2, in which specimen designations starting with an "S" refer to stiffened rectangular piers, and those starting with a "U" refer to circular piers. In each specimen, the number following the "S" or "U" is related to values of concrete-filled ratio. The values of width-thickness ratio parameters of flange plate (R_R), radius-thickness ratio parameter (R_t), and slenderness ratio parameter (λ) are defined by the following equations.

$$R_R = \frac{b}{t}\sqrt{\frac{\sigma_y}{E_s}\frac{12(1-\nu^2)}{\pi^2 k_R}} \tag{2.1}$$

$$R_t = \frac{R}{t}\frac{\sigma_y}{E_s}\sqrt{3(1-\nu^2)} \tag{2.2}$$

$$\lambda = \frac{2h}{r}\frac{1}{\pi}\sqrt{\frac{\sigma_y}{E_s}} \tag{2.3}$$

Here b = side length of square cross section, R = radius of the plate center position of circular cross section, t = steel plate thickness, E_s = Young's modulus, σ_y = yield stress, ν = Poisson's ratio, h = effective height, r = gyration radius of the cross section, k_R = $4n^2$ while n is the number of subpanels divided by longitudinal stiffeners in each plate panel.

The material properties of the SM490 and SS400 grade steel are shown in Table 2-3, and are obtained from tensile tests on three coupons in each series. The details of early strength concrete adopted for the specimens are given in Table 2-4, where f_c is compressive strength of the concrete which is determined by the average of uni-axial compressive strength values of three standard concrete cylinders (100 mm in diameter and 200 mm in length) in compression tests carried out on the day of the experiments.

Table 2-3. Material properties of steel

		E_s (GPa)	σ_y (Mpa)	ε_y (%)	σ_u (Mpa)	v
SM490	Measured	212	391	0.186	526	0.286
	Nominal	200	325	0.163	490~610	0.300
SS400	Measured	211	312	0.147	443	0.291
	Nominal	200	245	0.123	400~510	0.300

Table 2-4. Material properties of early strength concrete

Specimen	Age	E_c(GPa)	μ_c	f_c(MPa)
S-20	16	25.5	0.165	21.8
S-40	21	25.5	0.165	23.5
U-25	42	25.7	0.165	24.4
U-50	77	25.6	0.165	27.9

2.2.2 Concrete-filled Ratio

To determine the proper length of the filled-in concrete, the Specification (Japan Road Association 2012) recommends using the following formula in the practical seismic design.

$$h_c > \left(1 - \frac{M_{ys}}{M_a}\right) h \tag{2.4}$$

where h_c = concrete-filled length; h = length of the specimen from the base to the position on the top where inertial force is applied; $M_{ys} = (\sigma_{sy} - \sigma_{sN})Z_g$ which is the yield bending moment of the hollow steel cross section just above the filling concrete; σ_{sy} = yield stress or stress calculated by multiplying the allowable stress for local buckling by coefficient 1.7; σ_{sN} = stress due to axial force; Z_g = section modulus of hollow steel cross section; M_a = allowable bending moment of the steel-concrete composite cross section at the base.

In this study, it is planned to compare the seismic behavior of test specimens of above-mentioned sufficient concrete-filled ratio with that of those of low concrete-filled ratio, which introduced by Usami & Ge 1994. This calculation method of the filling length of concrete is based on the relation between the fully plastic moment of the steel-concrete composite cross section (M_{pc}) and the hollow steel cross section (M_{ps}). The height of the filled-in concrete is calculated by Eq. 2.5.

$$h_c = \left(1 - \frac{M_{ps}}{M_{pc}}\right) h \tag{2.5}$$

For the square sectional shape adopted in the tests, the fully plastic moment ratio is M_{ps}/M_{pc} ≈0.80, while the bending moment ratio becomes M_{ys}/M_a ≈ 0.59 by the above-mentioned equations. From these two calculations, 0.20*h* and 0.40*h* have been selected as the length of the filled-in concrete in this study. In the case of the length of the filled-in concrete being 0.20*h*, it is considered that the hollow steel section just above the concrete-filled portion would reach the fully plastic state earlier. While, for the length of the filled-in concrete being 0.40*h*, the composite cross-section at the base would reach the fully plastic state earlier.

In the case of test specimens of circular sectional shape, the bending moment ratio (M_{ys}/M_a) defined by Eq.2.4 is about 0.53, and the fully plastic moment ratio (M_{ps}/M_{pc}) obtained by Eq.2.4

is about 0.75. That is, the concrete-filled lengths of 0.50*h* and 0.25*h* are adopted for un-stiffened circular section steel piers in this study.

2.2.3 Load Sequence

Before conducting the hybrid loading test, the static cyclic loading test in a single horizontal direction will be performed to obtain the common fundamental properties of the test specimens. A constant axial load P/P_y =0.15, where P_y is the axial yield load calculated using the nominal yield stress of steel and cross-sectional area, is applied to all test specimens.

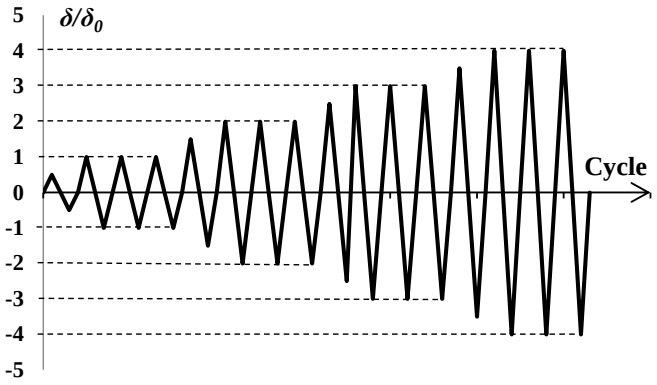

Fig. 2-2. Displacement history of the static cyclic single-axial loading test

The horizontal displacement history consists of a sequence of fully reversed displacement cycles as shown in Fig.2-2, that is, the peak displacements are increased stepwise after three successive cycles at each displacement level such as $\pm 0.5\delta_0$, $\pm 1\delta_0$ (3 cycles), $\pm 1.5\delta_0$, and $\pm 2\delta_0$ (3 cycles) until collapse. The displacement increment is the yield displacement (δ_0) of the steel pier without concrete filled, where δ_0 is defined as the displacement value corresponding to the yield strain (ε_y) at the bottom of the test specimen obtained from the tensile test. The corresponding load is defined as the yield strength H_0.

2.3 Experimental Results of Stiffened Rectangular Piers

2.3.1 Collapse Modes

In this section, behavior of specimens observed during the tests will be described in detail. In the Fig. 2-3, the features of three test specimens with different concrete-filled ratios after the static cyclic tests are presented.

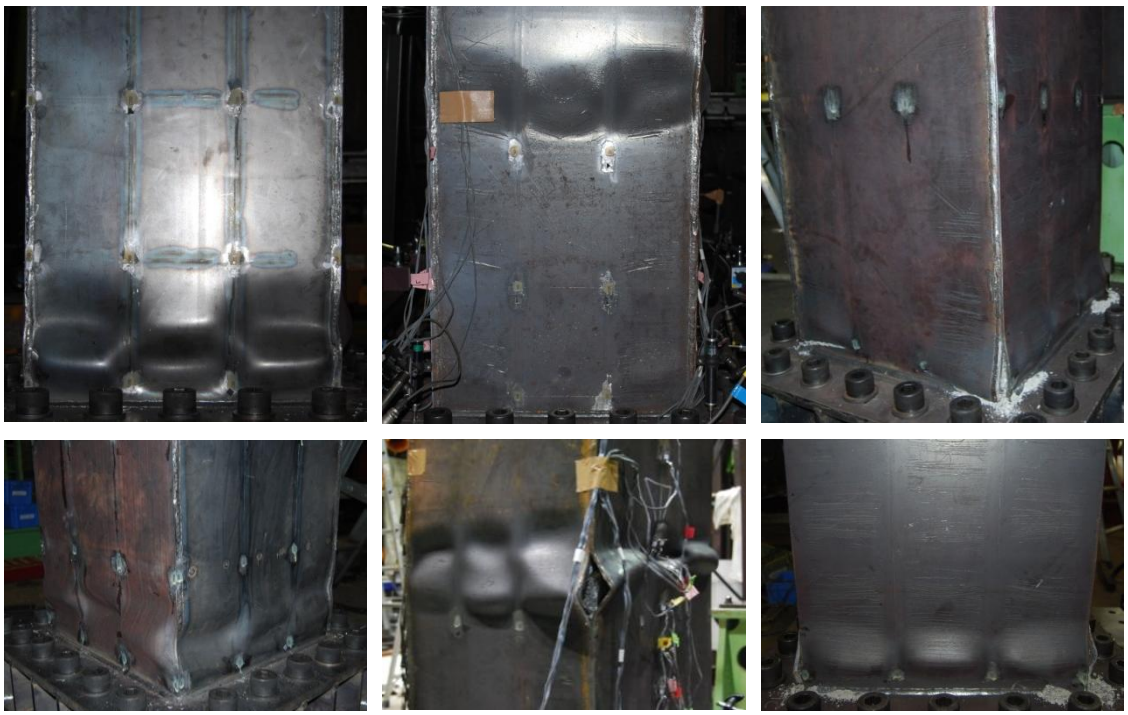

(a) S-00 (b) S-20 (c) S-40

Fig. 2-3. Failures of stiffened rectangular section specimens observed after static cyclic loading tests

For the stiffened test specimen without concrete infill (S-00), local plate buckling was first observed in the flange plates of the pier base immediately after the peak horizontal load, and then extended to the web plates, as shown in Fig.2-3(a). Once local buckling occurred, the plates were not fully straightened out during reversed loading. Buckling deformations progressively grew, and eventually the specimen lost its lateral resistance after either vertical

cracking in the weld material of flange-web junctions or fracture in the plate material became considerable. In this kind of test specimen, local buckling deformations were localized only in its base panels.

For the test specimen partially filled with low length of concrete (S-20) of the case of h_c=0.20h, the hollow steel section just above the diaphragm buckled severely as shown in Fig. 2-3(b). It indicates from the observation that the flange and web plates of the hollow steel section underwent significant inelastic action although the filled-in concrete participated in dissipating energy during the later loading stages. It is noted that this buckling also caused a large deterioration in post- buckling strength which will be discussed in the next section. It should also be pointed out that buckling occurred initially on the flange plates near the pier base, but it hardly grew as the loading was continued.

For the test specimen sufficiently filled with concrete (S-40), in the case h_c=0.40h, slight local buckling occurred only in the flange and web plates at the pier base. It was observed that the plates buckled outward before the cracks in weld or material took place. This is because the filled-in concrete prevented the buckling of plates inward. As shown in Fig. 2-3 (c), cracks along the welding in the corner of the cross sections were also observed after the loading was finished. Concrete behind the portions of plates buckled was seriously crushed. Because both the steel plates and filled-in concrete effectively participated in inelastic action, the specimen S-40 showed excellent earthquake-resistant performances, such as high strength, high ductility, and large energy absorption capacity.

2.3.2 Horizontal Load versus Horizontal Displacement Hysteretic Curves

Nondimensionalized horizontal load versus horizontal displacement hysteretic curves obtained

in cyclic tests of three stiffened rectangular specimens are shown in Fig. 2-4.

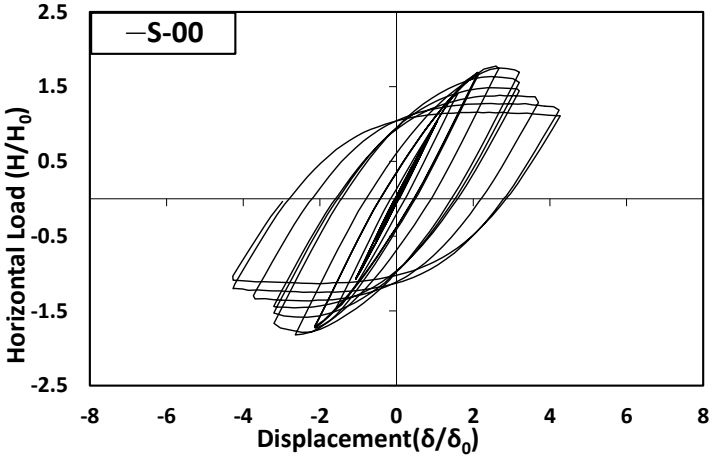

(a) h_c/h = 0.00

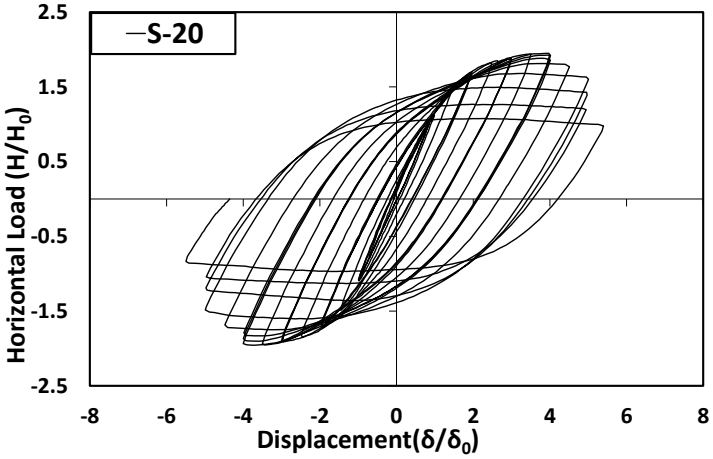

(b) h_c/h = 0.20

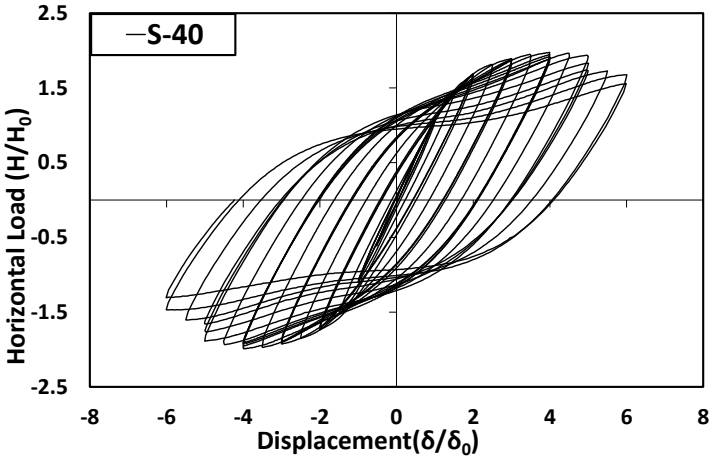

(c) h_c/h = 0.40

Fig. 2-4. Hysteretic curves of stiffened rectangular piers

The main parameters which indicate the strength and deformation capacity presented in the cyclic tests are summarized in Table 2-5. The load and the displacement are nondimensionalized by the yield displacement, δ_0=14.99 mm, and the corresponding yield load, H_0=233.42 kN, respectively, which refer to the yield point of specimen S-00. Plots (a) to (c) are sorted according to the length of filled-in concrete. It can be found in Fig. 2-4 that effect of filled-in concrete are significant. The comparison of these plots indicate that the hysteretic properties of specimen are improved as the length of filled-in concrete incresed.

Table 2-5. Static cyclic loading test results

Specimen	h_c/h	P/P_y	H_y/H_0	δ_y/δ_0	H_{max}/H_0	δ_m/δ_0	δ_{95}/δ_0	μ_m	μ_{95}
S-00	0.00	0.15	1.00	1.00	1.78	2.64	3.01	2.64	3.01
S-20	0.20	0.15	1.06	1.00	1.87	3.50	4.27	3.49	4.25
S-40	0.40	0.15	1.08	1.00	1.99	3.99	5.16	4.01	5.19

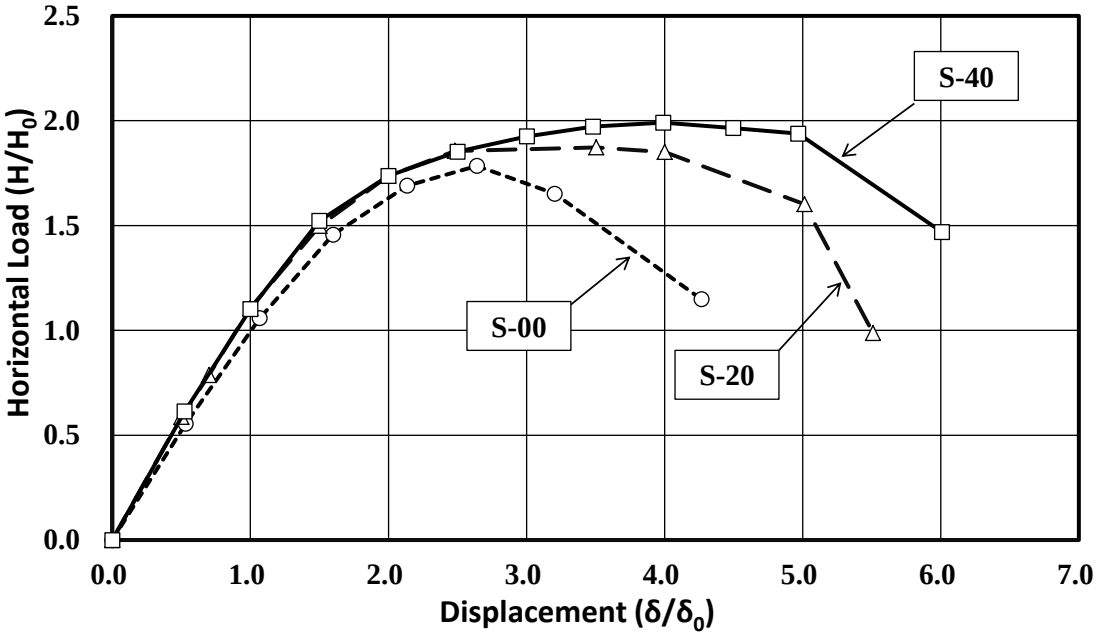

Fig. 2-5. Envelope curves of stiffened rectangular piers due to the static cyclic loading tests

Fig. 2-5 shows the envelope of the horizontal load-displacement hysteretic curves. From the Figs. 2-4 and 2-5 and Table 2-5 the following important facts are observed.

Fig. 2-5 indicates that in comparison with specimen S-00 without concrete filled, the maximum lateral loads were increased by about 5% and 12% in specimens S-20 and S-40, respectively which was filled up to the 0.20*h* and 0.40*h*. The corresponding displacement to the maximum load were 1.33 and 1.51 times larger than that of steel specimen S-00.

As a result, it can be concluded that by the presence of a diaphragm provided over the filled-in concrete, both the ultimate strength and deformation capacity of stiffened rectangular specimens are obviously improved in the filled-in concrete. In the case of h_c = 0.20*h*, a deterioration in strength was observed because local buckling occurred in the panels of the hollow steel section just above the filled-in concrete. On the other hand, specimen S-40 of h_c = 0.40*h* presented excellent deformation characteristics in undergoing the inelastic action due to slight buckling in the panels at the column base. It is worth noting that crack resulting from the low-cycle fatigue may occur at the corner near the weld.

2.3.3 Ductility Factor

Ductility is an important factor in a seismic design. The design strength, consequently cross sectional size of a pier can be substantially reduced if the pier is able to provide a good deformation capacity beyond the elastic limit by following constant energy law. The two kinds of ductility parameters, μ_m and μ_{95} are used usually for evaluating the deformation capacity of piers, which are showed in Table 2-5.

The ductility factor μ_m is defined as the ratio of the displacement corresponding to the maximum

lateral load, δ_m, to the horizontal displacement at which first yield occurs, δ_y:

$$\mu_m = \frac{\delta_m}{\delta_y} \tag{2.6}$$

In some cases, the degradation slope of the load-displacement curve is so gentle that the peak point is difficult to locate. Hence, another ductility parameter μ_{95} was proposed (Ge & Usami, 1996) in the following,

$$\mu_{95} = \frac{\delta_{95}}{\delta_y} \tag{2.7}$$

Here δ_{95} is the lateral displacement obtained when the lateral resistance load is reduced to 95% of the maximum load.

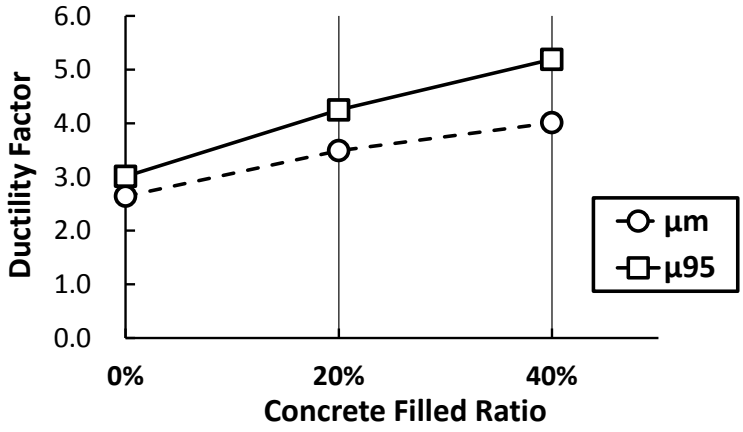

Fig. 2-6. Effect of filled-in concrete on ductility

The values of the ductility factors μ_m and μ_{95} are listed in Table 2-5, and plot of μ_m and μ_{95} against the concrete-filled ratio is shown in Fig. 2-6. As seen from the figure, the ductility factors μ_m and μ_{95} are considerably higher when the height ratio of the filled-in concrete increased. In other words, the ductility behavior of the stiffened rectangular piers can be largely improved by the filled-in concrete.

2.4 Experimental Results of Unstiffened Circular Piers

2.4.1 Collapse Modes

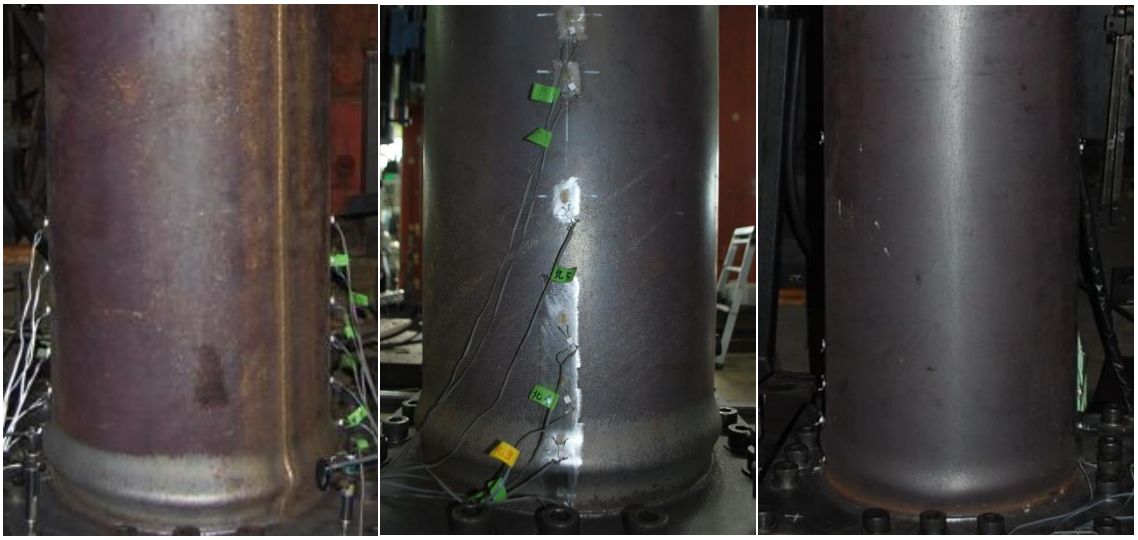

(a) U-00 (b) U-25 (c) U-50

Fig. 2-7. Failure mode of circular specimens observed after static cyclic tests

As seen in Fig. 2-7, the local buckling of plates was observed at the column base regardless of the length of the filled-in concrete. Similar to the specimens with a diaphragm over the concrete, such as S-20 and S-40 above-mentioned in the section 2.3, initial buckling occurred at the column base, just before the maximum load. This deformation, however, grew progressively when cyclic loading was continued because the load was not increased sufficiently to form buckling at the hollow steel section above the concrete-filled part.

2.4.2 Horizontal Load versus Horizontal Displacement Hysteretic Curves

The hysteretic curves of the static cyclic loading tests of circular piers are shown in Fig. 2-8.

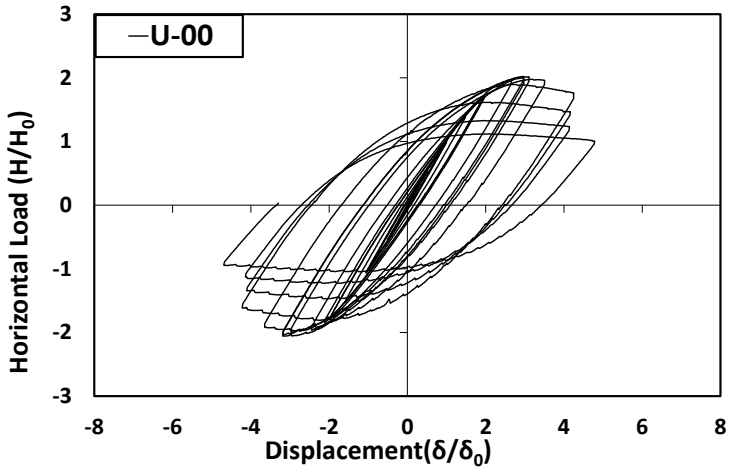

(a) h_c/h = 0.00

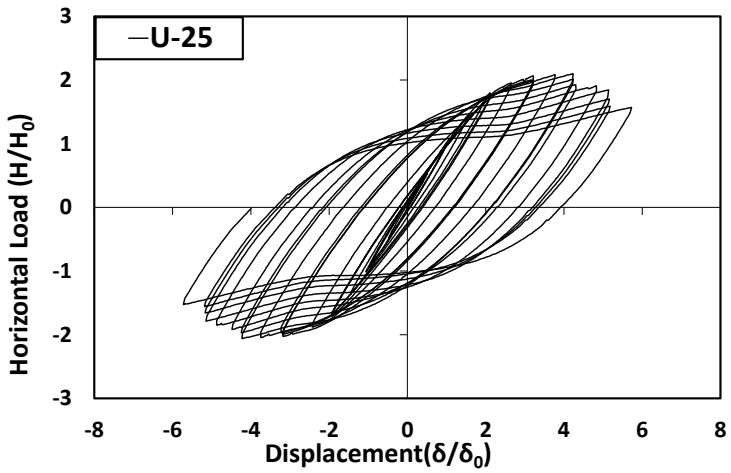

(b) h_c/h = 0.25

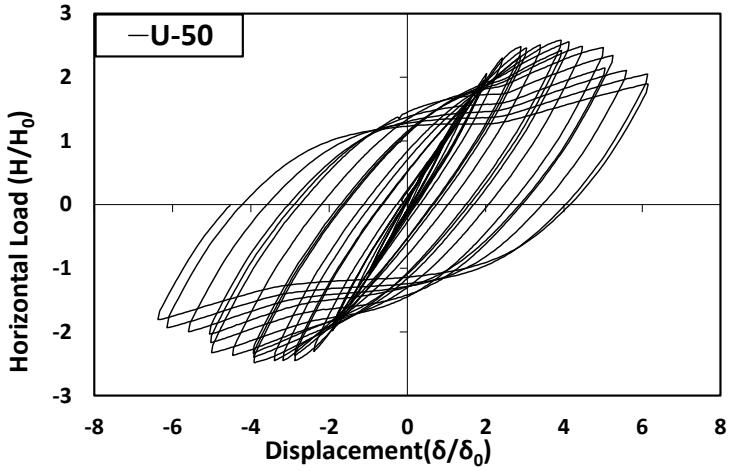

(c) h_c/h = 0.50

Fig. 2-8. Hysteretic curves of unstiffened circular piers

The envelope curves are shown in Fig. 2-9, where the horizontal displacement and horizontal load are non-dimensionallized by the yield displacement (δ_0 = 8.46 mm) and yield load (H_0 = 85.55 kN) of the specimen U-00, respectively. The cyclic loading test results are summarized in Table 2-6.

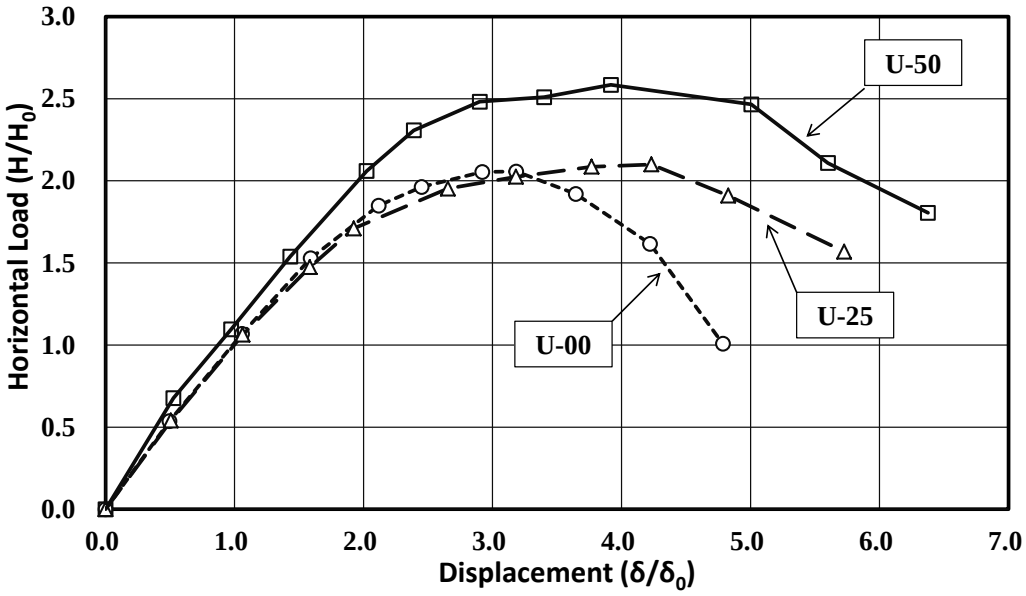

Fig. 2-9. Envelope curves of un-stiffened circular piers due to the static cyclic tests

Table 2-6. Static cyclic loading test results

Specimen	h_c/h	P/P_y	H_y/H_0	δ_y/δ_0	H_{max}/H_0	δ_m/δ_0	δ_{95}/δ_0	μ_m	μ_{95}
U-00	0.00	0.15	1.00	1.00	2.06	3.18	3.53	3.18	3.53
U-25	0.25	0.15	1.00	1.00	2.10	4.23	4.56	4.23	4.56
U-50	0.50	0.15	1.12	1.00	2.58	3.92	5.10	3.92	5.10

It can be observed from the Fig. 2-9 that, in comparison with specimen U-00 without concrete filled, the displacement at the maximum load of specimen U-25 with a length of 0.25*h* infill concrete increased by 33%, which showed its better deformation capacity. However, it is also shown that the filled-in concrete of an insufficient length made a very small contribution to the

maximum lateral load since the load was transmitted difficultly to the concrete only through the frictional contact between the external plate with internal concrete.

For the specimen U-50, in which concrete was filled sufficiently with a length of 0.50*h*, it can be seen from the Fig. 2-8 and Table 2-6 that both the maximum lateral load and deformation capacity are obviously improved by the filled-in concrete. Compared with the specimen U-00, the maximum lateral load of specimen U-50 significantly increased by 25%, and the displacement corresponding to the maximum load was 1.23 times larger than the displacement of specimen U-00.

The seismic performance of specimen U-50 has shown great different with that of specimen U-25, although both the specimens U-25 and U-50 were partially filled with concrete. This is because the specimen U-50 possesses a sufficient length of infill concrete, and the upper part of filled-in concrete could apply an axial force to the concrete at the base and transmit the load to the concrete through frictional contact between external steel plates and internal concrete.

2.4.3 Ductility Factor

The values of the ductility factors μ_m and μ_{95} obtained by the cyclic test results of un-stiffened circular piers are listed in Table 2-6, and plot of μ_m and μ_{95} against the concrete-filled ratio is shown in Fig. 2-10.

It can be seen from the Fig. 2-10 that, comparing with specimen U-00 without concrete infill, the ductility factors μ_m and μ_{95} of specimen U-25 of h_c = 0.25*h* respectively increased by 33% and 29%, in the case of specimen U-50 of h_c = 0.50*h*, the corresponding values increased by 23% and 44%, respectively. This can be attributed to the confinement of the internal concrete

which prevented local buckling of plates. Accordingly, some improvement of ductility capacity of the circular steel section due to the filled-in concrete can be expected even when a diaphragm is not provided on the concrete.

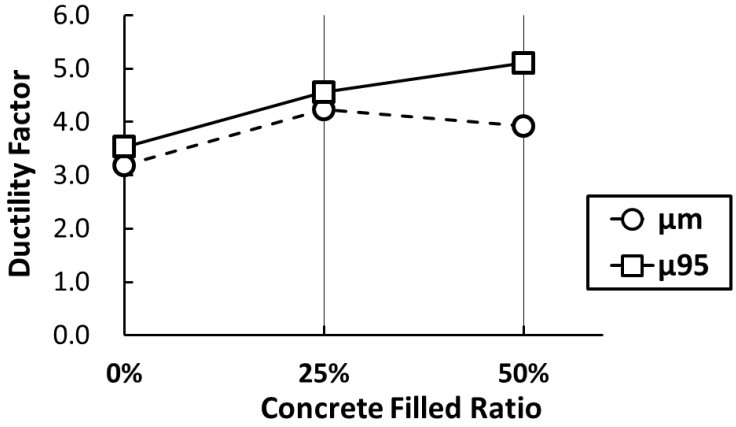

Fig. 2-10. Effect of filled-in concrete on ductility

2.5 Conclusions

A total of 6 column specimens including 3 stiffened rectangular piers and 3 circular piers were tested under constant axial compression and static cyclic lateral loads with varying displacement amplitude. Based on the experimental results, the following conclusions are drawn.

Partially concrete-filled steel piers under static cyclic loading showed generally prominent earthquake-resistant characteristics in undergoing the inelastic action.

For the stiffened rectangular piers, through the comparison among the specimens S-00 without concrete infill, S-20 (h_c/h = 0.20), and S-40 (h_c/h = 0.40), it is observed that both strength and ductility of steel piers can be significantly increased by filled-in concrete. This is because when inward local-plate buckling displacements are prevented by filled-in concrete, local buckling deformations are delayed in their initiation and also moderated considerably, which leads to an

increase in ductility and ultimate strength.

In the case of circular piers, the partially concrete-filled specimens U-25 (h_c/h = 0.25) and U-50 (h_c/h = 0.50) showed considerably better deformation capacity than specimen U-00 without encased concrete. However, for the specimen U-25, it is also shown that the filled-in concrete of an insufficient length made a very small contribution to the ultimate load since the load was hardly transmitted to the concrete through the frictional contact between the external plate with internal concrete. On the other hand, the specimen U-50 possesses a sufficient length of infill concrete, and the filled-in concrete was found to be effective in improving the strength and ductility of column.

CHAPTER 3
BEHAVIOR OF PARTIALLY CONCRETE-FILLED STEEL BRIDGE PIERS UNDER SINGLE- AND BI- DIRECTIONAL HYBRID TEST

3.1 General

In this chapter, the earthquake response of partially concrete-filled steel bridge piers obtained from the single- and bi- directional hybrid test will be presented.

In order to evaluate the seismic performance of a structure or a structural member, the following three kinds of test methods are used in general: the static cyclic loading test (quasi-static test), the shaking table test (dynamic test), and the hybrid test (pseudo-dynamic test).

To date, most of the existing experimental data were obtained from static cyclic loading test which was described in detail in the Chapter 2. Obviously, the seismic behavior of a structure evaluated on the basis of its static cyclic behavior would be different from what actually emerged during induced earthquake vibrations.

Shaking table test provides true dynamic loading. A model of a structure is mounted on a stiff platform, which is shaken so as to apply the appropriate base motion. Shaking table tests are often costly and cannot be efficiently conducted for isolated whole structure because of its too large scale. Special loading equipment is also necessary for the dynamic test and its loading capacity is usually limited so that test specimens have to be modeled in the small-scale range. To overcome these problems, the hybrid loading test method had been developed.

Fig. 3-1 shows a conceptual flow of the hybrid test. Hybrid test is a widely used alternative to

shaking-table test, in which the structural displacements due to the earthquake are calculated by computers using a stepwise integration procedure and applied quasi-statically to the test specimen. The resulting resistance forces are measured and feed back to the analysis model as part of the input for the next calculation step. It is advantage in simplifying the equipment needed and it allows for inspection of the behavior of structures during loading. Because the hybrid test simulates realistic dynamic testing without the need for dynamically rated actuators or very high oil flow rates, it can make full-scale testing feasible, so long as a sufficiently large strong floor and reaction wall are available.

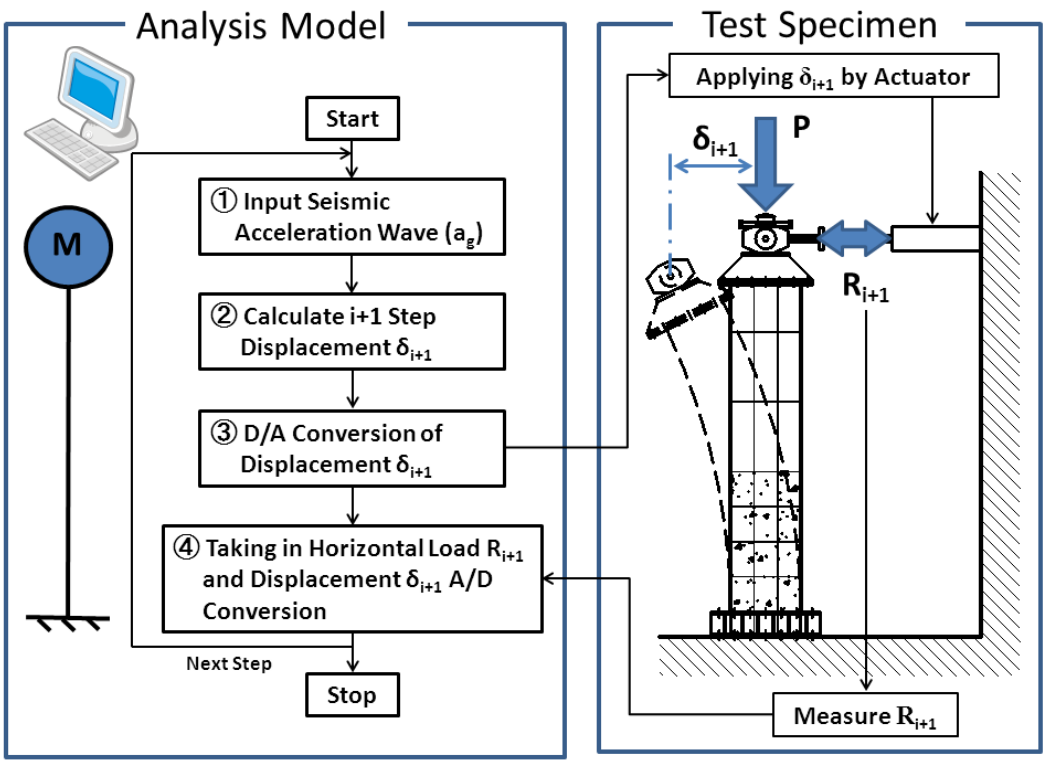

Fig. 3-1. A conceptual flow of hybrid test method

In a bi-directional hybrid loading test, the test specimen is modeled as a two-degree-of-freedom system, and the corresponding equation of motion is presented as follows,

$$\begin{bmatrix} m & 0 \\ 0 & m \end{bmatrix} \begin{Bmatrix} a_x \\ a_y \end{Bmatrix}_{n+1} + \begin{bmatrix} c & 0 \\ 0 & c \end{bmatrix} \begin{Bmatrix} v_x \\ v_y \end{Bmatrix}_{n+1} + \begin{Bmatrix} R_x \\ R_y \end{Bmatrix}_{n+1} = \begin{bmatrix} m & 0 \\ 0 & m \end{bmatrix} \begin{Bmatrix} a_{g,x} \\ a_{g,y} \end{Bmatrix}_{n+1} \quad (3.1)$$

where the properties of the actual bridge pier such as mass (m), initial rigidity (k_0), and the natural period (T) are determined on the basis of the static cyclic loading test results. The damping coefficient (c) is then obtained from the mass and stiffness with a value of 0.05 for the damping ratio (ζ). $\{a\}$ and $\{v\}$ are the acceleration and velocity at the gravity center of the mass, respectively, and $\{a_g\}$ is the seismic acceleration vector. The bi-directional restoring force $\{R\}$ of the actual pier can be calculated from real-time data measured in the specimen during the loading test. The subscript x and y indicate the N-S and E-W direction, respectively. The suffix n denotes the value at the time $n \times \Delta t$, where the time interval was chosen as Δt = 0.01s. The Newmark-β method (β = 1/6) was applied to solve for the displacement using the initial rigidity (k_0), as shown in the following equations,

$$\{\delta\}_{n+1} = \{\delta\}_n + \{v\}_n \Delta t + \frac{1}{2}\{a\}_n \Delta t^2 + \beta(\{a\}_{n+1} - \{a\}_n)\Delta t^2 \quad (3.2)$$

$$\{v\}_{n+1} = \{v\}_n + \frac{1}{2}(\{a\}_{n+1} + \{a\}_n)\Delta t \quad (3.3)$$

By introducing the measured and scaled restoring force vector$\{R\}$ at n step into Eq.(3.1), the response displacement, velocity, and acceleration at n+1 step can be calculated using Eq.(3.2) and Eq.(3.3).

To investigate the seismic performance of partially concrete-filled steel bridge piers under actual earthquake conditions, a total of 40 test specimens, including 27 stiffened rectangular piers and 13 circular piers, through single- and bi-directional hybrid tests. In the experimental work of hybrid tests, the effects of bi-directional loading and length of filled-in concrete on the main seismic performance parameters, such as maximum lateral load, maximum response displacement and residual displacement were studied in this chapter.

3.2 Outline of Experiment

3.2.1 Test System Setup

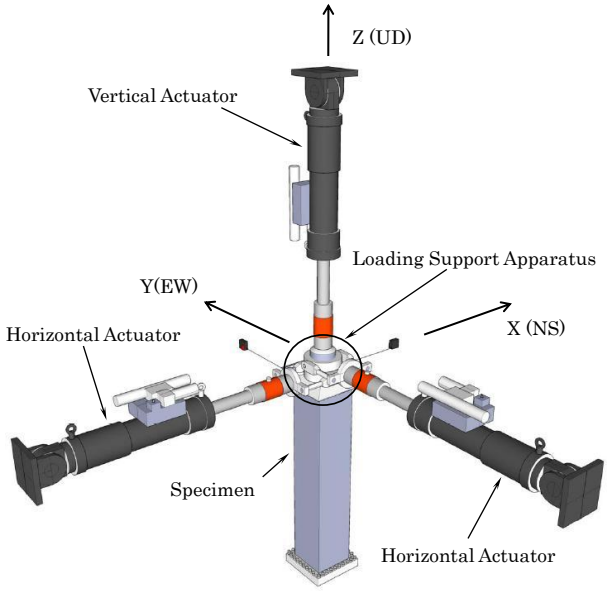

Fig.3-2. Tri-directional loading system

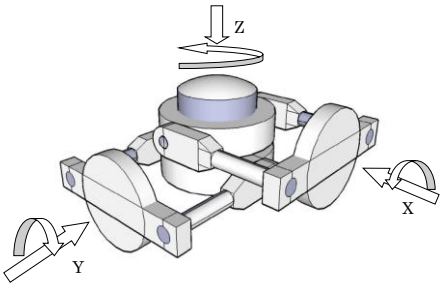

Fig. 3-3. Loading support apparatus

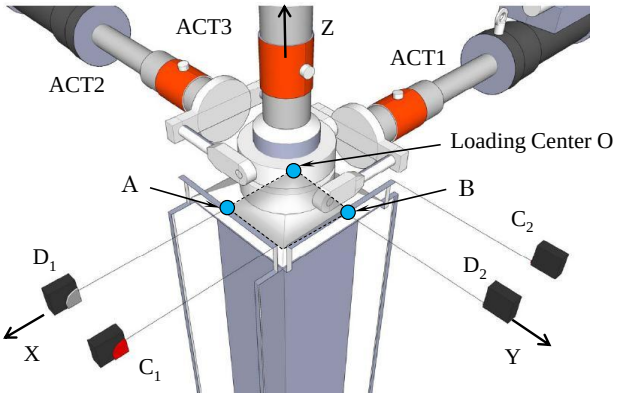

(a) Top

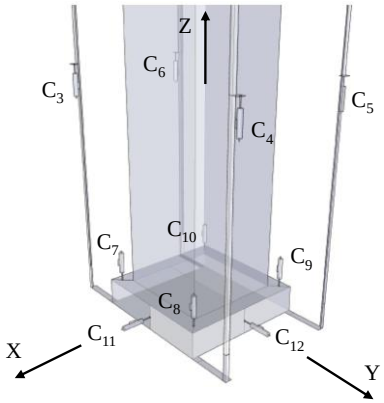

(b) Base

Fig. 3-4. Measuring system

The test system adopted in this study consisted of the tri-directional loading system and measuring system developed by Aoki et al (2007). The loading system is shown in Fig. 3-2.

Three 1000kN actuators and a loading support apparatus were used to apply tri-directional loads on the top of test specimens. The loading support apparatus included two loading arms and a core ball and circular bearings as illustrated in Fig. 3-3. The outer ends of the loading arms were rigidly connected to the two horizontal direction actuators. The inner ends could move along the core ball surface with negligible friction to keep the axes of the loading arms always pointing toward the center of the core ball and circular bearings.

The measuring system consisted of three groups of displacement transducers (DTs) and three load cells (ACTs) located at the end of the loading axis of each actuator. A complex displacement measuring system is required because the displacement of loading point O cannot be measured directly. The first group of DTs including the 4 string-pull type displacement meters C1, C2, D1, and D2, shown in Fig. 3-4 (a) were arranged in the measurement plane on the top of the specimen, where the measurement plane is defined as the plane perpendicular to the pier axis including the loading point O. The string ends of D1 and D2 were connected to the midpoints A and B at the side of the measurement plane to measure the bi-directional horizontal displacement of the loading center O. The string ends of C1 and C2 are linked to the corner of the measurement plane to obtain the Z-axis rotation of the measurement plane, as shown in Fig. 3-4 (a). The second group of DTs of the sliding-rod displacement meters C3 to C6 are located vertically at the four corners in the middle of the specimen for measuring the rotation angle of the measurement plane, as illustrated in Fig. 3-4 (b). The third group of DTs of C7 to C10 is used for determining the rotation angle, and C11 and C12 are used for measuring the horizontal shifts at the base of the specimen. The details of compensation are calculated from the measuring data to obtain the precise location of the loading point O and can be referred to the literature written by Dang et al. (2010).

3.2.2 Experimental Program

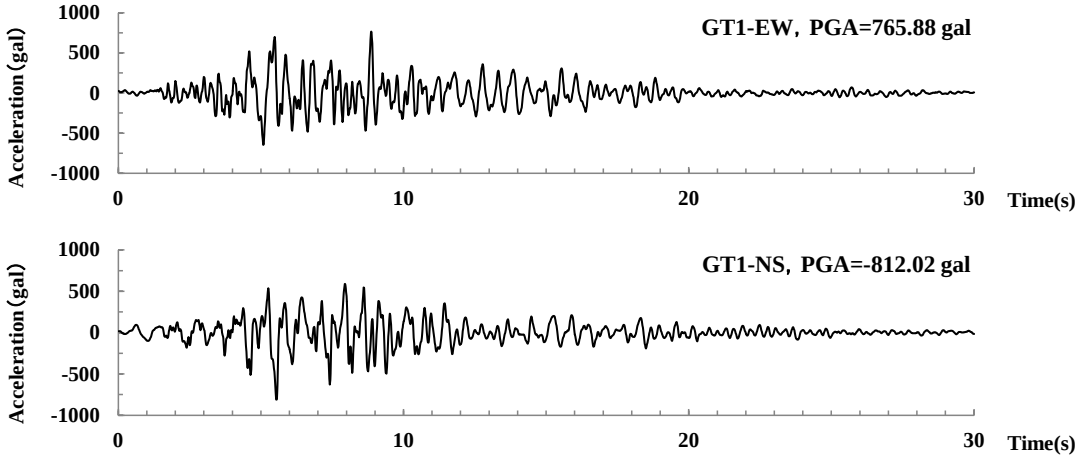

(a) JMA (Ground Type 1 – Hard Ground)

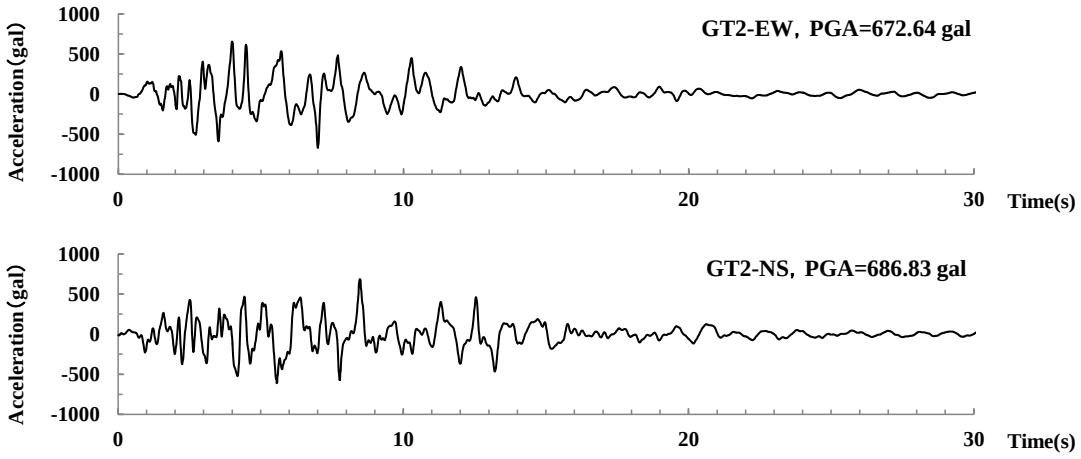

(b) JRT (Ground Type 2 – Medium Ground)

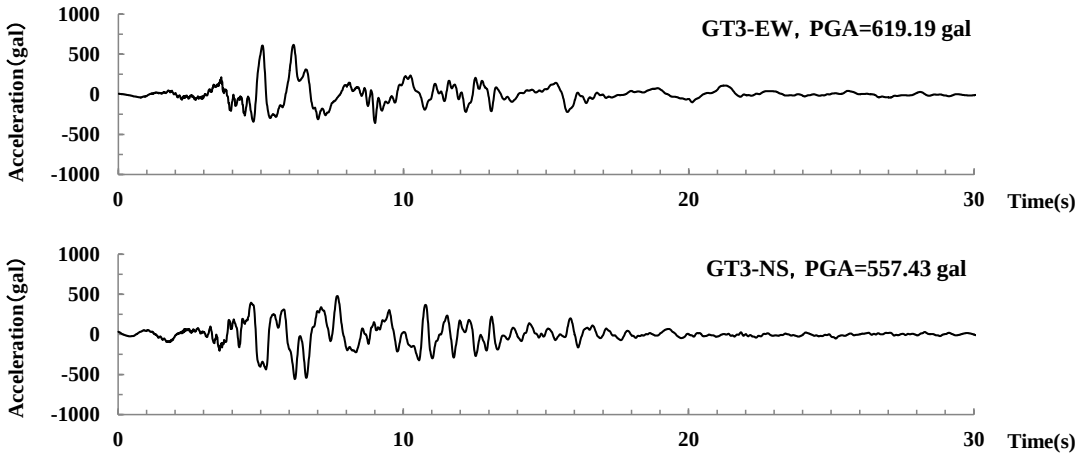

(c) PKB (Ground Type 3 – Soft Ground)

Fig. 3-5. Input earthquake accelerogram records in Kobe Earthquake

Three kinds of input acceleration data recorded in the 1995 Kobe Earthquake are used, which consisted of JMA, JRT, and PKB, corresponding to hard ground (Ground Type 1), medium ground (Ground Type 2), and soft ground (Ground Type 3), respectively. The acceleration time histories are presented in Fig. 3-5.

Table 3-1. Experimental program for stiffened rectangular piers

No.	*Specimen*	*Loading Mode*	*Ground Type*	*Concrete Filled Ratio*
1	S-H-00-1D-1	1D-EW	GT1 (JMA)	h_c/h = 0.00
2	S-H-00-1D-2	1D-NS		
3	S-H-00-2D-1	2D		
4	S-H-00-1D-3	1D-EW	GT2 (JRT)	
5	S-H-00-1D-4	1D-NS		
6	S-H-00-2D-2	2D		
7	S-H-00-1D-5	1D-EW	GT3 (PKB)	
8	S-H-00-1D-6	1D-NS		
9	S-H-00-2D-3	2D		
10	S-H-20-1D-1	1D-EW	GT1 (JMA)	h_c/h = 0.20
11	S-H-20-1D-2	1D-NS		
12	S-H-20-2D-1	2D		
13	S-H-20-1D-3	1D-EW	GT2 (JRT)	
14	S-H-20-1D-4	1D-NS		
15	S-H-20-2D-2	2D		
16	S-H-20-1D-5	1D-EW	GT3 (PKB)	
17	S-H-20-1D-6	1D-NS		
18	S-H-20-2D-3	2D		
19	S-H-40-1D-1	1D-EW	GT1 (JMA)	h_c/h = 0.40
20	S-H-40-1D-2	1D-NS		
21	S-H-40-2D-1	2D		
22	S-H-40-1D-3	1D-EW	GT2 (JRT)	
23	S-H-40-1D-4	1D-NS		
24	S-H-40-2D-2	2D		
25	S-H-40-1D-5	1D-EW	GT3 (PKB)	
26	S-H-40-1D-6	1D-NS		
27	S-H-40-2D-3	2D		

Table 3-2. Experimental program for unstiffened circular piers

No.	*Specimen*	*Loading Mode*	*Ground Type*	*Concrete Filled Ratio*
1	U-H-00-1D-1	1D-EW	GT2 (JRT)	h_c/h = 0.00
2	U-H-00-1D-2	1D-NS		
3	U-H-00-2D-1	2D		
4	U-H-25-1D-1	1D-EW	GT2 (JRT)	h_c/h = 0.25
5	U-H-25-1D-2	1D-NS		
6	U-H-25-2D-1	2D		
7	U-H-50-1D-1	1D-EW	GT2 (JRT)	h_c/h = 0.50
8	U-H-50-1D-2	1D-NS		
9	U-H-50-2D-1	2D		
10	U-H-50-1D-3	1D-EW	GT3 (PKB)	
11	U-H-50-1D-4	1D-NS		
12	U-H-50-1D-5	1D-PA		
13	U-H-50-2D-2	2D		

Table 3-3. Properties of actual bridge piers

Type	h_c/h	P/P_y	P (kN)	m (t)	k_0 (kN/mm)	c (t/s)	T (s)
Stiffened Rectangular	0.00	0.15	648	1058	62.9	815.8	0.81
	0.20	0.15	648	1058	65.9	835.0	0.80
	0.40	0.15	648	1058	67.4	844.4	0.79
Unstiffened Circular	0.00	0.15	315	514	44.3	477.2	0.68
	0.25	0.15	315	514	46.2	487.3	0.66
	0.50	0.15	315	514	61.3	561.3	0.58

The experimental programs for stiffened rectangular piers and circular piers are listed in Table 3-1 and Table 3-2, respectively. In the tables, specimen designations starting with an “S” refer to stiffened rectangular piers, and those starting with a “U” refer to circular piers. The ground type is represented by “GT”, and “H” indicates the hybrid loading test, the following number denotes the height ratio of the filled-in concrete, and “1D” or “2D” refers to the single- or bi-directional hybrid test, respectively.

A constant axial load (P/P_y = 0.15) was applied to all test specimens, and the properties of the actual bridge piers, such as mass, initial rigidity, damping coefficient and the natural period, are listed in Table 3-3.

3.3 Experimental Study on Stiffened Rectangular Piers

3.3.1 Collapse Modes

During the experiments, it was observed that the test specimens loaded by seismic waves of medium and soft grounds (GT2 and GT3) have shown much greater damage than those in hard ground (GT1). The piers of low concrete-filled ratio or without concrete infill quickly collapsed in the bi-directional loading tests of soft ground (GT3). Therefore, in order to give complete and clear information for explaining the effect of bi-directional loading and filled-in concrete on the seismic response of test specimens, phenomena observed during the hybrid tests of medium ground (GT2) will be described in detail in this section.

Fig. 3-6 shows the different failure modes of piers after hybrid tests, in which plots placed in row 1, 2, and 3 correspond to the test results of piers without concrete infill (h_c = 0.00h), with low concrete-filled ratio (h_c = 0.20h), and sufficiently filled with concrete (h_c = 0.40h), respectively. The left two columns of plots are the results due to single-directional loading, while the rightmost plots represent the results due to bi-directional loading.

It can be clearly seen from the Fig.3-6 that the specimens due to bi-directional loading suffered much more damage than those due to single-directional loading, no matter what kind of concrete-filled ratio. It also can be observed that as the length of filled-in concrete increased, the conditions of damage were gradually improved, whether under single-directional loading or bi-directional loading.

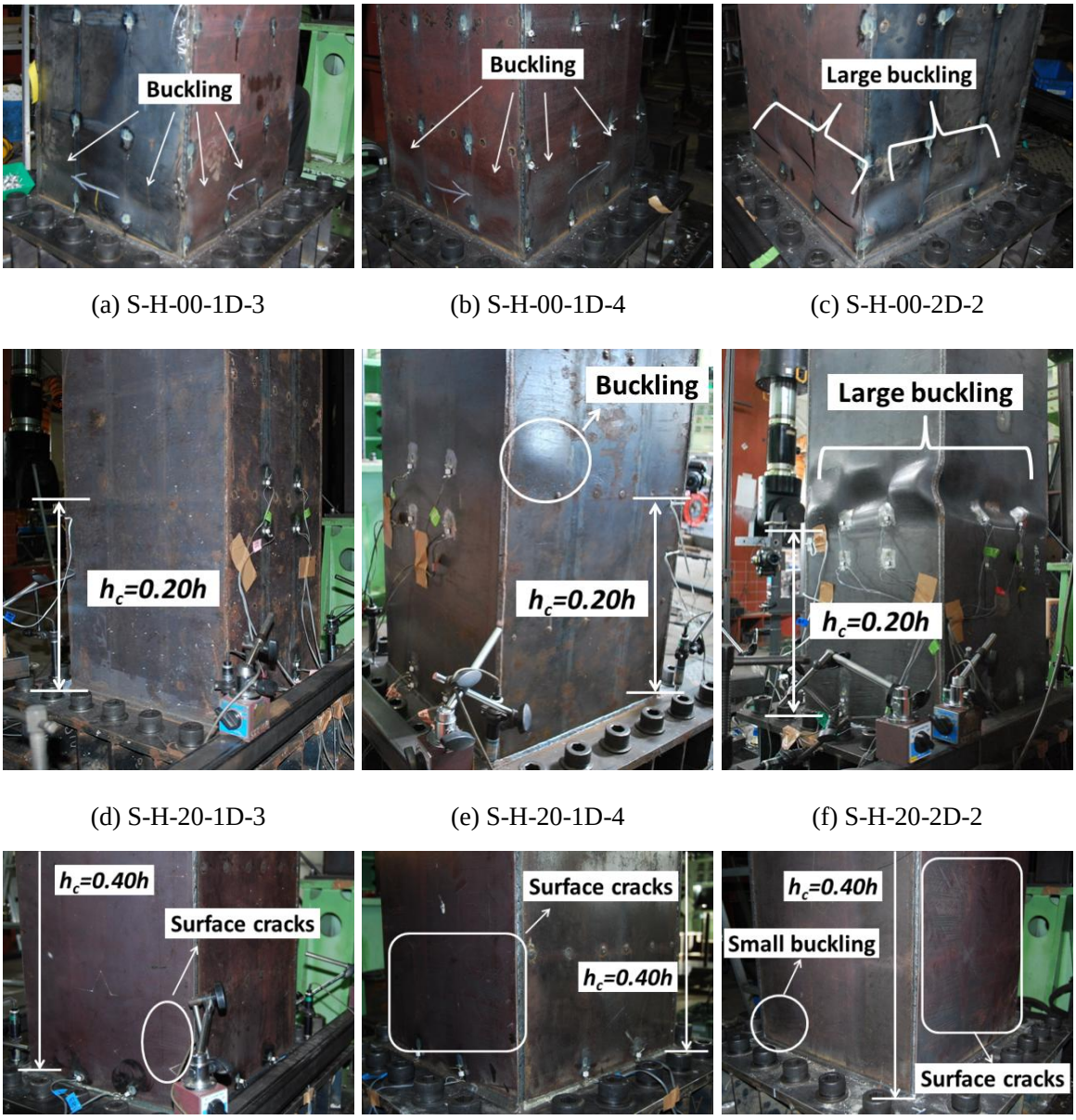

(a) S-H-00-1D-3 (b) S-H-00-1D-4 (c) S-H-00-2D-2

(d) S-H-20-1D-3 (e) S-H-20-1D-4 (f) S-H-20-2D-2

(g) S-H-40-1D-3 (h) S-H-40-1D-4 (i) S-H-40-2D-2

Fig.3-6. Stiffened rectangular specimens after loading tests of medium ground (GT2)

For the stiffened rectangular test specimens without concrete infill (h_c = 0.00h), whether in single-directional loading tests or in bi-directional loading tests, local plate buckling was first observed in the flange plates at the pier base immediately after the peak horizontal load, and then extended to the web plates. Once local buckling occurred, the plates were not fully

straightened out during reversed seismic loading, buckling deformations progressively grew and the response displacement on the top of the piers became considerable, especially in the case of bi-directional loading as illustrated in plot (c). In this kind of test specimens, local buckling deformations were localized only in their base panels as shown in plots (a) to (c).

For the stiffened specimens S-H-20-1D-3 (GT2-EW) and S-H-20-1D-4 (GT2-NS), both in the case of $h_c = 0.20h$, only some surface cracks were observed on the plates near the column base and in the hollow steel section above filled-concrete, and slight local buckling took place in the flange plates of the hollow steel section immediately after the peak horizontal load, as shown in plots (d) and (e). But the buckling deformations hardly grew until the test was finished. However, for the specimen S-H-20-2D-2 (GT2-2D), which was tested under bi-directional loading, some small surface cracks and slight local buckling deformations were first observed in the base flange plate and the panel of the hollow steel section, as shown in plot (f). As the loading was continued, the buckling waves progressively grew and most of the lateral deformation took place in the hollow steel section, which resulted in the large horizontal displacements of the top of specimen in NS and EW direction as reflected in Fig.3-8 (c) and (d).

For the specimens sufficiently filled with concrete at the bottom of the case of $h_c = 0.40h$, the earthquake damage was smallest among these three kinds of specimens. For the specimens S-H-40-1D-3 (GT2-EW) and S-H-40-1D-4 (GT2-NS) under single-directional loading, it was observed that large number of surface cracks appeared on the flange and web plates from base to upper hollow steel section during the loading. But until the end of test, no severe damage was observed in the test specimens. For the specimen S-H-40-2D-2 (GT2-2D), even under bi-directional seismic loading, there was only slight outward buckling deformation occurred in the base panel following by a large number of surface cracks.

3.3.2 Effect of Bi-directional Loading

Table 3-4. Results of hybrid tests for stiffened rectangular piers

No.	*Specimen*	*Loading Mode*	δ_{max}/δ_0	δ_r/δ_0	H_{max}/H_0	$\Sigma E/E_0$	h_c/h
1	S-H-00-1D-1	GT1-1D-EW	2.86	0.72	1.86	12.43	
2	S-H-00-1D-2	GT1-1D-NS	3.69	1.43	1.56	21.84	
3	S-H-00-2D-1	GT1-2D	3.33	1.00	1.49	34.86	
4	S-H-00-1D-3	GT2-1D-EW	4.82	2.09	1.65	42.90	
5	S-H-00-1D-4	GT2-1D-NS	5.46	1.98	1.80	74.80	0.00
6	S-H-00-2D-2	GT2-2D	7.40	4.13	1.71	123.83	
7	S-H-00-1D-5	GT3-1D-EW	5.20	2.32	1.61	30.60	
8	S-H-00-1D-6	GT3-1D-NS	5.18	2.95	1.64	34.49	
9	S-H-00-2D-3	GT3-2D	15.76	15.76	1.55	61.70	
10	S-H-20-1D-1	GT1-1D-EW	2.99	0.68	1.90	13.76	
11	S-H-20-1D-2	GT1-1D-NS	3.76	0.77	1.89	22.58	
12	S-H-20-2D-1	GT1-2D	3.44	0.47	1.85	38.42	
13	S-H-20-1D-3	GT2-1D-EW	3.40	0.09	1.97	38.48	
14	S-H-20-1D-4	GT2-1D-NS	4.73	0.68	1.94	66.28	0.20
15	S-H-20-2D-2	GT2-2D	7.82	6.49	1.81	121.09	
16	S-H-20-1D-5	GT3-1D-EW	4.51	1.65	2.04	28.14	
17	S-H-20-1D-6	GT3-1D-NS	4.25	1.38	1.96	30.96	
18	S-H-20-2D-3	GT3-2D	10.04	10.04	1.81	47.88	
19	S-H-40-1D-1	GT1-1D-EW	3.11	0.72	2.04	13.96	
20	S-H-40-1D-2	GT1-1D-NS	3.73	0.55	2.12	25.47	
21	S-H-40-2D-1	GT1-2D	3.68	0.31	1.91	41.73	
22	S-H-40-1D-3	GT2-1D-EW	3.22	0.06	2.05	36.91	
23	S-H-40-1D-4	GT2-1D-NS	4.24	0.07	2.14	55.58	0.40
24	S-H-40-2D-2	GT2-2D	5.59	0.51	2.07	107.25	
25	S-H-40-1D-5	GT3-1D-EW	3.57	0.95	2.12	22.49	
26	S-H-40-1D-6	GT3-1D-NS	3.69	0.91	2.10	28.12	
27	S-H-40-2D-3	GT3-2D	7.18	1.66	2.08	69.94	

The hybrid test results obtained under single- and bi- directional loading, including maximum horizontal load H_{max}/ H_0, the maximum displacement δ_{max}/ δ_0, the residual displacement δ_r /δ_0, and the cumulative absorbed energy $\sum E /E_0$, are listed in Table 3-4. The cumulative absorbed

energy parameters $\sum E$ and E_0 are defined by

$$\Sigma E = \int_0^t H d\delta \, , E_0 = \frac{1}{2} H_0 \delta_0 \tag{3.4}$$

On the basis of test results, the effects of bi-directional loading and length of filled-in concrete on the main seismic performance parameters, such as maximum lateral load, maximum response displacement and residual displacement will be discussed in detail in the following section.

(1) Displacement Time History Curve

Fig. 3-7 to Fig. 3-9 respectively present the displacement time history curves of the test specimens with different concrete-filled ratios measured during hybrid loading tests. In these figures, displacement response obtained in the single- and bi- directional loading tests are represented by broken lines and solid lines, respectively. It can be seen obviously from these figures that the maximum displacement and residual displacement due to bi-directional loading (solid lines) are generally larger than those due to single-directional loading (broken lines), particularly in medium and soft ground (GT2 and GT3), because the steel plates buckled severely resulting in large stiffness degradation and greater deformation.

In the cases of specimens S-H-00-2D-3 and S-H-20-2D-3, as illustrated in the plots (e) and (f) of Fig. 3-7 and Fig. 3-8, respectively, the center of displacement response oscillation gradually slid off the time axis owing to bi-directional loading. Before the end of time history, the loading test has to be stopped midway for the low residual bearing capacity and extremely large displacement accompanied by significant local buckling and cracks, as shown in Fig.3-10.

However, for the specimens in hard ground (GT1), the displacement responses show not much difference between single- and bi- directional loadings. It is probably attributed to the effect of characteristic differences between seismic waves.

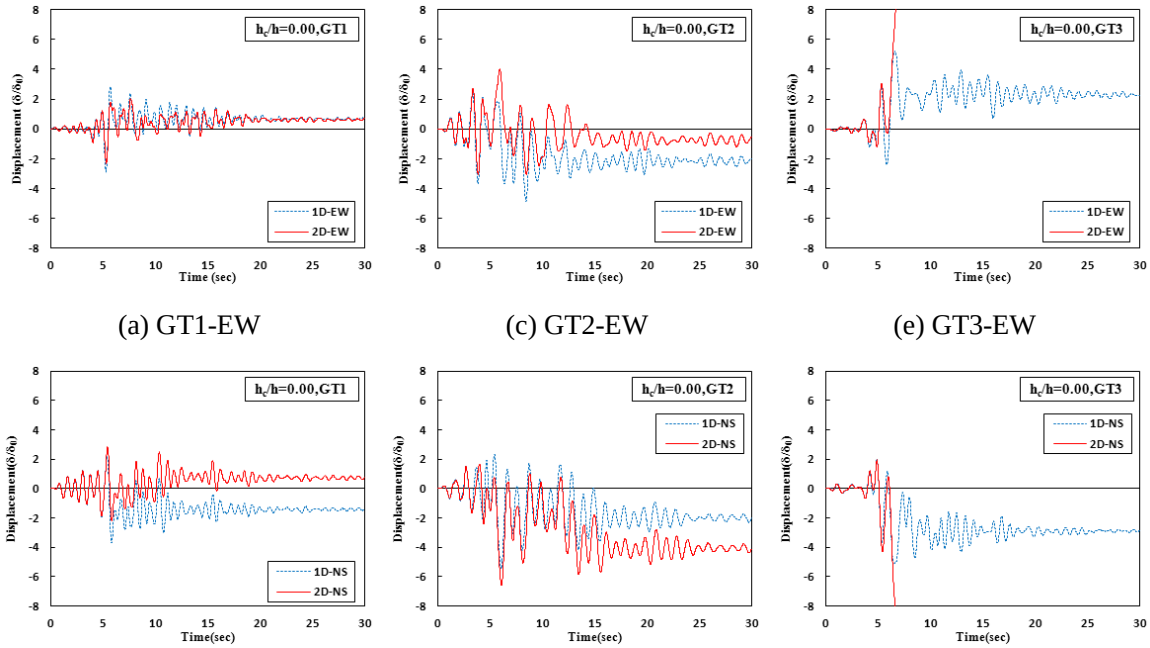

(a) GT1-EW (c) GT2-EW (e) GT3-EW

(b) GT1-NS (d) GT2-NS (f) GT3-NS

Fig. 3-7. Displacement time history curves of specimens without concrete infill (h_c/h = 0.00)

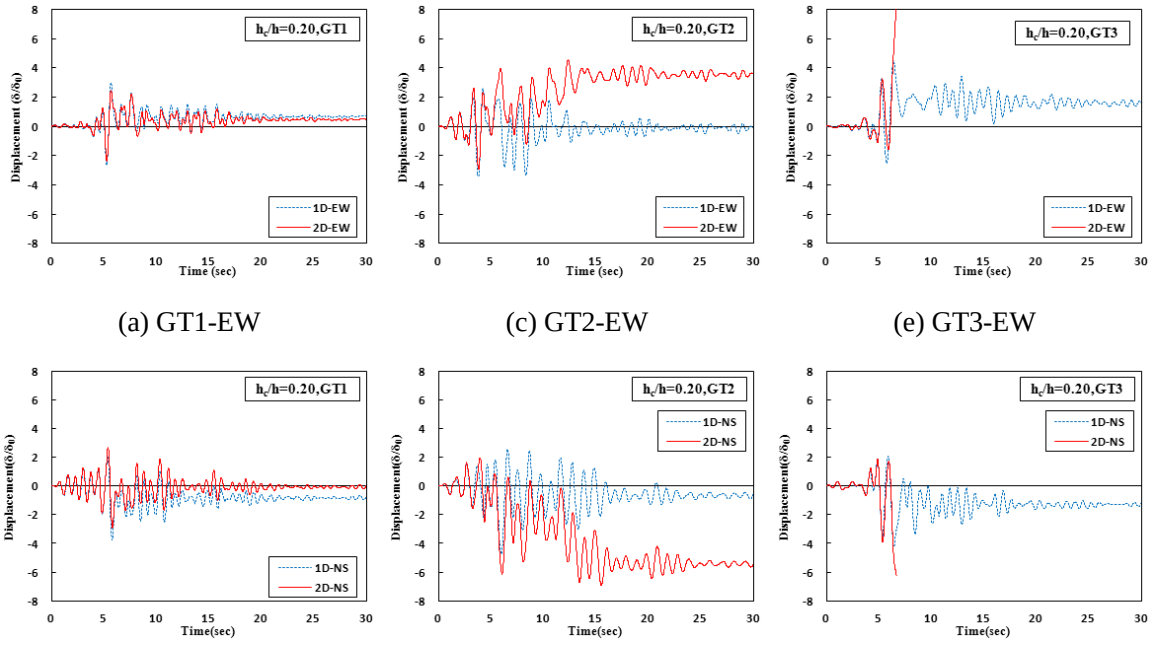

(a) GT1-EW (c) GT2-EW (e) GT3-EW

(b) GT1-NS (d) GT2-NS (f) GT3-NS

Fig. 3-8. Displacement time history curves of specimens of h_c/h = 0.20

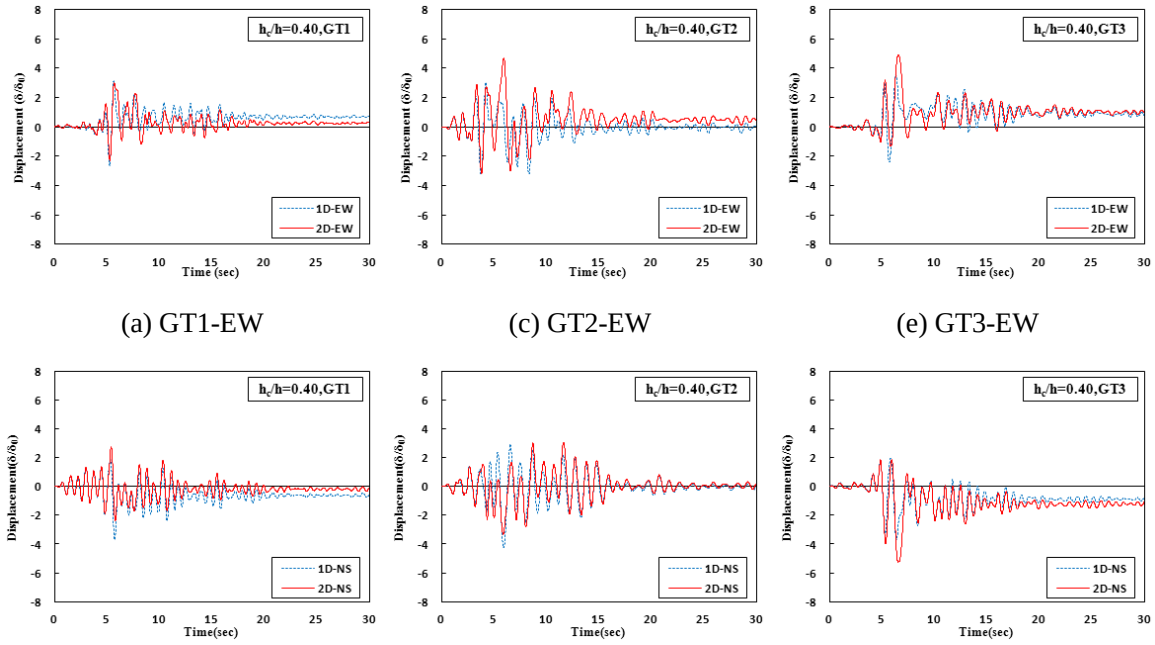

(a) GT1-EW (c) GT2-EW (e) GT3-EW

(b) GT1-NS (d) GT2-NS (f) GT3-NS

Fig. 3-9. Displacement time history curves of specimens of h_c/h = 0.40

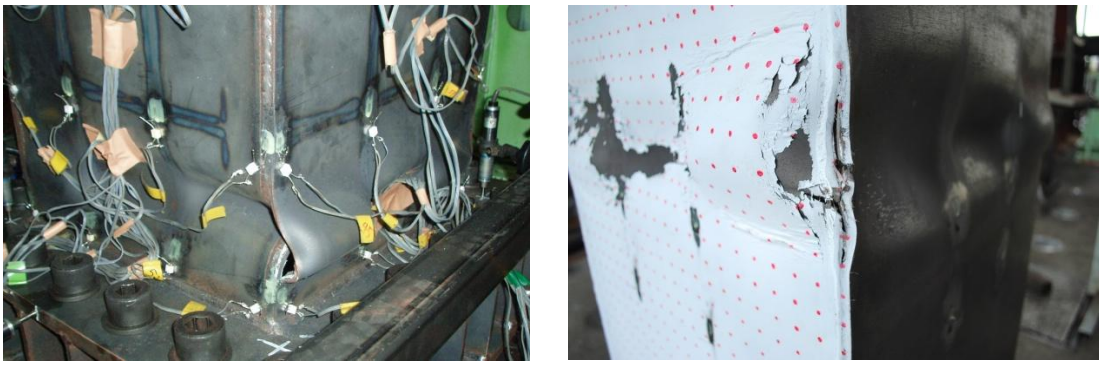

(a) S-H-00-2D-3 (b) S-H-20-2D-3

Fig. 3-10. Failure conditions due to bi-directional loading effect in soft ground (GT3)

Take specimen S-H-20-1D-2 as an example, the displacement response due to single ground motion in NS direction reached its maximum value 2.00δ_0 at 5.4sec in positive side, and soon peaked -3.76δ_0 at 5.8sec in negative side as can be seen in Fig.3-8 (b). Whereas, the maximum displacement of specimen S-H-20-2D-1 in NS direction under bi-directional loading showed

$2.69\delta_0$ at 5.4sec in positive side, which is $0.69\delta_0$ larger than specimen S-H-20-1D-2 because of stiffness degradation caused by local buckling. From that point, the displacement time history curve of specimen S-H-20-2D-1 under bi-directional loading moved toward positive side and then reached the peak point $-2.91\delta_0$ at 5.8sec in negative side, which is $0.85\delta_0$ less than that of specimen S-H-20-1D-2 of single-directional loading, and almost left no residual displacement, while $-0.77\delta_0$ large residual displacement was caused by single-directional loading. These changes in processes are reflected in the displacement response comparisons, and the values of maximum displacement and residual displacement obtained in bi-directional loading tests even show a little less than those of single-directional loading tests.

(2) Displacement Trajectories

The displacement trajectories of the center of the mass point at the pier tops in the horizontal plane measured in single- and bi-directional loading tests are represented by broken and solid lines, respectively, in Fig. 3-11, in which the horizontal and vertical axes indicate the response displacement in the EW and NS directions, respectively.

As seen from the Fig. 3-11, it can be found that the displacement trajectories were stretched toward Northwest owing to bi-directional loading, especially for the cases in the soft ground (GT3). The comparison among plots of GT1, GT2, and GT3 revealed that the shapes of the response displacement trajectories change significantly along with the change of input ground motions. It is also observed from the comparison that the displacement trajectories of specimens with 0.40*h* concrete infill under bi-directional loading show much closer to results of single-directional loading than cases of 0.00*h* and 0.20*h*.

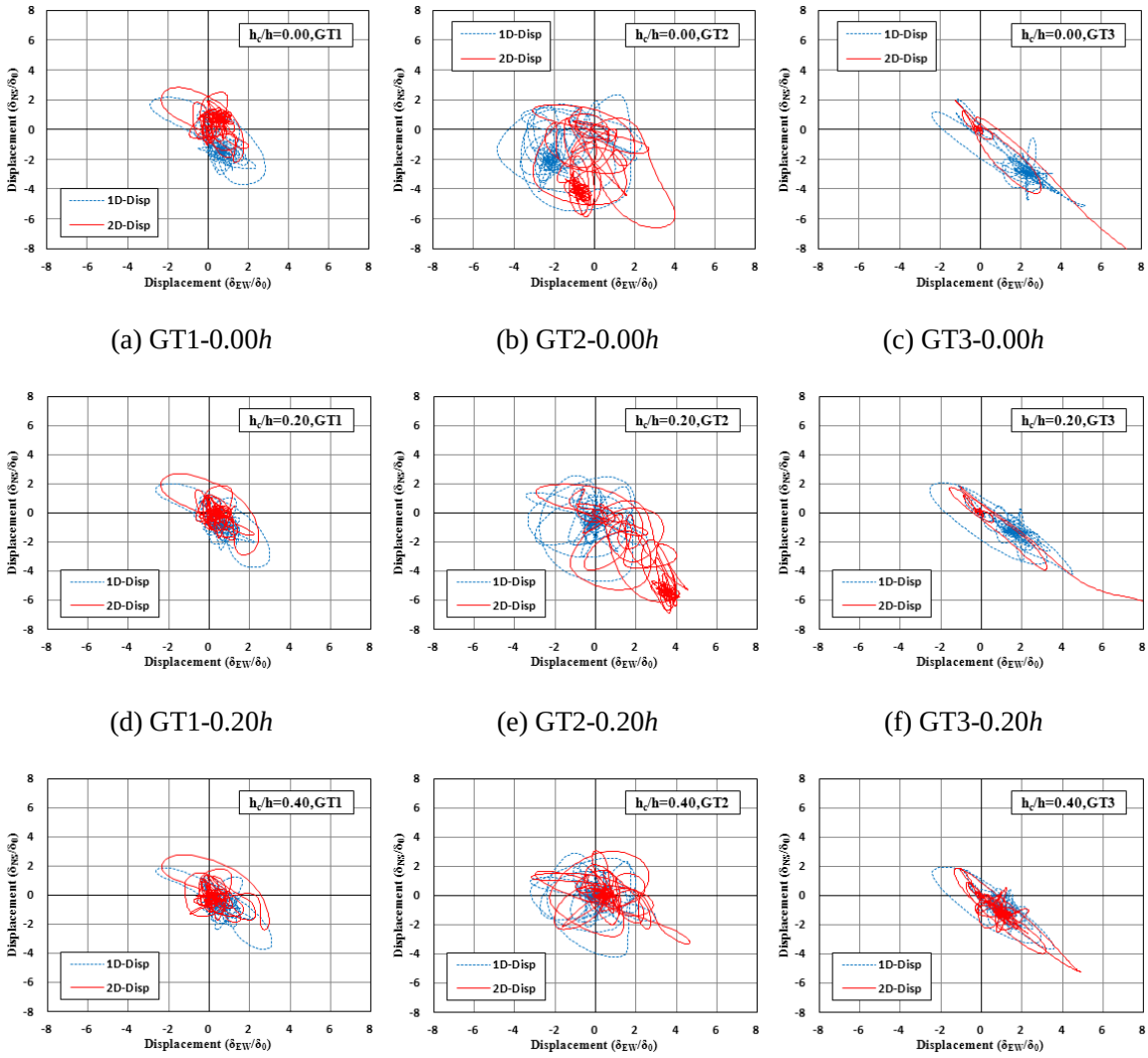

(a) GT1-0.00*h* (b) GT2-0.00*h* (c) GT3-0.00*h*

(d) GT1-0.20*h* (e) GT2-0.20*h* (f) GT3-0.20*h*

(g) GT1-0.40*h* (h) GT2-0.40*h* (i) GT3-0.40*h*

Fig.3-11. Response displacement trajectories in the horizontal plane

(3) Maximum Displacement and Residual Displacement

Plots (a) and (b) of Fig. 3-12 show the comparison of maximum displacement and residual displacement between single- and bi-directional loading test results, respectively.

It is clear from Fig. 3-12 (a) that the maximum response displacement, especially those caused by bi-directional loading depicted as the solid column in the figures, increases as a function of

the ground types from hard to soft in all three concrete-filled ratios. The average values of maximum displacements due to single-directional loading for specimens without concrete infill are 3.28, 5.14, and 5.19 for hard ground (GT1), medium ground (GT2), and soft ground (GT3), respectively. The corresponding values due to bi-directional loading are 3.33, 7.40, and 15.76, respectively. The ratios of the maximum displacements caused by bi-directional loading to those due to single-directional loading vary with the different ground types as 1.02, 1.44, and 3.04, respectively. Then, for the specimens of h_c = 0.20h, the corresponding ratios vary with the different ground types as 1.02, 1.92, and 2.29, respectively. In the case of h_c = 0.40h, the ratios change to 1.08, 1.53, and 1.98, respectively. Therefore, it is thought that the maximum response displacement of steel piers without or with concrete-filled caused by actual bi-directional strong earthquake loading cannot be adequately predicted from single-directional loading tests or analysis.

Fig. 3-12 (b) compares the residual displacement due to single- and bi- directional loadings, in which the two left-hand columns list the results of single-directional and the rightmost column lists the results of bi-directional loading tests. The residual displacement limit provided in the specification for highway bridges of Japan is 1% of the pier height, which is corresponding to 1.60δ_0 for the tested piers and is shown by the dash line in the plots. Compared with Fig. 3-12 (a), the difference between single- and bi- directional loadings is expanded in Fig. 3-12 (b), especially for the specimens with 0.2h height of concrete filled. In the case of h_c = 0.20h, the residual displacement ratios of bi-directional loadings to single-directional loadings are 0.64, 16.73, and 6.62 for GT1, GT2, and GT 3, respectively. For the specimens of h_c = 0.40h, the corresponding ratios change to 0.48, 7.83, and 1.79, respectively. These results also indicate that it is inadequate to evaluate residual displacement under actual bi-directional loading based only on conventional single-directional loading tests or analysis.

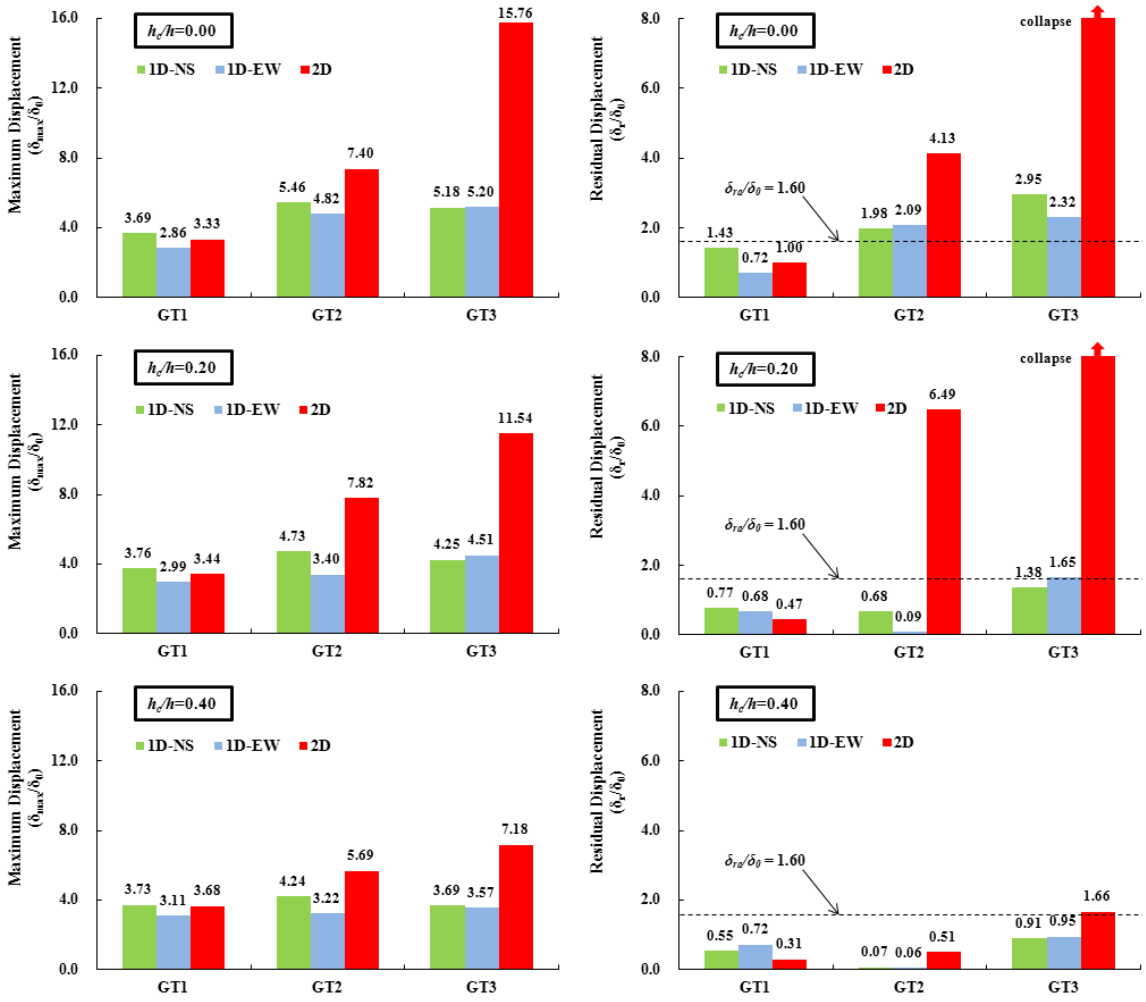

(a) Maximum displacement (b) Residual displacement

Fig. 3-12. Comparison of single- and bi- directional loading

In Fig.3-12, a similar tendency of the residual displacement and the maximum displacement is observed. In the design specifications, Eq.(3.5) is proposed with the coefficients C_R = 0.45 and r = 0.1 to estimate the residual displacement of partially concrete-filled steel piers under strong earthquake loading, which is shown as a straight line in Fig. 3-13.

$$\frac{\delta_r}{\delta_0} = C_R\left(\frac{\delta_{max}}{\delta_0} - 1\right)(1 - r) \tag{3.5}$$

To determine the relationship between residual displacement and maximum displacement, test

data except for the results of the specimens S-H-20-2D-2 and S-H-20-2D-3, which show much larger residual displacement values than the limit value, were selected and plotted in Fig. 3-13. The plotted points for specimens with 0.20*h* and 0.40*h* concrete infill heights are indicated by circular shape (○) and square shape (□), respectively. The results due to single- and bi-directional loadings are represented by hollow and solid marks, respectively.

It can be observed that the design specifications provide an accurate estimation of residual displacement for sufficiently concrete-filled piers (h_c/h = 0.40) except for the case due to bi-directional loading in the soft ground (GT3). But in the case of low concrete-filled ratio, this estimation equation does not well meet the results obtained in medium ground and soft ground due to either single- or bi-directional loadings.

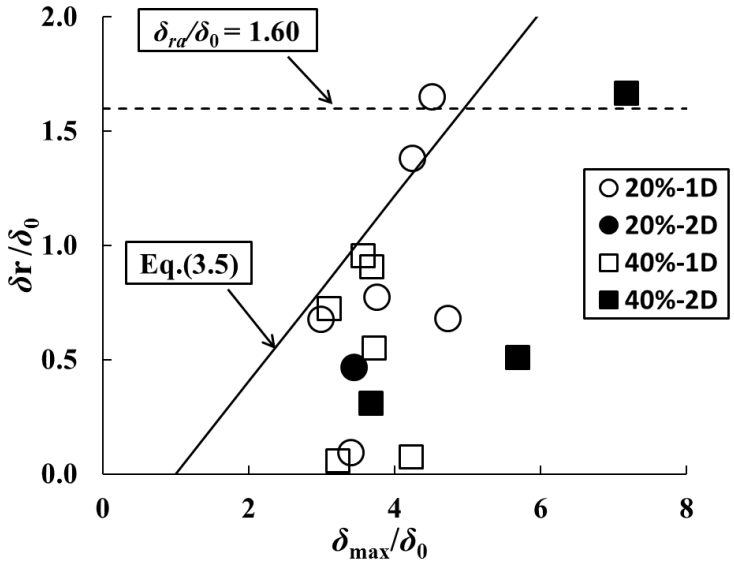

Fig.3-13. Relationship between the maximum displacement and residual displacements

(4) Hysteretic Curves

The hysteretic curves measured during the single- and bi- directional loading tests are represented by broken lines and solid lines in Figs.3-14 to 3-16, respectively, in which plots

placed in column 1, 2, and 3 correspond to the test results of piers in hard ground (GT1), medium ground (GT2), and soft ground (GT3), respectively.

As seen from Figs.3-14 to 3-16, compared to the results of single-directional loading tests, the specimens for the bi-directional loading hybrid tests presented a considerable degree of degradation in resistance force accompanied by an increase in displacement. For the cases of hard ground (GT1) and medium ground (GT2), the average attenuation ratios were about 14% and 10% large respectively, while a greater average attenuation value of 22% was calculated for soft ground (GT3). The degradation of lateral restoring force resulted from the local buckling deformation accelerated by the bi-directional loading. Once local buckling occurred, the plates were not fully straightened out during reversed loading, buckling deformations progressively grew, and the lateral resistance of the specimen gradually reduced.

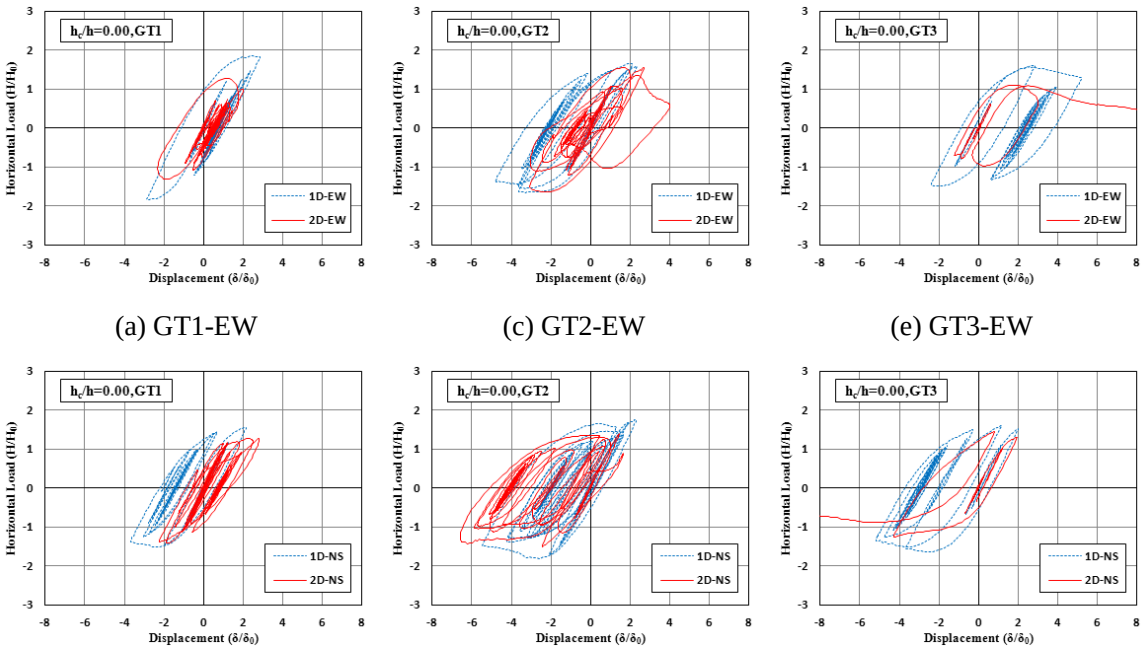

(a) GT1-EW (c) GT2-EW (e) GT3-EW

(b) GT1-NS (d) GT2-NS (f) GT3-NS

Fig. 3-14. Hysteretic curves of specimens without concrete infill (h_c/h = 0.00)

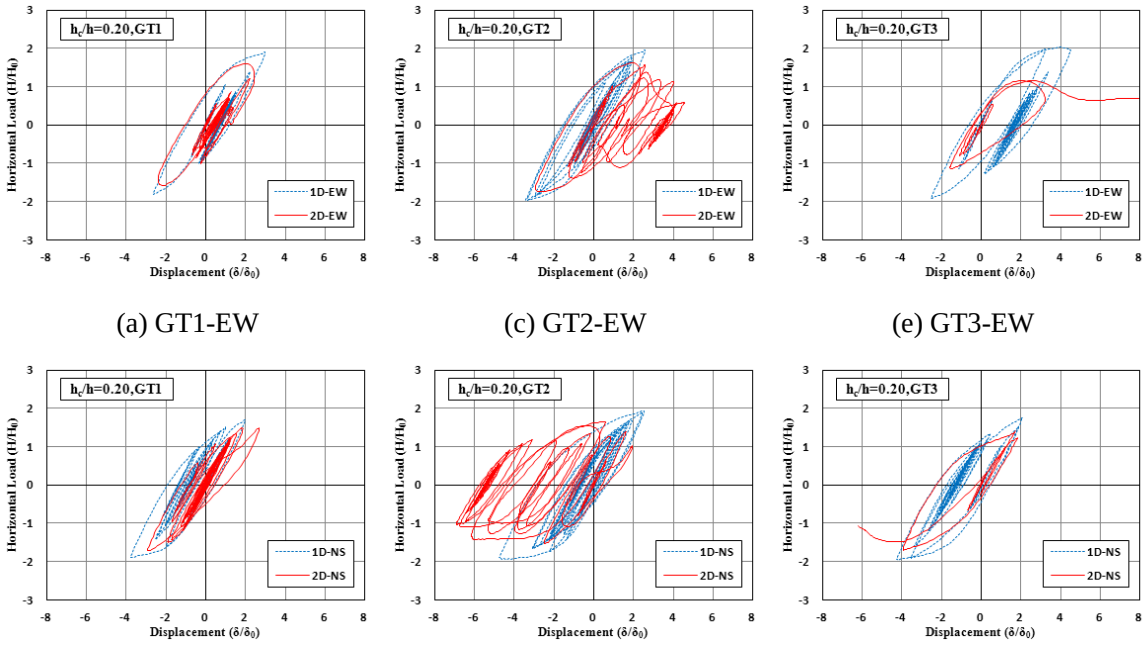

(a) GT1-EW (c) GT2-EW (e) GT3-EW

(b) GT1-NS (d) GT2-NS (f) GT3-NS

Fig. 3-15. Hysteretic curves of specimens of h_c/h = 0.20

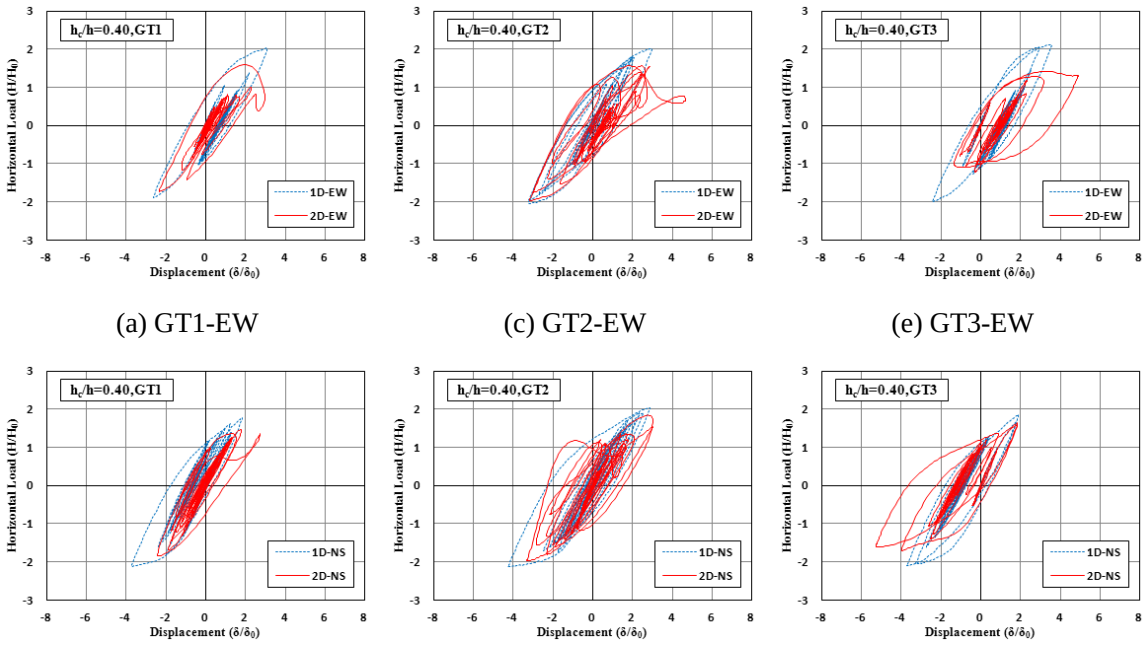

(a) GT1-EW (c) GT2-EW (e) GT3-EW

(b) GT1-NS (d) GT2-NS (f) GT3-NS

Fig. 3-16. Hysteretic curves of specimens of h_c/h = 0.40

(5) Lateral Resistance Trajectories

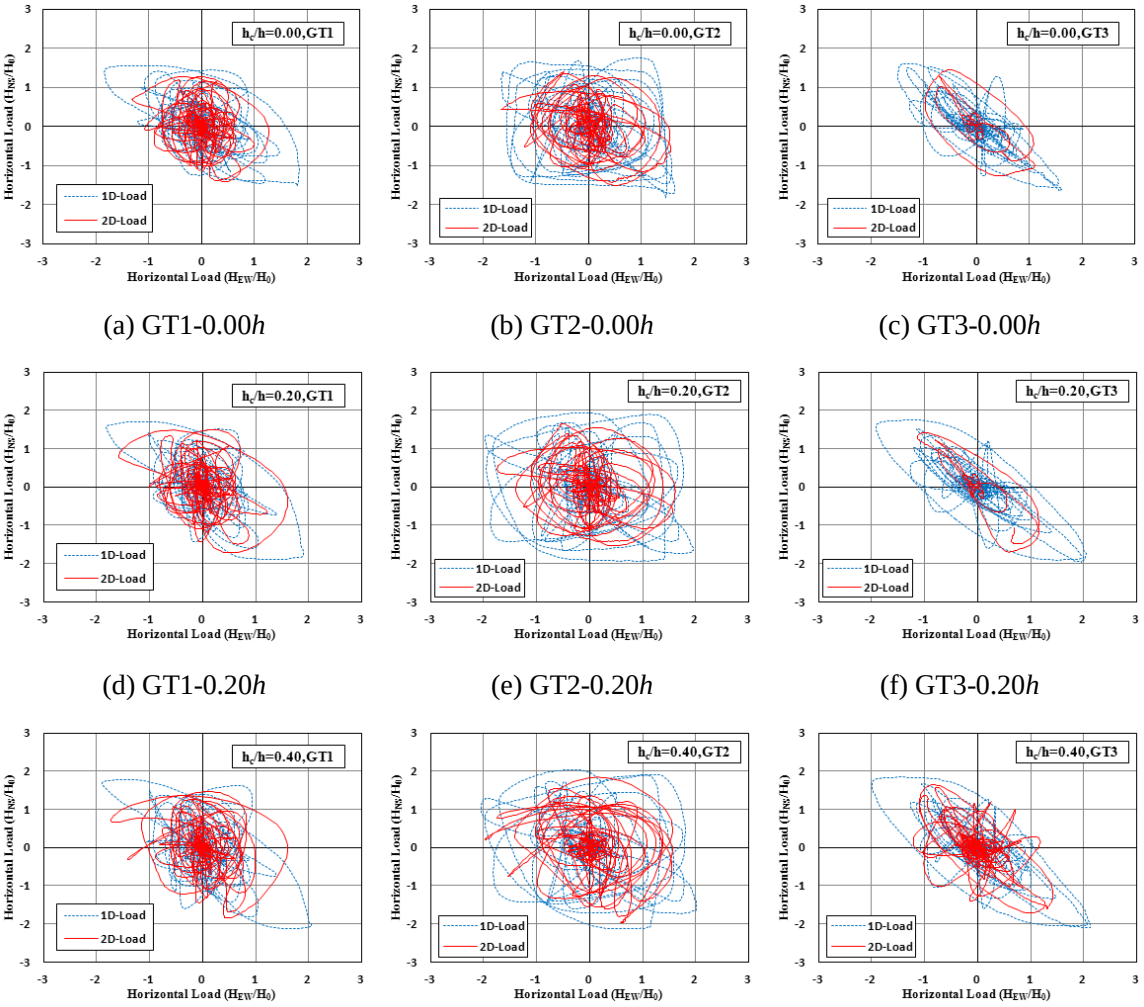

(a) GT1-0.00*h* (b) GT2-0.00*h* (c) GT3-0.00*h*

(d) GT1-0.20*h* (e) GT2-0.20*h* (f) GT3-0.20*h*

(g) GT1-0.40*h* (h) GT2-0.40*h* (i) GT3-0.40*h*

Fig.3-17. Lateral resistance trajectories in the horizontal plane

Bi-directional lateral resistance force trajectories in the horizontal plane are shown in Fig.3-17, in which the vertical and horizontal axes represent the horizontal force of the piers in the NS and EW directions, respectively. The solid lines in all the plots of Fig.3-17, representing the results due to bi-directional loading tests, exhibit circular-like patterns which are generally enveloped by the fusiform-like single-directional loading results presented by the broken lines. Accordingly, the synthesis of two lateral forces analyzed independently in the two orthogonal

directions can result in larger force standard, which will lead to an over-estimation of the hysteretic horizontal force of the actual bi-directionally loaded steel piers with partially concrete infill.

(6) Maximum Horizontal Load

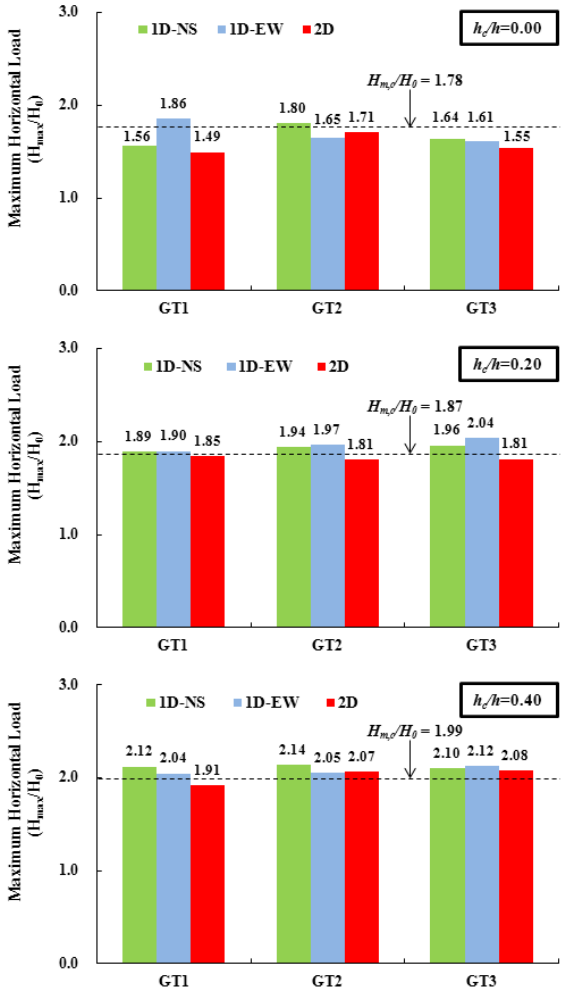

Fig. 3-18. Maximum horizontal load comparison between single- and bi- directional loading

Fig. 3-18 compares the maximum horizontal load, $H_{max,2D}$ subjected to bi-directional loading and $H_{max,NS}$ and $H_{max,EW}$ under single-directional loading. The maximum loads of stiffened

rectangular piers due to static cyclic loading $H_{m,c}$ are presented by the dash line in the plots of Fig. 3-18.

As shown in Fig. 3-18, $H_{m,c}$ due to static cyclic loading are generally about 5% smaller than those of single-directional hybrid loadings, because the static cyclic loading tests make specimens loaded by incremental displacement that lead to larger fatigue damage accumulation than single-directional hybrid tests. It also can be observed from Fig. 3-18 that, in the case of bi-directional strong earthquake loading, $H_{max,2D}$ of test specimens with three different concrete-filled ratios (i.e., h_c/h = 0.00, 0.20 and 0.40) presented a small degree of degradation about 6.2%, 6.5% and 3.7%, respectively, in comparison with results obtained by single-directional loading tests on an average for the three ground types. The test specimens of inadequate concrete-filled ratio (h_c/h = 0.20) showed almost the same deterioration in strength as steel piers without filled concrete, because of local buckling deformation that was more prone to occur in the panels of the hollow steel section just above the lower positioning concrete.

(7) Cumulative Energy Absorption

Fig. 3-19 presents a comparison of the cumulative energy absorption values between the single- and bi-directional hybrid loading tests. It can be observed that the largest difference is obtained among the ground types and the cumulative energy absorption due to bi-directional loading tests is generally larger than those due to single-directional loading tests.

The cumulative energy absorption time history curves of sufficiently concrete-filled test specimens due to bi-directional hybrid loadings tests are illustrated in Fig.3-20, in which plots (a) to (c) represented the results obtained in hard ground (GT1), medium ground (GT2), and soft ground (GT3), respectively.

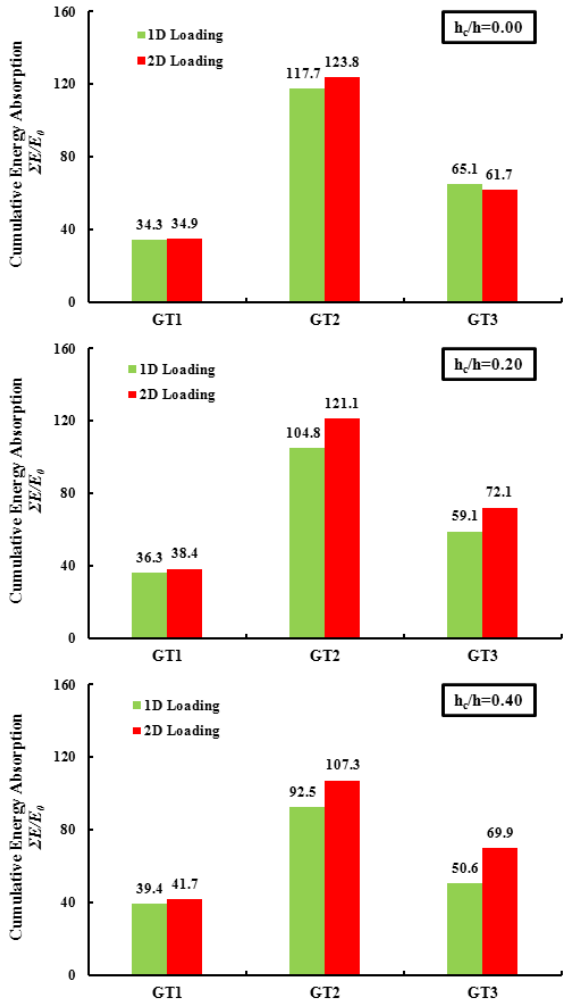

Fig. 3-19. Cumulative energy absorption comparison between single- and bi- directional loading

It can be seen from the plot (a) of Fig.3-20 that during the 5.0 to 5.8 second after loading the energy absorption in NS direction rapidly reached 70% of all the energy and finished left 30% slowly in the next 5 seconds, while in the EW direction the test specimen absorbed almost all of the energy from 5.0 to 5.7 second. Compared to the cases of hard ground (GT1), the specimen of medium ground (GT2) absorbed much more energy, as shown in plot (b). In the case of EW directional component, the specimen absorbed 50% of all the energy from 3.0 to 4.2 second and reached its peak at 10.2 second, while in the NS direction the specimen finished its 50% energy 2.5 seconds later than that of EW direction. Then slowly absorbed energy and the peak appeared

until 15.5 second. For the cases of soft ground (GT3), as shown in plot (c), the energy absorption value of EW directional component is nearly as much as that of NS directional component during from 5.0 to 6.3 second. Therefore, it can be pointed that the specimens of medium and soft grounds (GT2 and GT3) will suffer much more damage caused by strong earthquake loading than those of hard ground (GT1).

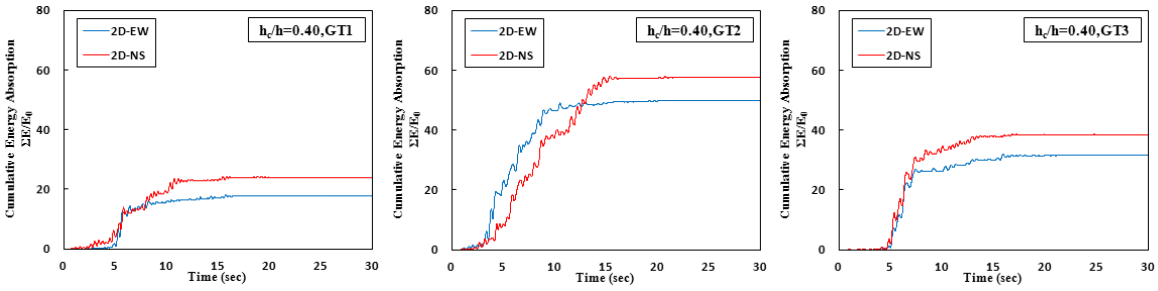

(a) Hard Ground (GT1) (b) Medium Ground (GT2) (c) Soft Ground (GT3)

Fig.3-20. Energy absorption time history curves due to bi-directional loading (h_c = 0.40h)

3.3.3 Effect of Filled-in Concrete

(1) Maximum Displacement

The change of maximum displacement as a function of the concrete-filled ratio is shown in Fig. 3-21. It can be found that great change does not emerge in hard ground (GT1) regardless of the encase concrete. In contrast, for the medium (GT2) and soft ground (GT3), the maximum displacement response due to bi-directional loading gradually decreased with increasing height of the filled-in concrete. Compared to the piers without concrete infill, the maximum displacements due to bi-directional loadings were reduced by about 14% and 38% on an average for the three ground types, when the concrete is filled up to 0.2h and 0.4h height, respectively.

The difference between results due to single- and bi- directional loading was also reduced by about 15% and 55%, respectively.

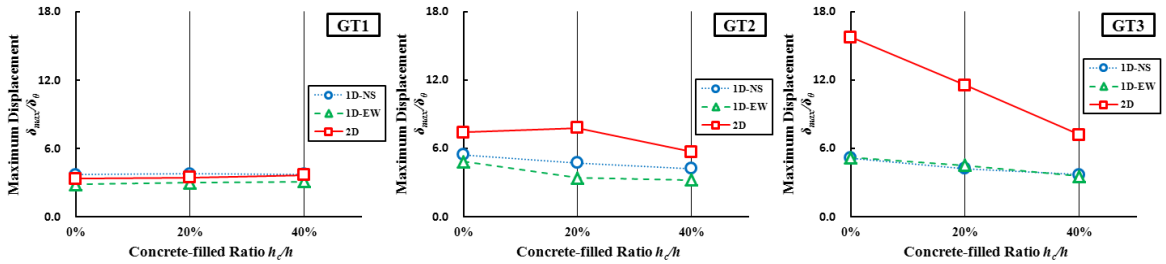

(a) Hard Ground - GT1 (b) Medium Ground - GT2 (c) Soft Ground - GT3

Fig.3-21. Maximum displacement as a function of different concrete-filled ratios

(2) Residual Displacement

The reduction of residual displacement along with the growth of concrete-filled height is also observed in Fig. 3-22 as well as the maximum displacement in Fig. 3-21.

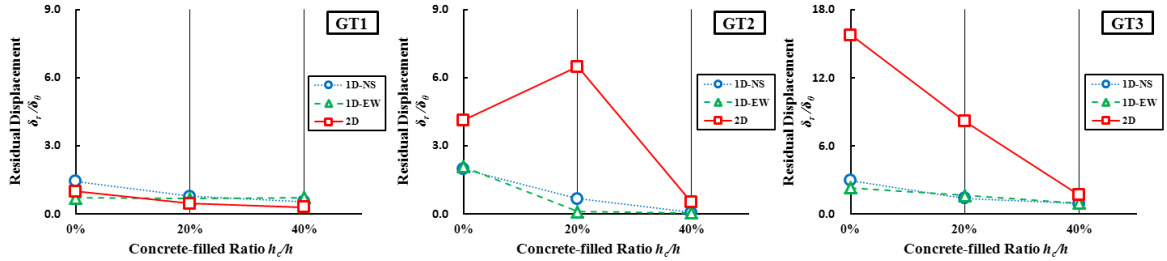

(a) Hard Ground - GT1 (b) Medium Ground - GT2 (c) Soft Ground - GT3

Fig.3-22. Residual displacement as a function of different concrete-filled ratios

By comparison to the result of pier without concrete infill, the residual displacement due to single-directional loading was significantly reduced by about 53% and 72% through filling 0.20*h* and 0.40*h* length concrete in the piers, respectively. In the case of bi-direction loading, it is also observed that the reduction of residual displacement attributing to the effect of filled-in

concrete is remarkable, especially in soft ground (GT3). The residual displacement has shown about 42% and 88% less by a height of 0.20*h* and 0.40*h* concrete filled than the case without concrete infill, respectively. If a bridge pier, especially in medium ground (GT2) and soft ground (GT3), is filled up to 0.40*h* with concrete, the difference in the residual displacement between the single- and bi-directional loadings diminishes. It is owing to the sufficient height of encase concrete which can prevent local buckling deflection of the outer steel plates of cross section toward inside and increase the strength and ductility of the outer steel plates during the strong earthquake loading. However, for the pier of a low concrete-filled ratio, it is unsafe to estimate the residual displacement based only on the single-directional loading test results.

(3) Maximum Horizontal Load

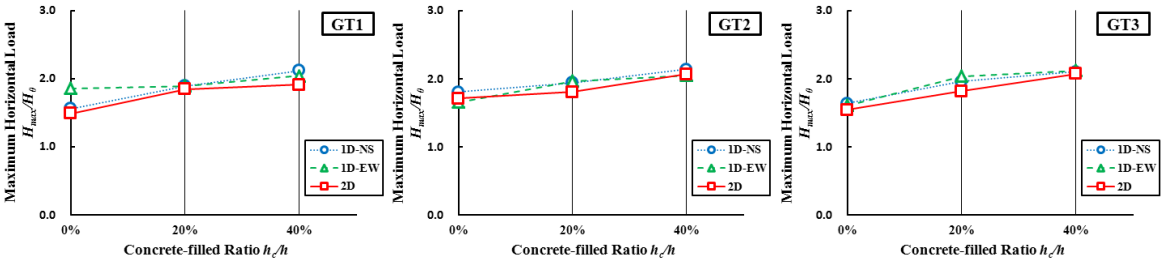

(a) Hard Ground - GT1 (b) Medium Ground - GT2 (c) Soft Ground - GT3

Fig.3-23. Maximum horizontal load as a function of different concrete-filled ratios

Fig.3-23 presents comparisons of the maximum horizontal load with the different filled-in concrete heights for the three different ground types. It can be observed that the maximum load of the pier with a concrete-filled height of 0.2*h* and 0.4*h* was increased by about 15% and 25% on an average for the three ground types, respectively, in comparison with the piers without concrete. The effect of filled-in concrete is clear from these results.

However, the maximum load of the piers would not significantly improve even if the height of filled-in concrete increases, because the pier with sufficient concrete filling height always fractures at the bottom end of piers, as shown in Fig. 2-3 (c) of Chapter 2, and then loses its lateral resistance.

(4) Cumulative Energy Absorption

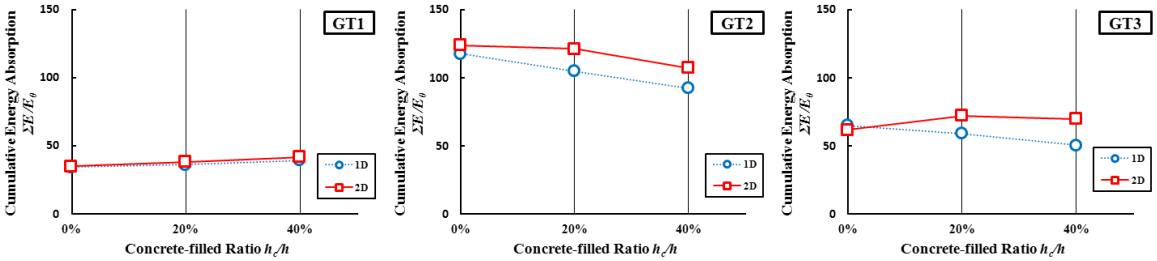

(a) Hard Ground - GT1 (b) Medium Ground - GT2 (c) Soft Ground - GT3

Fig.3-24. Cumulative energy absorption as a function of different concrete-filled ratios

It can be observed from Fig. 3-24 that the cumulative absorbed energy does not greatly change in the hard ground (GT1) when the concrete-filled ratio increased. However, in the case of medium ground and soft ground (GT2 and GT3), the reduction of cumulative hysteresis dissipation energy along with the growth of concrete-filled height were generally observed in plots (b) and (c), since the displacement response was considerably decreased while the lateral load changed little as the concrete-filled ratio increased. For the specimen S-H-00-2D-1 (h_c/h = 0.00) under bi-directional loading, in the case of soft ground (GT3), the loading test was stopped midway because the pier had suffered great damage before the end of time history, and resulted in a low value of cumulative energy absorption.

3.4 Experimental Study on Circular Piers

3.4.1 Collapse Modes

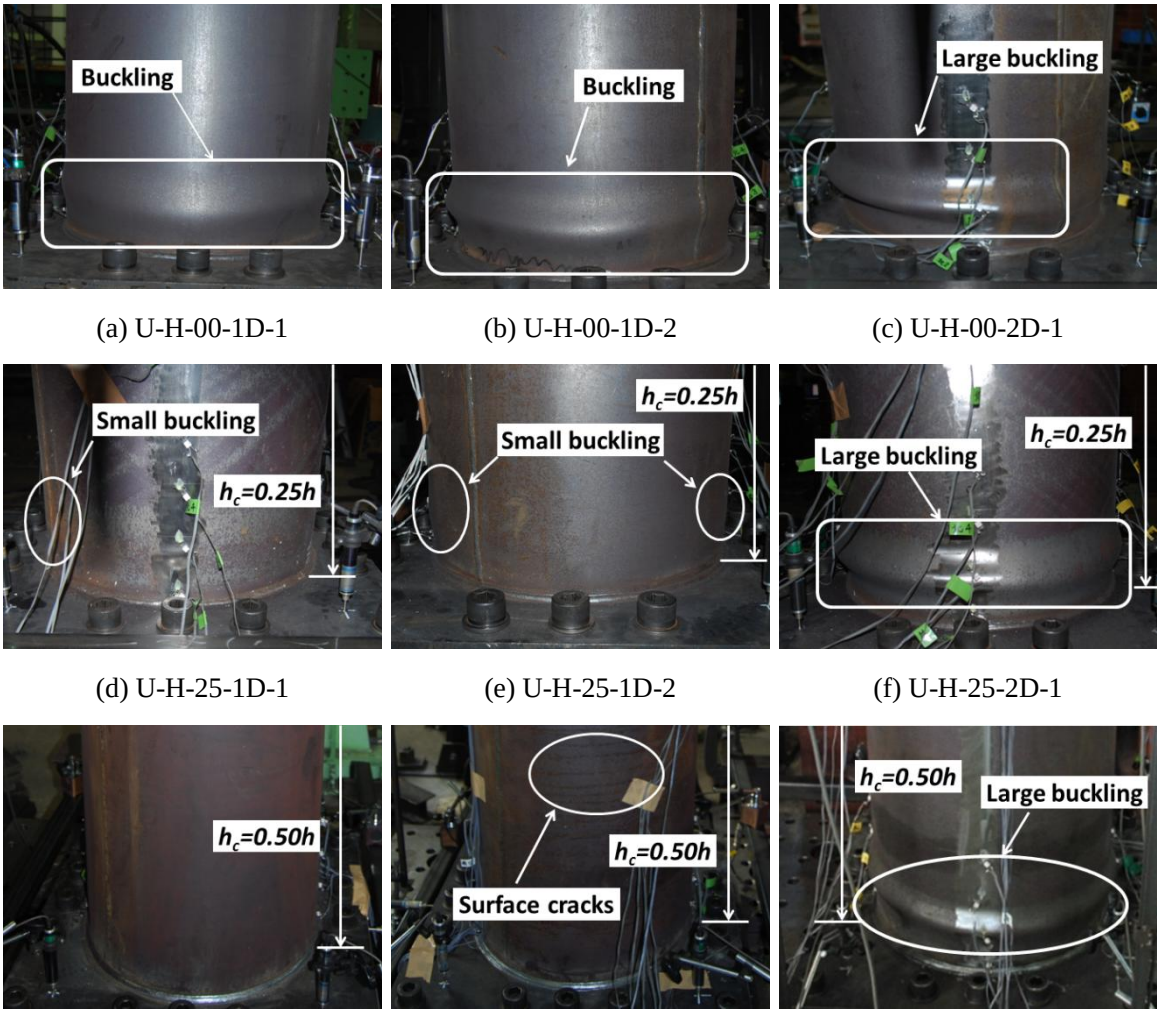

(a) U-H-00-1D-1 (b) U-H-00-1D-2 (c) U-H-00-2D-1

(d) U-H-25-1D-1 (e) U-H-25-1D-2 (f) U-H-25-2D-1

(g) U-H-50-1D-1 (h) U-H-50-1D-2 (i) U-H-50-2D-1

Fig.3-25. Circular specimens after loading tests of medium ground (GT2)

As above mentioned in section 3.3.2, the specimens of medium ground (GT2) absorbed the most energy among the three kinds of grounds. The obvious differences of seismic performance between single-directional loading and bi-directional loading in medium ground (GT2) were also observed for stiffened rectangular piers. Therefore, the damage modes of circular piers in

medium ground (GT2) will be studied in this section.

Fig. 3-25 shows the different failure modes of piers after hybrid tests, in which photos placed in row 1, 2, and 3 correspond to the test results of piers without concrete infill (h_c = 0.00h), with low concrete-filled ratio (h_c = 0.25h), and sufficiently filled with concrete (h_c = 0.50h), respectively. The left two columns of photos are the results due to single-directional loading, while the rightmost plots represent the results due to bi-directional loading.

As seen in the Fig. 3-25, the local buckling of plates was observed at the column base regardless of the length of concrete infill, because a diaphragm was not designed over the filled-in concrete in specimens.

Similar to the stiffened rectangular specimens, it can be clearly seen from the Fig.3-25 that the effects of bi-directional loading and filled-in concrete on the collapse modes of circular specimens are significant. The test specimens due to bi-directional loading damaged more severely than those due to single-directional loading, no matter what kind of concrete- filled ratio. The conditions of damage were considerably improved as the length of filled-in concrete increased, whether under single-directional loading or bi-directional loading.

3.4.2 Effect of Bi-directional Loading and Filled-in Concrete

The hybrid test results obtained under single- and bi- directional loading, including maximum horizontal load H_{max}/ H_0, the maximum displacement δ_{max}/ δ_0, the residual displacement δ_r /δ_0, and the cumulative absorbed energy $\sum E /E_0$, are listed in Table 3-5. On the basis of test results obtained in the medium ground (GT2), the effects of bi-directional loading and length of filled-in concrete on the main seismic performance parameters, such as maximum lateral load,

maximum displacement and residual displacement will be discussed in detail in the following.

Table 3-5. Results of hybrid tests for unstiffened circular piers

No.	*Specimen*	*Loading Mode*	δ_{max}/δ_0	δ_r/δ_0	H_{max}/H_0	$\Sigma E/E_0$	h_c/h
1	U-H-00-1D-1	GT2-1D-EW	8.10	4.18	2.05	101.07	
2	U-H-00-1D-2	GT2-1D-NS	6.66	3.14	2.14	147.29	0.00
3	U-H-00-2D-1	GT2-2D	15.45	15.45	2.06	82.94	
4	U-H-25-1D-1	GT2-1D-EW	4.93	1.25	2.32	83.69	
5	U-H-25-1D-2	GT2-1D-NS	6.84	0.21	2.39	107.26	0.25
6	U-H-25-2D-1	GT2-2D	11.37	8.63	2.28	260.16	
7	U-H-50-1D-1	GT2-1D-EW	4.59	0.40	2.98	74.14	
8	U-H-50-1D-2	GT2-1D-NS	4.56	0.09	3.04	61.22	0.50
9	U-H-50-2D-1	GT2-2D	8.59	3.39	2.94	209.45	

(1) Displacement Time History Curve

Fig. 3-26 present the displacement time history curves of the test specimens with three different concrete-filled ratios, which were measured during the hybrid loading tests. The displacement response obtained in the single- and bi- directional loading tests are represented by broken lines and solid lines, respectively. For the specimen U-H-00-2D-1of the case of h_c/h = 0.00, the bi-directional loading test had to be stopped midway before the end of time history, as shown in plots of the top row in Fig. 3-26, because significant local buckling occurred in the steel plates at the base, which caused low residual bearing capacity and extremely large displacement of the specimen.

It can be seen clearly from Fig. 3-26 that the displacement components in EW and NS directions due to bi-directional loading are much larger than those due to single-directional loading, particularly in the case of low concrete-filled ratios, because the steel plates at the base buckled severely resulting in large stiffness degradation and greater deformation. It also can be found

that as the length of filled-in concrete increased the displacement response was effectively improved, especially in the case of bi-directional loading.

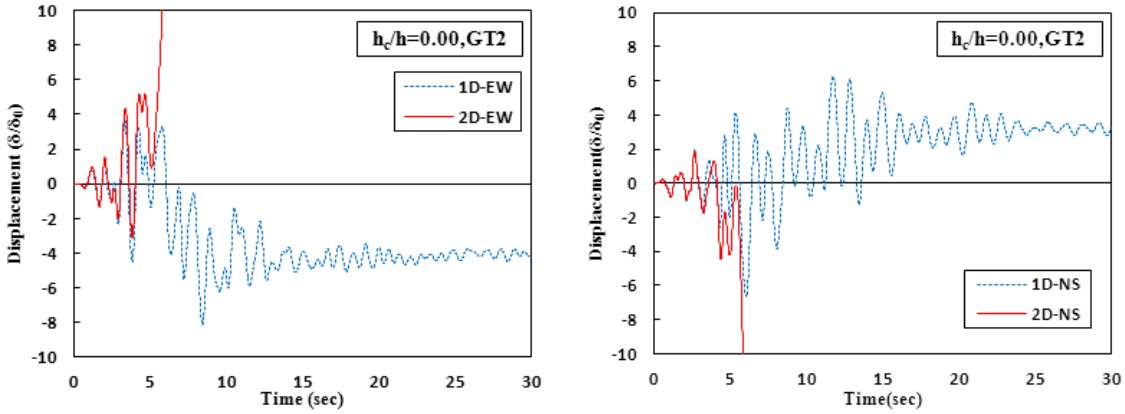

(a) h_c = 0.00h

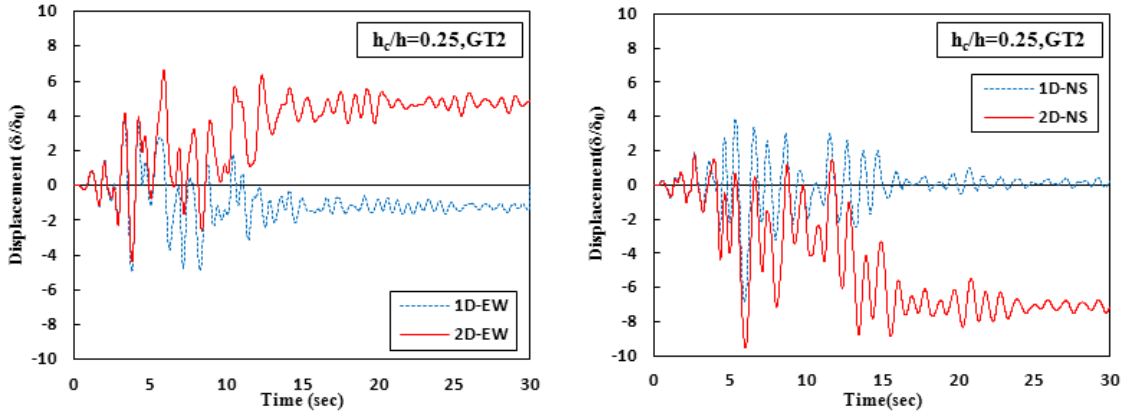

(b) h_c = 0.25h

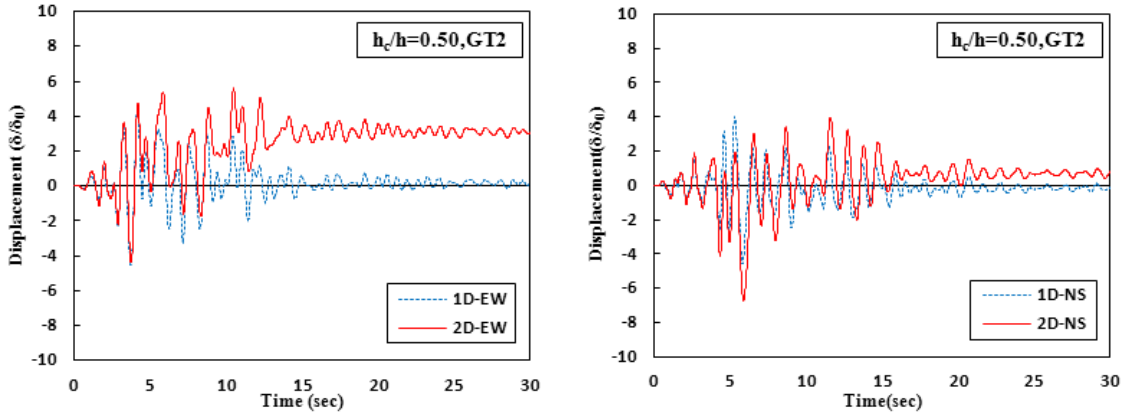

(c) h_c = 0.50h

Fig. 3-26. Displacement time history curves of unstiffened circular specimens (GT2)

(2) Displacement Trajectories

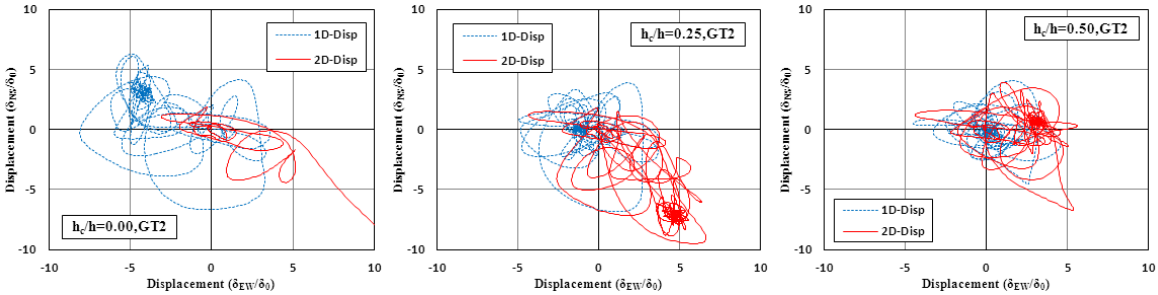

(a) h_c = 0.00h (b) h_c = 0.25h (c) h_c = 0.50h

Fig.3-27. Response displacement trajectories in the horizontal plane

The displacement trajectories of the mass point at the pier top due to single- and bi-directional loadings, including three different kinds of specimens, are represented in Fig. 3-27 by broken lines and solid lines, respectively.

As seen from the Fig. 3-27, it can be found that the displacement trajectories were stretched toward Southeast owing to bi-directional loading. It is also observed from the comparison that the displacement trajectories of specimens with an adequate length of filled-in concrete (h_c = 0.50h) under bi-directional loading show much closer to results of single-directional loading than results of 0.00h and 0.25h.

(3) Maximum Displacement and Residual Displacement

Fig. 3-28 shows the comparison of maximum displacement of circular piers with three different concrete-filled ratios between single- and bi-directional loading test results.

It is clear from Fig. 3-28 that the maximum response displacement caused by bi-directional

loading depicted as the solid column was much larger than results of single-directional loading. The non-dimensional average values of maximum displacements due to single-directional loading for specimens of h_c = 0.00*h*, 0.25*h* and 0.50*h* are 7.38, 5.89 and 4.58, respectively. The ratios of the maximum displacements caused by bi-directional loading to results due to single-directional loading vary with the different concrete-filled ratios as 2.09, 1.93, and 1.88, respectively.

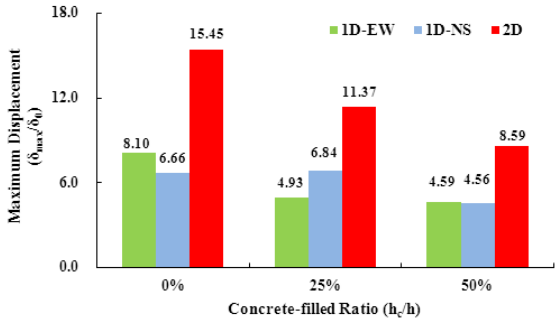

Fig. 3-28. Maximum displacement comparison

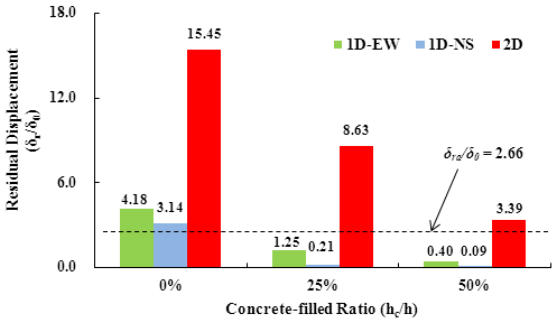

Fig. 3-29. Residual displacement comparison

It also can be found in Fig. 3-28 that the maximum displacement response, particularly due to bi-directional loading, significantly decreased with increasing the length of the filled-in concrete. Compared to the piers without concrete fill, when the concrete was filled up to 0.25*h* and 0.50*h* height, the maximum displacements due to bi-directional loadings were reduced by about 26% and 44%, respectively. It is because the sufficient height of encase concrete can prevent local buckling deflection of the outer steel plates of cross section toward inside and increase the strength and ductility of the outer steel plates during the strong earthquake loading.

Fig. 3-29 compares the residual displacement due to single- and bi- directional loadings, in which the two left-hand columns list the results of single-directional and the rightmost column lists the results of bi-directional loading tests. The residual displacement limit provided in the specification for highway bridges of Japan is 1% of the pier height, which is corresponding to

$2.66\delta_0$ for the test piers, and is shown by the dash line in the figure.

It is clear that the difference between single- and bi- directional loadings was significant as seen from Fig. 3-29, in which all residual displacements due to bi-directional loading exceeded the limit value while the majority of results due to single-directional loading located under the limit. This means that the design based on single-directional loading test results leads to unsafe side.

The reduction of residual displacement along with the growth of concrete-filled height is also observed in Fig. 3-29 as well as the maximum displacement in Fig. 3-28. In comparison with the results of piers without concrete infill, the residual displacement due to single-directional loading was significantly reduced by about 80% and 93% through filling concrete up to 0.25*h* and 0.50*h* height in the piers, respectively. In the case of bi-directional loading, the residual displacements of specimens of h_c = 0.25*h* and 0.50*h* have shown about 44% and 78% less than the result of specimen without concrete infill, respectively.

In addition, a certain correlation between the maximum and residual displacements is also observed from Figs. 3-28 and 3-29. Like rectangular piers, test data of concrete-filled circular piers collected under both single- and bi-directional loading were selected and plotted in Fig. 3-30. Single- and bi-directional loading test results are represented by white and black solid marks, respectively. In Fig. 3-30, result for specimen H-25-2D of bi-directional loading was excluded because it showed greater residual values than the limits stated in the specifications. Eq. (3.5) for estimating residual displacement is represented by the straight line in the figure.

From Fig. 3-30, we observe that the seismic design code provides a near-upper bound level estimation of residual displacement when a partially concrete-filled circular pier (hc/h = 0.25, 0.50) under single-directional loading or with adequate concrete fill ratio (hc/h = 0.50) under bi-directional loading. However, in the case of a low concrete fill ratio pier (hc/h = 0.25) under

bi-directional loading, residual displacement is far beyond the value calculated by the Eq.(3.5).

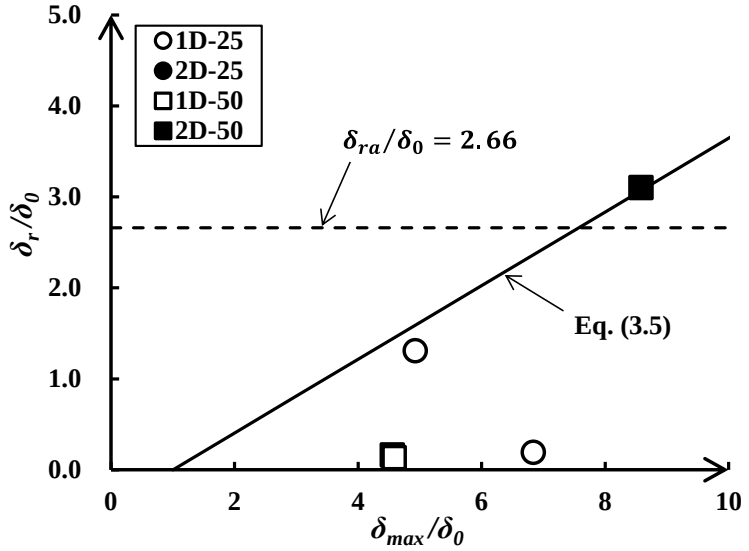

Fig. 3-30. Relationship between the maximum displacement and residual displacements

(4) Hysteretic Curves

The hysteretic curves measured during the single- and bi-directional loading tests are represented by broken lines and solid lines in Figs. 3-31, respectively, in which plots of row 1, 2, and 3 correspond to the results of piers of h_c = 0.00*h*, 0.25*h* and 0.50*h*, respectively.

As seen from Figs. 3-31, compared with the results of single-directional loading tests, the specimens tested under bi-directional loading presented a considerable degree of degradation in horizontal load accompanied by a great increase in displacement.

For the specimens of three different concrete-filled ratios, the average attenuation ratios of horizontal load component of bi-directional loading to single-directional loading were about 13%, 12% and 9% large, respectively. The degradation of restoring force resulted from the local buckling deformation accelerated by the bi-directional loading. Once local buckling occurred, the plates were not fully straightened out during reversed loading and buckling deformations

progressively grew, then the lateral resistance of the specimen gradually reduced.

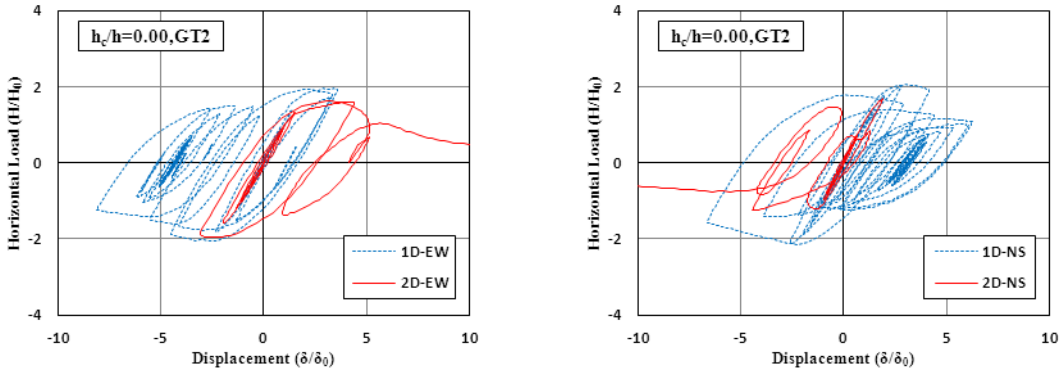

(a) h_c = 0.00h

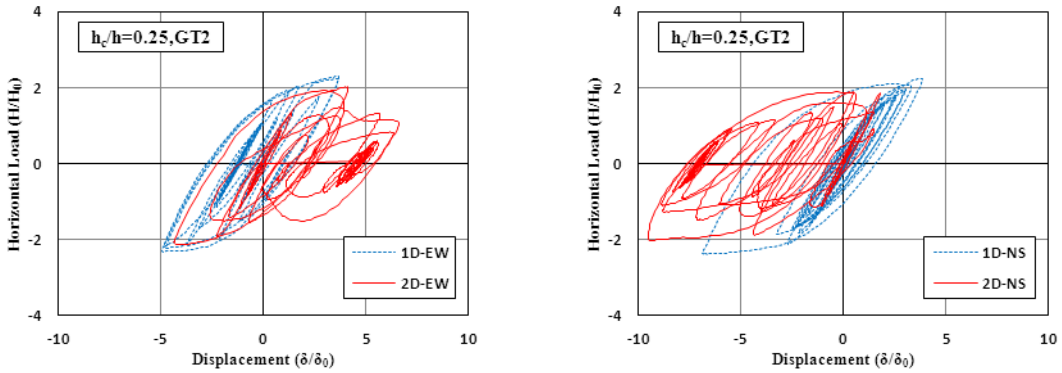

(b) h_c = 0.25h

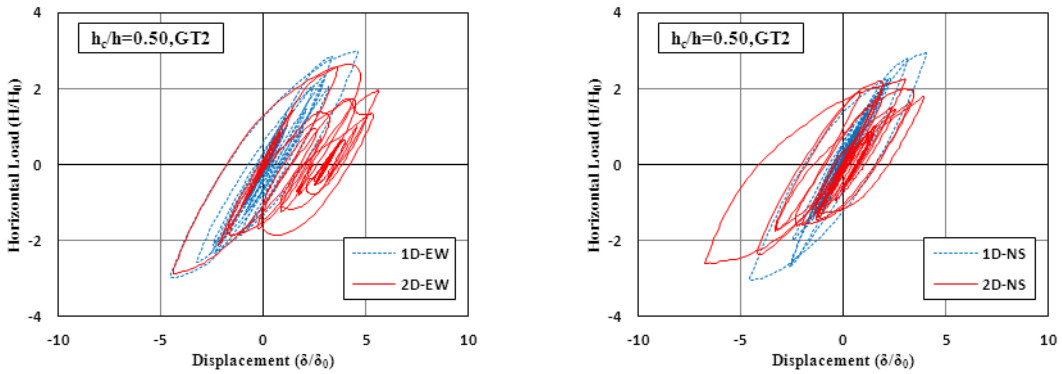

(c) h_c = 0.50h

Fig. 3-31. Hysteretic curves of circular specimens (GT2)

(5) Lateral Resistance Force Trajectories

The lateral resistance force trajectories in the horizontal plane for circular piers are shown in Fig.

3-32, in which the vertical and horizontal axes represent the horizontal force of the piers in the NS and EW directions, respectively. The solid lines in all the plots of Fig. 3-32, indicating the results due to bi-directional loading tests, are generally enveloped by the single-directional loading results presented by the broken lines. The range of the horizontal resistance trajectories became larger as the concrete-filled ratio increased, which means the strength of the piers can be effectively improved by filling concrete in the piers.

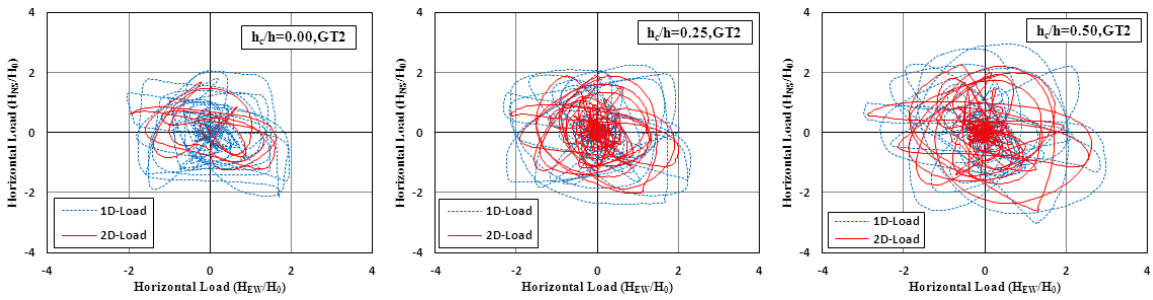

(a) h_c = 0.00h (b) h_c = 0.25h (c) h_c = 0.50h

Fig. 3-32. Horizontal resistance force trajectories in the horizontal plane

(6) Maximum Horizontal Load

Fig. 3-33 compares the maximum horizontal load, $H_{max,2D}$ subjected to bi-directional loading and $H_{max,NS}$ and $H_{max,EW}$ under single-directional loading. It can be found from Fig. 3-33 that, in the case of bi-directional strong earthquake loading, $H_{max,2D}$ of test specimens with three different concrete-filled ratios (i.e., h_c/h = 0.00, 0.25 and 0.50) presented a small degree of degradation about 1.7%, 3.2% and 2.3%, respectively, in comparison with average results of single-directional loading tests.

It also can be observed that the maximum horizontal loads of the piers partially filled with a height of 0.25h and 0.50h concrete were increased by about 12% and 43%, respectively, in

comparison with the piers without concrete infill. The effect of filled-in concrete is clear from these results.

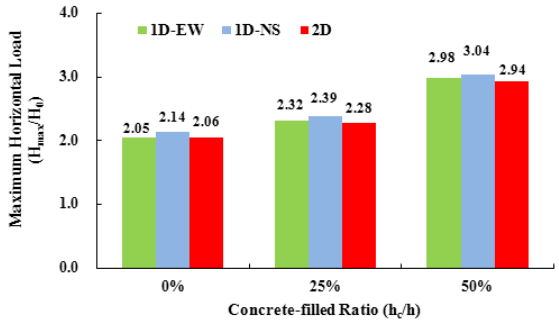

Fig. 3-33. Maximum horizontal load comparison

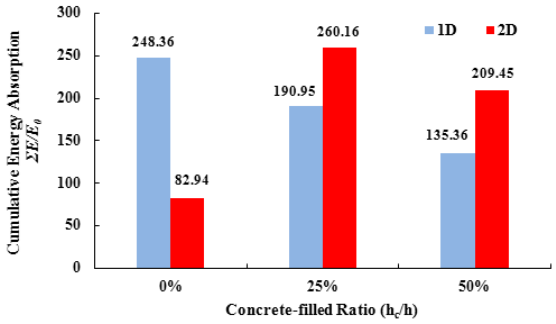

Fig. 3-34. Cumulative energy absorption

(7) Cumulative Energy Absorption

Fig. 3-34 presents a comparison of the cumulative energy absorption values between the single- and bi-directional hybrid loading tests.

It can be clearly seen from the Fig. 3-22 that the cumulative energy absorption due to bi-directional loading tests is generally much larger than those due to single-directional loading tests. For the specimen U-H-00-2D-1 subject to bi-directional loading of the case of h_c/h = 0.00, the loading test was stopped midway before the end of time history because the pier had suffered great damage caused by severe buckling occurred at the base, which resulted in a low value of cumulative energy absorption.

The reduction of cumulative energy absorption along with the growth of concrete-filled height was observed in Fig. 3-34, because the displacement response was significantly reduced as the concrete-filled ratio increased, as shown in Fig. 3-26, while the increment rate of lateral load was much less than the reduction rate of displacement .

3.5 A New Evaluation Method for Piers under Bi-directional Loading

As above stated in the section 3.3, the partially concrete-filled steel piers on the soft ground (GT3) suffered most severe damage due to bi-directional loading among three different ground types. According to the above discussion about the effect of bi-directional loading on seismic performance of bridge piers, it is also clear that to evaluate the seismic behavior of steel piers under bi-directional loading through conventional single-directional loading test or analysis is improper and difficult.

Therefore, a new seismic-behavior evaluation method for steel piers under bi-directional loading is developed, and the validity of this method is verified by the hybrid test results of circular piers on the soft ground (GT3).

3.5.1 Principal Component Analysis of Ground Motion Data

The eveluation method is developed on the basis of principal component analysis (PCA), which is a standard tool in modern data analysis, in diverse fields from neuroscience to computer graphics. It is a simple and non-parametric method for extracting relevant information from confusing data sets. The goal of PCA is to identify the most meaningful basis, i.e. the first principal component for re-expressing a data set of bi-directional ground motions. The aim is that the single-directional loading test on the basis of the first principal component could acquire the similar results to those due to bi-directional loading test. In other wards, if this procedure is clarified to be effective, far simple test method due to single-directional loading compared with that of bi-directional loading will become a usefull tool as realising the behaviour of piers under actual holyzontally bi- directional seismic oscilations.

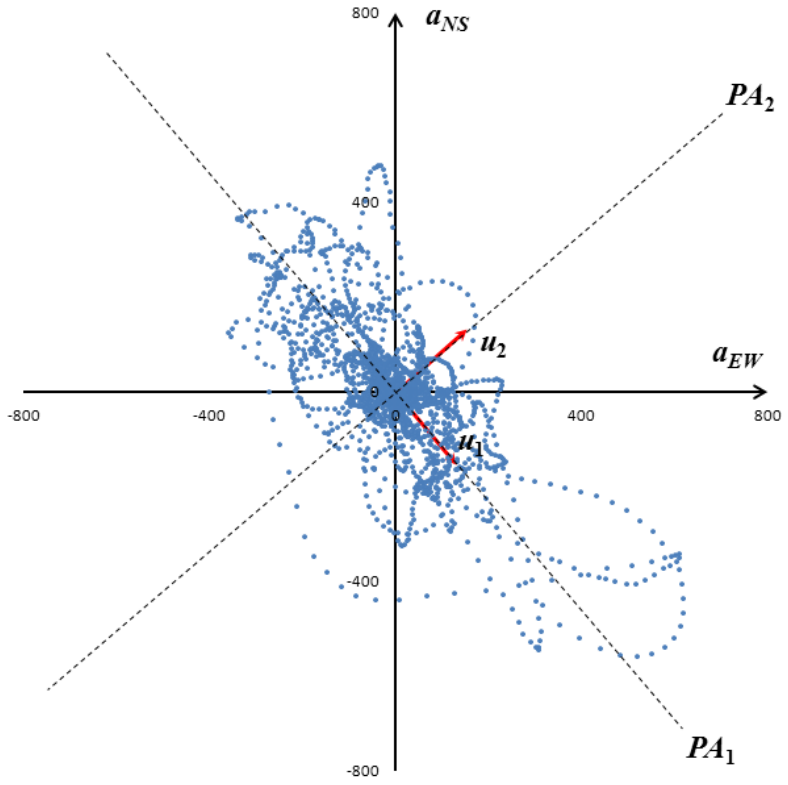

Fig. 3-35. PCA of PKB earthquake accelerogram records (GT3)

The PKB earthquake accelerogram records in EW and NS directions as shown in Fig. 3-5, which were obtained on the soft ground (GT3) in Kobe Earthquake, are respectively named as a_{EW} (gal) and a_{NS} (gal), and illustrated as points in Fig. 3-35, in which the horizontal and vertical axes indicate the ground motion data in the EW and NS directions, respectively. The origin of the coordinate system are determined by the average values of the ground motion data,

$$\begin{pmatrix}\bar{a}_{EW}\\ \bar{a}_{NS}\end{pmatrix} = \begin{pmatrix}\sum_{i=1}^{5000} a_{EW,i}/5000\\ \sum_{i=1}^{5000} a_{NS,i}/5000\end{pmatrix} = \begin{pmatrix}-0.43\\ 0.14\end{pmatrix} \tag{3.6}$$

The variance covariance matrix V, whose (i, j) entry is the covariance of data vectors in EW and NS directions, is calculated by following Eq.3.7.

$$V = \frac{1}{5000}\begin{pmatrix}\Sigma_{i=1}^{5000}(a_{EW,i}-\bar{a}_{EW})^2 & \Sigma_{i=1}^{5000}(a_{EW,i}-\bar{a}_{EW})(a_{NS,i}-\bar{a}_{NS})\\ \Sigma_{i=1}^{5000}(a_{NS,i}-\bar{a}_{NS})(a_{EW,i}-\bar{a}_{EW}) & \Sigma_{i=1}^{5000}(a_{NS,i}-\bar{a}_{NS})^2\end{pmatrix}$$

$$= \begin{pmatrix} 7501 & -5751 \\ -5751 & 9364 \end{pmatrix} \tag{3.7}$$

The eigenvalues of the variance covariance matrix V are $\lambda_1 = 14260$ and $\lambda_2 = 2606$, and the corresponding unit eigenvectors are as follows:

$$u_1 = \begin{pmatrix} 0.6481 \\ -0.7615 \end{pmatrix}, \qquad u_2 = \begin{pmatrix} 0.7615 \\ 0.6481 \end{pmatrix} \tag{3.8}$$

The pricinple axes determined by the unit eigenvectors are decipted by the dashed lines in the Fig. 3-35. Let $U = (u_1\ u_2)$, the new viriables $\xi_{1,i}$, $\eta_{2,i}$ are defined by Eq.3.9,

$$\begin{pmatrix} a_{EW,i} - \bar{a}_{EW} \\ a_{NS,i} - \bar{a}_{NS} \end{pmatrix} = U \begin{pmatrix} \xi_{1,i} \\ \eta_{2,i} \end{pmatrix} \tag{3.9}$$

To solve the $\xi_{1,i}$ and $\eta_{2,i}$, Eq.3.9 can be rewritten as follows,

$$\begin{pmatrix} \xi_{1,i} \\ \eta_{2,i} \end{pmatrix} = U^{-1} \begin{pmatrix} a_{EW,i} - \bar{a}_{EW} \\ a_{NS,i} - \bar{a}_{NS} \end{pmatrix} = U^{T} \begin{pmatrix} a_{EW,i} - \bar{a}_{EW} \\ a_{NS,i} - \bar{a}_{NS} \end{pmatrix} \tag{3.10}$$

that is,

$$\begin{cases} \xi_{1,i} = 0.6481\left(a_{EW,i} - \bar{a}_{EW}\right) - 0.7615\left(a_{NS,i} - \bar{a}_{NS}\right) \\ \eta_{2,i} = 0.7615\left(a_{EW,i} - \bar{a}_{EW}\right) + 0.6481\left(a_{NS,i} - \bar{a}_{NS}\right) \end{cases} \tag{3.11}$$

The time history curve of first principal component $\{\xi_1\}$, which describes the direction of maximum variance of ground motion data, is shown in Fig. 3-36.

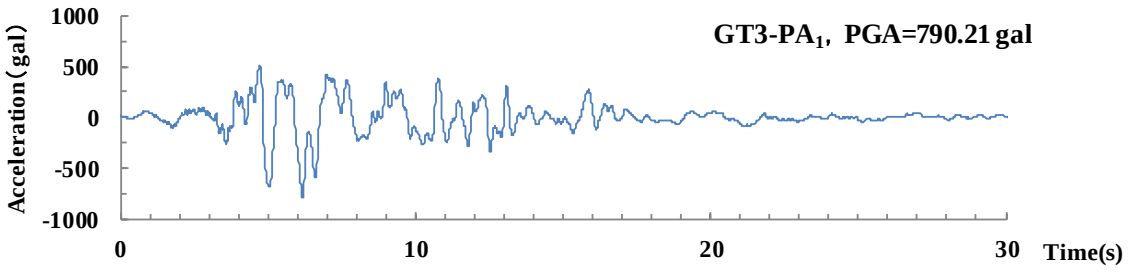

Fig. 3-36. Acceleration time history curve of first principal component of PKB seismic wave

3.5.2 Experimental Verification of Proposed Method

To verify the validy of proposed method, a total of 4 circular piers, were investigated in this study. The hybrid test results obtained under single- and bi- directional loading on the soft ground (GT3) are listed in Table 3-6.

Table 3-6. Hybrid test results of circular piers on GT3

No.	*Specimen*	*Loading Mode*	δ_{max}/δ_0	δ_r/δ_0	H_{max}/H_0	$\Sigma E/E_0$	h_c/h
1	U-H-50-1D-3	GT3-1D-EW	3.81	0.24	2.96	31.76	0.50
2	U-H-50-1D-4	GT3-1D-NS	4.37	0.14	3.09	72.40	
3	U-H-50-1D-5	GT3-1D-PA	8.82	3.64	2.99	123.26	
4	U-H-50-2D-2	GT3-2D	9.32	4.28	3.05	141.39	

It can be observed from the Table 3-6 that there is a wide gap between the results of No.4 specimen in the case of bi-directional loading and the test results of No.1 and No.2 specimens subjected to conventional single-directional loading. However, the proposed new single-directional loading results of No.3 specimen, tested by adopting the first principal component, showed little differences from those of No.4 specimen. The comparison of seismic behavior due to proposed new single-directional loading mode (1D-PA) and bi-directional loading is to be discussed in detail as follows.

(1) Displacement Time History Curve

Plots (a) to (d) of Fig. 3-37 compared the displacement time history curve due to bi-directional loading with results due to three different single-directional loading modes, respectively. In these plots, displacement response obtained in the single- and bi- directional loading tests are represented by broken lines and solid lines, respectively. In Plots (a) and (b), the displacement

response components in EW and NS directions due to bi-directional loading showed so much larger than those due to conventional single-directional loading. It is feasible to accurately evaluate the complicated inelastic behavior of steel piers subjected to bi-directional seismic loading on the basis of results of conventional single- directional loading tests.

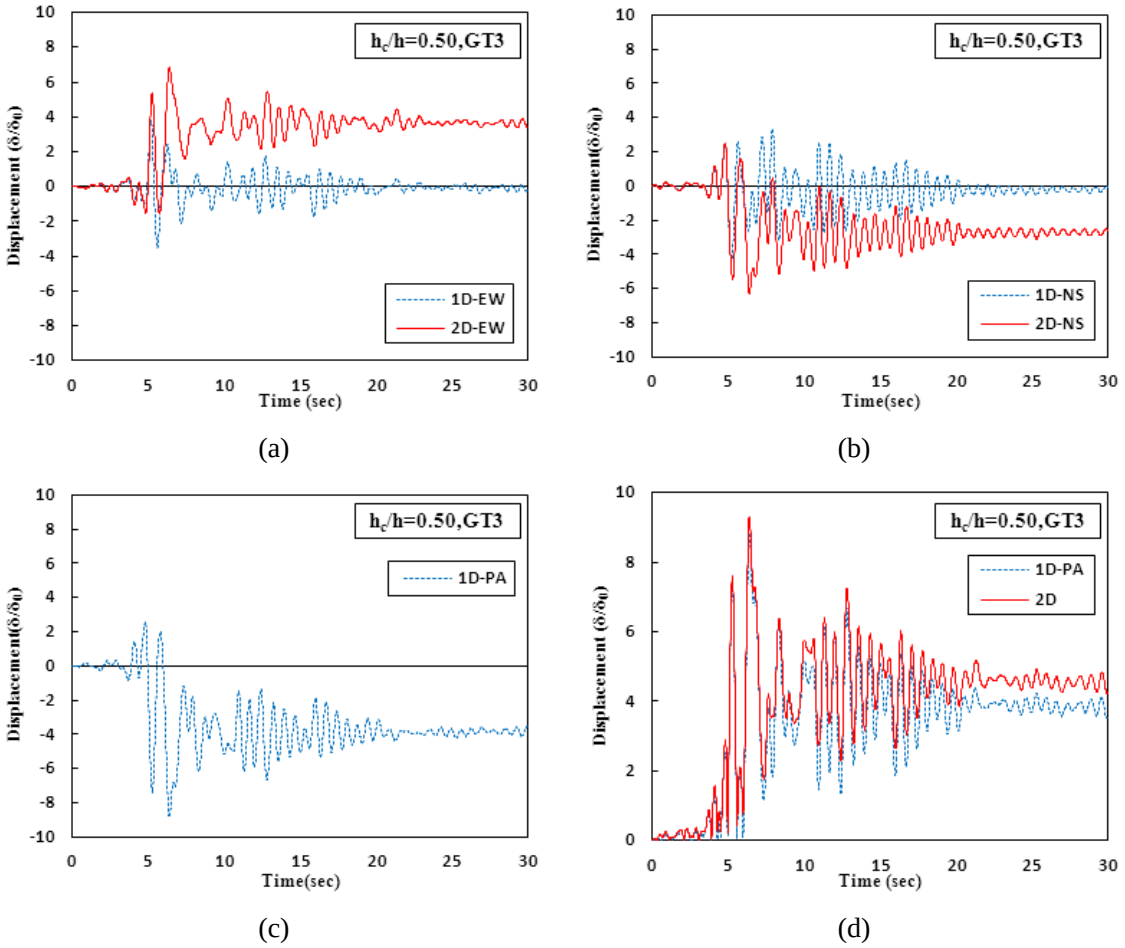

Fig. 3-37. Displacement time history curves of circular specimens (GT3)

Because the displacement trajectories due to bi-directional loading were located in a horizontal plane while the displacement responses due to 1D-PA loading mode were limited on an axis as shown in Plot (c), the absolute values of displacement vectors were adopted in Plot (d) to ensure that it is possible to make a displacement comparison between No.3 and No.4 specimens.

It can be easily seen from Plot (d) that the gap between displacement time histories curves named as "1D-PA" and "2D" is very small. The non-dimensional values of maximum displacement and residual displacement due to 1D-PA loading mode for specimens of $h_c = 0.50h$ are 8.82 and 3.64 on the soft ground (GT3), respectively. The corresponding values due to bi-directional loading are 9.32 and 4.28, respectively. The tolerances of the maximum displacement and residual displacement between bi-directional loading and 1D-PA loading are about 5.7% and 17.6%, respectively.

Therefore, it is thought that the displacement response of circular steel piers caused by actual bi-directional strong earthquake loading on the soft ground (GT3) could be practically predicted from proposed new single-directional loading test (1D-PA).

(2) Hysteretic Curve

The hysteretic curves measured in the hybrid loading tests conducted on soft ground (GT3) are represented in the Fig. 3-38.

As seen from Plots (a) and (b), compared to the results of conventional single-directional loading tests, the No.4 specimen of bi-directional loading test presented a considerable degree, about 26%, of degradation in lateral resistance accompanied by an large increase in displacement. The degradation of lateral resistance force resulted from the severe local buckling deformation accelerated by the bi-directional loading.

Plot (c) of Fig. 3-38 shows the hysteretic curves due to 1D-PA loading test, which presented a significant larger hysteresis than those obtained in the conventional single-directional hybrid loading tests, i.e. "1D-EW" and "1D-NS" curves, respectively as illustrated in Plots (a) and (b).

In order to compare between the two hysteretic curves due to 1D-PA loading and 2D loading, using the same processing method as the above mentioned, the absolute values of displacement and load vectors of 1D-PA and 2D loading modes were depicted in Plot (d) by broken lines and solid lines, respectively.

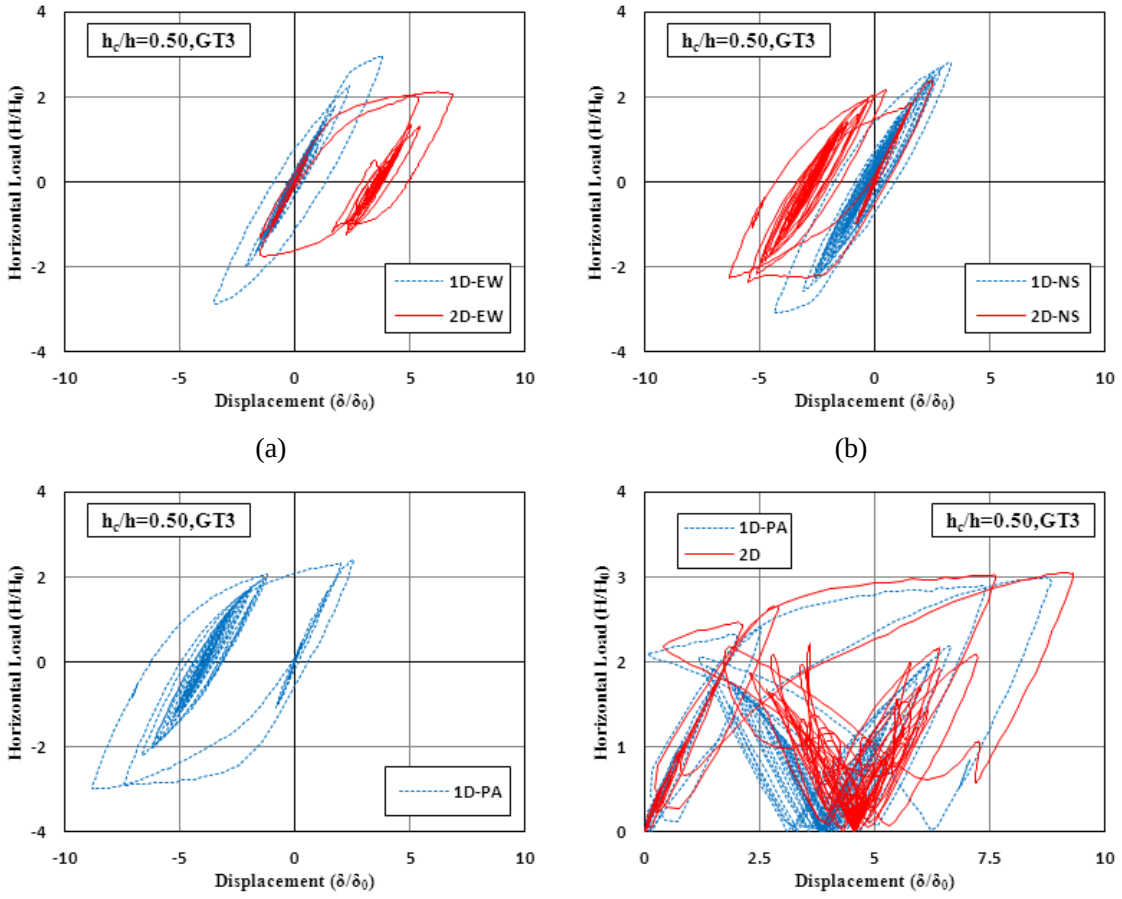

Fig. 3-38. Hysteretic curves of circular specimens (GT3)

Both curves named as “1D-PA” and “2D” showed a very similar hysteresis of absolute values. The non-dimensional values of maximum lateral resistance due to 1D-PA loading mode is 2.99 on the soft ground (GT3), and the corresponding value due to 2D loading is 3.05, only about 2% tolerance.

(3) Cumulative Energy Absorption Time History Curve

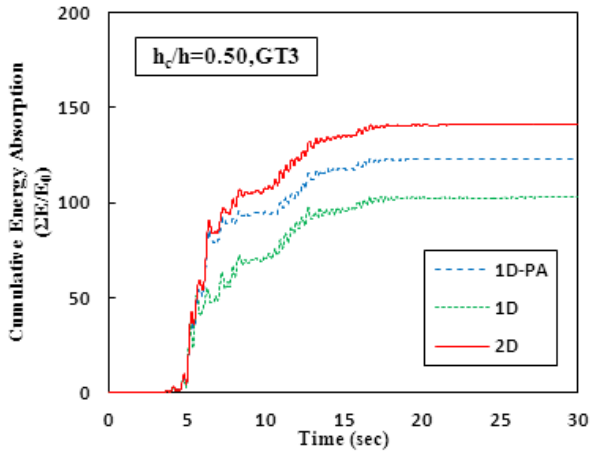

Fig. 3-39. Hysteretic curves of circular specimens (GT3)

The three kinds of cumulative energy absorption time history curves names as “1D-PA”, “1D” and “2D”, which are depicted by dash lines, dot lines and solid lines in Fig. 3-39, respectively, were obtained by the results of proposed 1D-PA loading test, by the sum of results of conventional 1D loading tests in EW and NS directions, and by the test results due to 2D hybrid loading, respectively. It can be observed that the cumulative energy absorption due to bi-directional loading test is larger than those due to single-directional loading tests. In comparison with the result of bi- directional loading, the ultimate cumulative energy absorption of 1D-PA loading mode shows about 13% smaller, while the sum of conventional 1D loading presents about 27% degradation in energy absorption.

Through the above comparisons, the complex seismic behavior caused by bi-directional earthquake loading on the soft ground (GT3) is considered to be approximately simulated by the results of proposed new single-directional loading test or analysis more accurately than conventional single- directional loading test.

3.6 Seismic Design Considerations

3.6.1 Maximum Displacement

The admissible displacement δ_{ma} for partially concrete-filled bridge piers advised in the seismic design specifications is determined as the displacement when the load of specimen reached its peak point in repeated cyclic loading tests or analysis. In this study, the non-dimensional admissible displacement (δ_{ma}/δ_0) for stiffened rectangular steel piers of three different concrete-filled ratios, i.e., h_c/h = 0.00, 0.20 and 0.40, was obtained by static cyclic loading tests as 2.64, 3.50 and 3.99 (referred to as δ_m/δ_0 in Table 2-5), respectively. For the circular steel piers of h_c/h = 0.00, 0.25 and 0.50, the corresponding admissible value was 3.18, 4.23 and 3.92, respectively.

As shown in Fig. 3-12 (a), for the stiffened rectangular section piers without concrete fill or with inadequate concrete-filled ratio (h_c/h = 0.20), the admissible value was beyond by a majority of the hybrid test results due to either single- or bi-directional loading in medium and soft grounds (GT2 and GT3). In the case of circular piers, as shown in Fig. 3-28, all of the hybrid test results in medium ground (GT2) exceeded the admissible value.

Therefore, the cross-section size or the stiffened-plate rigidity of the stiffened rectangular steel piers with low concrete-filled ratio should be modified in line with the routine design procedure on the basis of single-directional loading test results. For the circular piers, the steel grade, diameter of cross section or the thickness of steel plate should be modified, and a diaphragm over filled-in concrete is recommended as an alternative improvement if possible.

However, for the stiffened rectangular piers of sufficient concrete-filled ratio (h_c/h = 0.4), only those results acquired by bi-directional loading tests conducted in medium and soft grounds (GT2 and GT3) exceeded the corresponding admissible displacement. That is why an

adjustment of displacement is required to ensure the seismic performance of piers under actual strong earthquakes.

3.6.2 Residual Displacement

The admissible residual displacement is provided in the seismic design specifications as 1/100 of the pier height, which corresponds to $1.60\delta_0$ and $2.66\delta_0$ for the stiffened rectangular piers and the circular piers used in this study, respectively.

For the steel piers without concrete infill, except in the cases of hard ground (GT1), all residual displacements after the end of the tests exceeded the admissible value, whether under single-directional loading or bi-directional loading.

For the partially concrete-filled steel piers, the residual displacements due to single-directional loading were all located in the range of admissible value. However, when the piers under bi-directional loading, especially in the soft ground (GT3), this value was exceeded by both results of test specimens with filled-in concrete.

For the stiffened rectangular piers of h_c/h = 0.20, or the circular piers of h_c/h = 0.25, which suffered severe damage due to bi-directional loadings, regarding the maximum response displacement, the enough increment of concrete-filled height is recommended to ensure the basic seismic performance.

3.6.3 Maximum Horizontal Load

Whether for stiffened rectangular piers or circular piers, the values of maximum lateral resistance obtained in the bi-directional loading tests showed nearly the same as the results of

single-directional loading tests. The insignificant differences (2%~7%) between bi- and single-directional loadings can be ignored in practical design.

Therefore, regarding the maximum resistance under actual seismic bi-directional loading conditions, the average of conventional single-directional loading results can be used for three different ground types.

3.6.4 A New Bi-Directional Seismic Verification Method

As stated above, the partially concrete-filled steel bridge piers, which may have an ability to withstand damage caused by single-directional loading in the test, will probably suffer severe damage or even collapse due to actual bi-directional earthquake actions, especially in the medium and soft grounds (GT2 and GT3).

Therefore, on the basis of the conventional single-directional verification method, we consider a more rational design treatment according to the difference in displacement response between single- and bi-directional loading tests. The procedure for a new bi-directional seismic verification method is explained in the following steps.

(1) First, following the conventional single-directional verification method, apply the earthquake motions in longitudinal and transverse directions separately and verify the dynamic response of a partially concrete-filled bridge pier through the ultimate displacement limit δ_{ma} and residual displacement limit δ_{ra}. If the pier fails to satisfy the verification check, then increase concrete-filled height or thicken the steel plate to ensure basic seismic performance.

(2) After a pier meets the above requirements, verify the maximum response displacement $\delta_{m,2D}$ from Eq.(3.12), in which values of $\delta_{m,1D\text{-}EW}$ and $\delta_{m,1D\text{-}NS}$ are obtained in step (1).

$$\delta_{m,2D} = C_{m,2D} \cdot max(\delta_{m,1D-EW},\quad \delta_{m,1D-NS}) < \delta_{ma} \tag{3.12}$$

Here the maximum displacement correction factor $C_{m,2D}$, which is given by maximum response displacement ratio of bi- to single-directional loading for a pier filled with adequate concrete, can be referred to Table 3-4 as 1.08, 1.53, and 1.98 for stiffened rectangular piers in the hard, medium, and soft grounds (GT1~3), respectively. The value of $C_{m,2D}$ is possible to change according to different pier parameters.

(3) If the safety verification check was satisfied, verify the residual displacement of the pier through the following equation.

$$\delta_{r,2D} = C_R(\frac{\delta_{m,2D}}{\delta_y} - 1)(1 - r)\delta_y < \delta_{ra} \tag{3.13}$$

(4) The pier under bi-directional earthquake loading is confirmed to be safe if $\delta_{m,2D}$ and $\delta_{r,2D}$ are satisfied; otherwise, the pier needs steel strength upgrades or a redesign in cross-sectional area.

(5) If experimental equipment for bi-directional hybrid loading is available or there is an accurate model suitable for the practical design of actual bi-directional strong earthquake loading, apply EW and NS directional earthquake components simultaneously and check that the response displacements $\delta_{m,2D}$ and $\delta_{r,2D}$ are smaller than the displacement limits.

3.7 Conclusions

To clarify the seismic behavior of partially concrete-filled steel bridge piers subjected to actual seismic earthquake forces, a total of 40 test specimens, including 27 stiffened rectangular piers and 13 circular piers, subjected to single- and bi- directional hybrid loadings were tested in this study. On the basis of the test results, the conclusions can be summarized as follows:

(1) Obvious differences between single- and bi- directional loadings were observed in the hysteretic curves and displacement time history curves of partially concrete-filled steel bridge piers. The maximum displacement and residual displacement during an actual earthquake cannot be correctly estimated by conventional single- directional loading test results for medium and soft ground. The seismic design specification based only on single-directional loading test results may lead to unsafe side decision in some cases.

(2) The piers with low concrete-filled ratio or even without concrete infill, which may have an ability to withstand damage caused by single-directional loading, will probably suffer severe damage or even collapse due to actual bi-directional earthquake actions, especially in the medium and soft grounds (GT2 and 3). However, the piers of adequate concrete-filled ratio showed excellent earthquake-resistant performances under either single- or bi-directional loading due to the effect of sufficient encase concrete.

(3) The maximum displacement caused by the bi-directional loading, especially in the medium and soft ground (GT2 and GT3), showed much larger than results due to single-directional loading. Then a modified admissible displacement method is proposed for the seismic design considering the bi-directional loading effect.

(4) The residual displacement of the test results showed similarities with the maximum displacement. However, it should be noticed that the difference between the single- and bi-directional loadings was enlarged several times in the case of piers with low concrete-filled ratio, which results in an unsafe region. The design specifications provide an accurate estimation of residual displacement for sufficiently concrete-filled piers except for the case due to bi-directional loading in the soft ground (GT3), and hence the residual displacement correction factor is also proposed for the seismic design.

(5) The maximum horizontal load caused by bi-directional loading was only about 2%~7% lower on an average than that of the single-directional loading tests. Therefore, it is possible to predict the maximum horizontal load of the steel box section piers in actual bi-directional loading conditions from conventional single-directional loading test results. The maximum load of the pier increased gradually along with the increment of concrete-filled height but this growth trend might reach threshold value.

(6) For the cumulative energy absorption, the largest difference appeared among the three ground types, and the cumulative energy absorption caused by the bi-directional loading is generally larger than that due to single- directional loading.

(7) For the circular specimens on the soft ground (GT3), the complex seismic behavior caused by bi-directional earthquake loading can be approximately simulated by the results of proposed new single-directional loading test method which is developed on the basis of principal component analysis (PCA) for the input earthquake acceleration data.

CHAPTER 4
MULTIPLE-SPRING MODEL FOR BI-DIRECTIONAL HYSTERETIC BEHAVIOR OF STEEL PIERS

4.1 General

As stated in the Chapter 1, a complete assessment of the seismic design of steel bridge piers often requires a nonlinear dynamic analysis. It is known that the dynamic characteristics of steel bridge piers subjected to bi-directional seismic forces can be obtained by the hybrid loading tests. As discussed in the Chapter 3, the seismic response of a thin-walled bridge pier to earthquake excitations depends on several factors, such as earthquake characteristics, ground conditions and structural properties. In order to clarify the seismic performance of steel bridge piers under actual earthquake loading, it is necessary to carry out hybrid loading tests using a variety of seismic waves as much as possible. However, the cost on experiment including loading system and test specimens is often substantial, especially for large scale models.

Therefore, results from these tests are then used in the development and calibration of hysteretic models that permit the extrapolation of the limited test data to other cases of dynamic response. These models can be divided into three main categories in accordance with the increasing level of refinement and complexity: global empirical models, discrete finite element models, and microscopic finite element models.

Based on the research conducted to examine the stability and ductility of steel bridge piers under cyclic loading, some single degree of freedom global empirical models such as bi-linear kinematic hardening model, tri-linear kinematic hardening model, 2-parameter model and

damage index model have been developed to express the in-plane hysteretic behavior of steel bridge piers. These models are useful in the preliminary design phase for estimating displacement ductility demands. However, the global empirical models are based on too crude approximations and yield too little information on the forces, deformations and damage distribution in the structure, and such models are restricted to the region where only in-plane hysteretic behavior of bridge piers is considered.

For the microscopic finite element models, members and joints of structures are discretized into a large number of finite elements, like shell elements or fiber elements. Constitutive and geometric nonlinearity is typically described at the stress-strain level or averaged over a finite region. Physical nonlinearities, including bond deterioration between steel and concrete, interface friction at the cracks, creep, relaxation and thermal phenomena, can be studied with this kind of models. However, these models are computationally expensive for large scale nonlinear dynamic analyses, where the model of a steel bridge pier involves thousands of degrees of freedom.

In the case of discrete finite element models, a pier is modeled as an assembly of interconnected elements that describe the hysteretic behavior of steel or concrete members. Constitutive nonlinearity is either introduced at the element level in an average sense or at the section level. This study concentrates on the discrete finite element models, which are the best compromise between simplicity and accuracy in nonlinear seismic response studies. A multiple-spring model is one of such models.

Lai et al. (1984) proposed a five spring model to simulate the hysteretic and stiffness degrading behavior of reinforced concrete members subjected to axial force and biaxial bending interaction. The proposed model consists of two inelastic elements at the two ends of a

reinforced concrete member sandwiching a linear elastic line element, as shown in Fig. 4-1. For each inelastic element, there are four inelastic steel springs at each corner representing the stiffness of the effective steel bars, with a fifth spring, not shown in the figure, at the center of the section which was only effective when the concrete is in compression. In Lai's model, the force-deformation relation for the effective steel springs follows Takeda's model, a maximum point directional bilinear model.

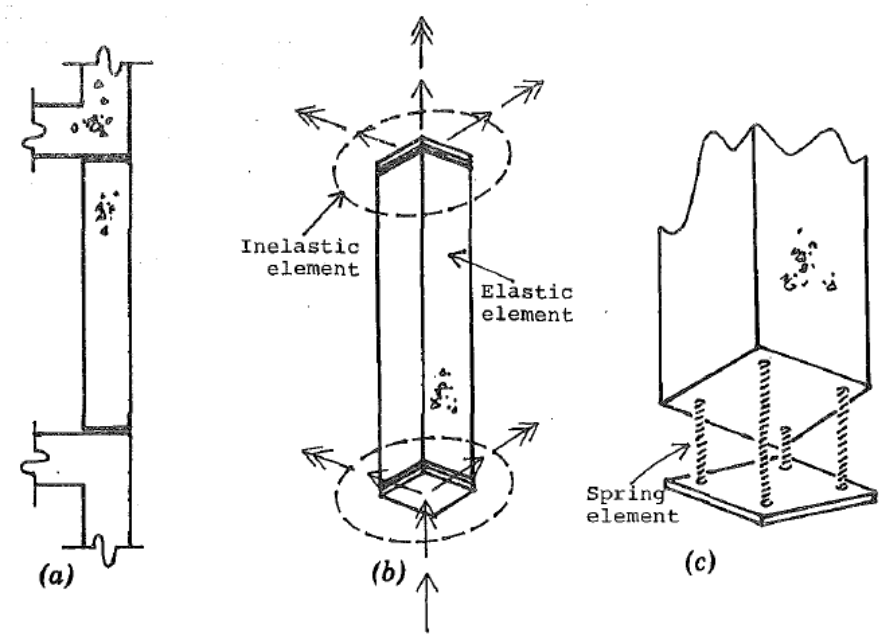

Fig. 4-1. Lai's model: (a) member in frame; (b) member model; (c) inelastic element

As above-mentioned in Chapter 1, Jiang et al. (2001) also proposed a hysteretic model, consisting of a concentrated mass and a rigid bar with multiple nonlinear springs located at the base, as shown in Fig. 4-2 (a), for thin-walled circular steel piers under biaxial bending to predict the ultimate seismic behavior of cantilever-type piers. The constitutive relations for nonlinear spring adopted in Jiang's model, as illustrated in Fig. 4-2 (b), in which the tension side is expressed by the bi-linear curve while the compression side is by the tri-linear curve with a

descending part that represents the strength deterioration due to local buckling, are determined by the in-plane behavior of thin-walled circular steel piers. Herein, the in-plane behavior is predicted by the 2-parameter model, a global empirical model.

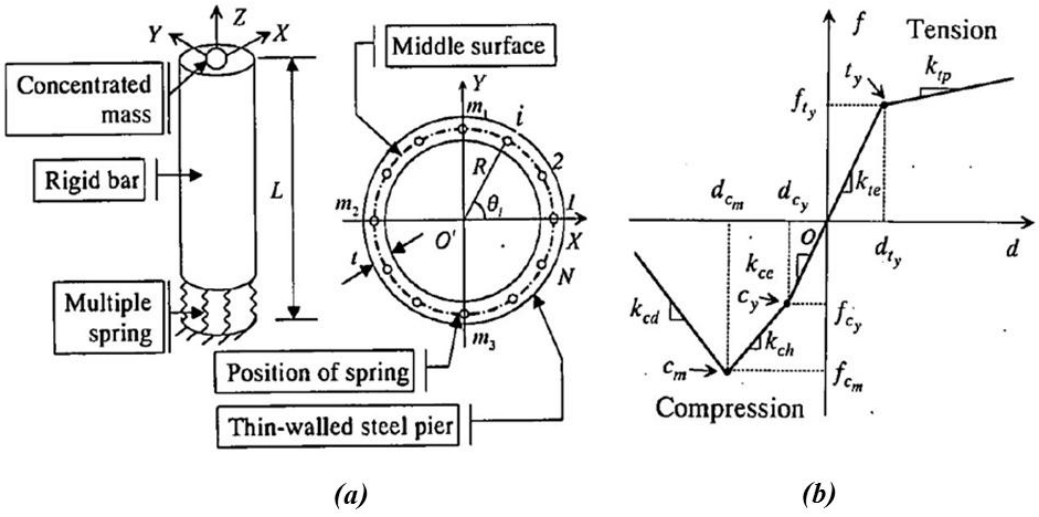

Fig. 4-2. Jiang's model: (a) multiple-spring model for thin-walled circular steel piers;

(b) constitutive model for each spring

The two above-mentioned models, by their simplistic constitutive relations of spring element, are not claimed to be precise to express the hysteretic behavior of bridge piers, especially in the case of bi-directional dynamic loading, but rather, tried to bridge the gap between the microscopic finite element models and the very crude empirical models.

In order to reproduce accurately the hysteresis characteristic of the steel bridge piers, in this study, a series of approximate curves, whose parameters are determined by the static cyclic loading test results, have been adopted to describe the complicated nonlinear behavior of spring element exactly. To examine the validity of the proposed multiple spring model, the analytical results obtained by the proposed model are compared with experimental results due to static cyclic loading, single- and bi-directional hybrid loading.

4.2 Analytical Method of Multiple Spring Model

4.2.1 Multiple-Spring Model for Thin-Walled Steel Piers

As a three-dimensional hysteretic model for thin-walled steel piers, the proposed model consists of a concentrated mass representing weight of the superstructure and a rigid bar with multiple nonlinear springs located at the pier base, as illustrated in Fig. 4-3. The springs are arranged with equal intervals along the middle surface of the cross section, and become symmetric with respect to both X and Y axes. It is assumed that no horizontal relative displacement occurs at the base of the pier.

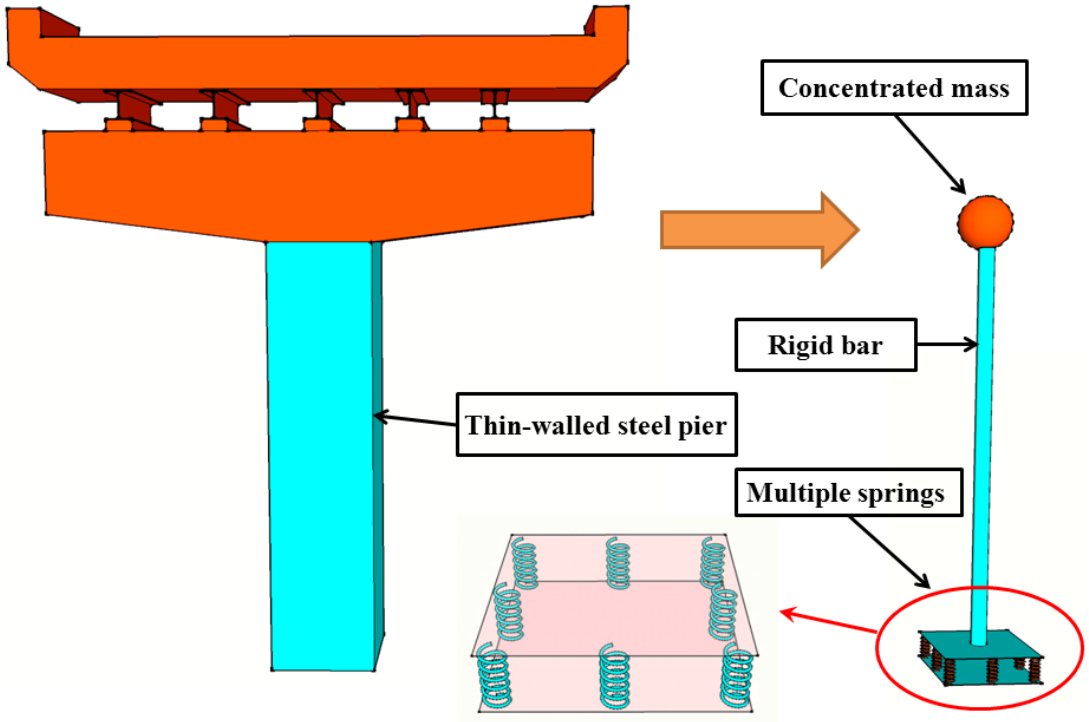

Fig. 4-3. Multiple-spring model for steel pier

From the plane cross-section assumption and kinematic relation, the incremental vertical displacement of the *i*-th spring Δd_i is expressed as

$$\Delta d_i = -\frac{1}{h}(x_i \Delta D_X + y_i \Delta D_Y) + \Delta D_Z \tag{4.1}$$

where h is the height of the pier; ΔD_X , ΔD_Y and ΔD_Z are three incremental translational displacement components at the top of the pier; x_i and y_i are vertical and horizontal coordinates of i-th spring on the cross section, respectively, as shown in Fig. 4-4.

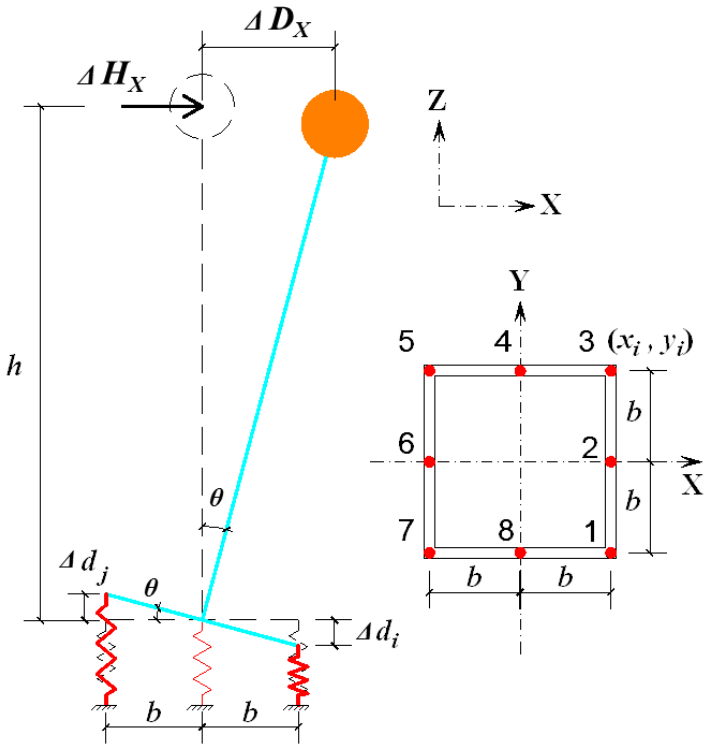

Fig. 4-4. Kinematic relation between incremental displacements of pier and springs

The moment equilibrium and the vertical force equilibrium at the base of the pier lead to

$$\Delta H_X = -\frac{1}{h}\sum_{i=1}^{N} x_i \Delta f_i \tag{4.2}$$

$$\Delta H_Y = -\frac{1}{h}\sum_{i=1}^{N} y_i \Delta f_i \tag{4.3}$$

$$\Delta V_Z = \sum_{i=1}^{N} \Delta f_i \tag{4.4}$$

where ΔH_X , ΔH_Y and ΔV_Z are three incremental force components applied at the top of the

pier; Δf_i is the incremental force of the *i*-th spring and *N* of the form 2^n is the total number of springs. For each nonlinear spring, the following constitutive relation holds.

$$\Delta f_i = k_i \Delta d_i \tag{4.5}$$

where k_i is the tangent stiffness of the *i*-th spring. From Eqs. (4.1) to (4.5), the incremental force-displacement relation at the top of the pier can be written as the following equation,

$$\begin{Bmatrix} \Delta H_X \\ \Delta H_Y \\ \Delta V_Z \end{Bmatrix} = \begin{bmatrix} a_{11} & a_{12} & a_{13} \\ a_{21} & a_{22} & a_{23} \\ a_{31} & a_{32} & a_{33} \end{bmatrix} \begin{Bmatrix} \Delta D_X \\ \Delta D_Y \\ \Delta D_Z \end{Bmatrix} \tag{4.6}$$

where

$$a_{11} = \frac{1}{h^2} \sum_{i=1}^{N} k_i {x_i}^2 \tag{4.7}$$

$$a_{12} = a_{21} = \frac{1}{h^2} \sum_{i=1}^{N} k_i x_i y_i \tag{4.8}$$

$$a_{13} = a_{31} = -\frac{1}{h} \sum_{i=1}^{N} k_i x_i \tag{4.9}$$

$$a_{22} = \frac{1}{h^2} \sum_{i=1}^{N} k_i {y_i}^2 \tag{4.10}$$

$$a_{23} = a_{32} = -\frac{1}{h} \sum_{i=1}^{N} k_i y_i \tag{4.11}$$

$$a_{33} = \sum_{i=1}^{N} k_i \tag{4.12}$$

4.2.2 Constitutive Model for Nonlinear Spring

In a multiple-spring model, it is critically important to determine the constitutive relations for nonlinear springs so that the model can properly express the complex seismic behavior of the steel pier due to coupling effect of multiple-directional loading, $P-\Delta$ effect and local buckling. In our proposed model all the springs are assumed to have the same constitutive

relations.

The hysteretic curves of steel piers due to cyclic loading or hybrid loading, as presented in the figures in the Chapter 2 and 3, manifested in the form of a series of smooth curves. In order to faithfully reproduce the hysteretic behavior of steel piers, the constitutive relations for springs are approximately expressed by cubic curves and straight lines as shown in Fig. 4-5.

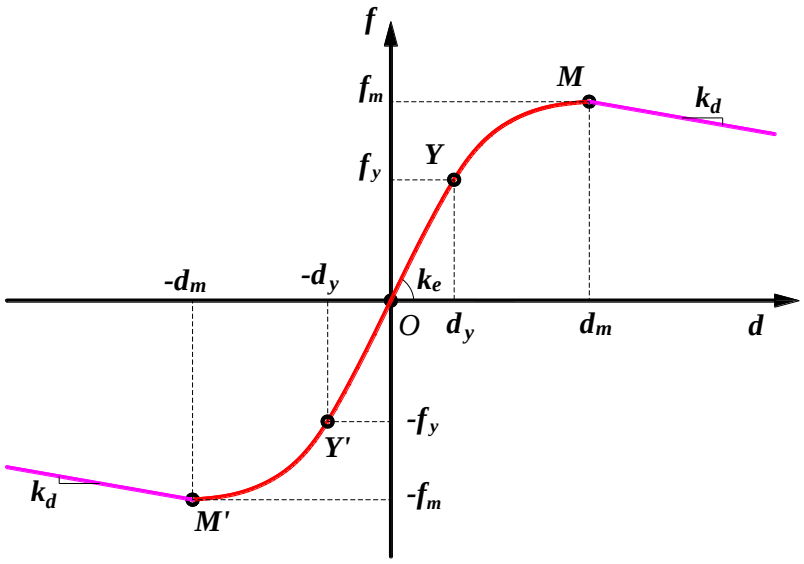

Fig. 4-5. Skeleton curve of spring

The skeleton curve of a spring reflects the behavior of steel piers. To determine the parameters of the proposed constitutive model, the in-plane horizontal force-displacement relation at the top of the pier, given by static cyclic loading test, is adopted. In such loading test, effects of local buckling and large displacement cyclic loading are considered. In order to take into account the $P-\Delta$ effect, the equivalent horizontal force is used, which is given by

$$H_{eq} = \frac{M}{h} = H + \frac{P\Delta}{h} \tag{4.13}$$

Here M is the bending moment caused by the vertical force P and the horizontal force H.

Based on the force-displacement envelop curves of the piers due to static cyclic loading tests, as shown in Figs. 2-5 and 2-8, the parameters of the skeleton curve of the spring model are obtained. Herein, the horizontal force at the top of pier is applied only in the *X* direction. From Eq.(4.6), the incremental in-plane (*X*-*Z* plane) force-displacement relations are derived as following, respectively,

$$\Delta H_X = a_{11}\Delta D_X + a_{13}\Delta D_Z \tag{4.14}$$

$$\Delta V_Z = a_{31}\Delta D_X + a_{33}\Delta D_Z = 0 \tag{4.15}$$

When pier is in elastic state, the tangent stiffness of the *i*-th spring k_i can be taken as the elastic constant, that is, $k_i = k_e$. Then, Eqs.(4.14) and (4.15) can be rewritten as

$$\Delta H_X = k_e(b_{11}\Delta D_X + b_{13}\Delta D_Z) \tag{4.16}$$

$$\Delta V_Z = k_e(b_{13}\Delta D_X + b_{33}\Delta D_Z) = 0 \tag{4.17}$$

where

$$b_{11} = \frac{1}{h^2}\sum_{i=1}^{N} {x_i}^2 \tag{4.18}$$

$$b_{13} = b_{31} = -\frac{1}{h}\sum_{i=1}^{N} x_i \tag{4.19}$$

$$b_{33} = N \tag{4.20}$$

It should be noted that $\sum_{i=1}^{N} x_i = 0$ when the springs are located symmetrically with respect to the *Y*-axis. Therefore, Eqs.(4.16) and (4.17) can be reduced to

$$\Delta H_X = k_e b_{11}\Delta D_X \tag{4.21}$$

$$\Delta D_Z = 0 \tag{4.22}$$

Eq.(4.21) is used to determine the elastic tangent stiffness k_e

$$k_e = \frac{\Delta H_X}{b_{11}\Delta D_X} = \frac{K_e}{b_{11}} \tag{4.23}$$

where K_e is the initial elastic stiffness of pier.

After the pier reaches the maximum horizontal load, as illustrated in Fig.4-5, the skeleton curve of the spring model presents as a straight line. Similar to the elastic tangent stiffness, the tangent stiffness of spring in softening or hardening state can be obtained as following

$$k_d = \frac{K_d}{b_{11}} \tag{4.24}$$

where K_d is the tangent stiffness of pier in softening or hardening range.

The displacement coordinates of yield point $Y(d_y, f_y)$ and the initial maximum point $M(d_m, f_m)$ are determined from the plane cross-section assumption and kinematic relation

$$d_y = \frac{b}{h}D_y, \qquad d_m = \frac{b}{h}D_m \tag{4.25}$$

Here D_y and D_m are the yield displacement and the displacement corresponding to maximum lateral force of the pier due to cyclic loading test. In this constitutive model for spring, it is assumed that the origin point *O*, the yield point *Y* and the initial maximum point *M* are located on a cubic curve. Therefore, the constraint conditions of displacement-force relation for this cubic curve can be expressed as

$$f_y = c_3 {d_y}^3 + c_2 {d_y}^2 + c_1 d_y \tag{4.26}$$

$$f_m = c_3 {d_m}^3 + c_2 {d_m}^2 + c_1 d_m \tag{4.27}$$

$$f_o{}' = 3c_3 {d_o}^2 + 2c_2 d_o + c_1 = k_e \tag{4.28}$$

Then, the coefficients of this cubic curve can be expressed as functions of (f_y, f_m),

$$c_3 = \frac{1}{{d_y}^2(d_y - d_m)} f_y - \frac{1}{{d_m}^2(d_y - d_m)} f_m + \frac{k_e}{d_y d_m} \tag{4.29}$$

$$c_2 = -\frac{d_m}{{d_y}^2(d_y - d_m)} f_y + \frac{d_y}{{d_m}^2(d_y - d_m)} f_m - \frac{k_e(d_y + d_m)}{d_y d_m} \tag{4.30}$$

$$c_1 = k_e \tag{4.31}$$

According to the moment equilibrium, the yield moment M_y and the maximum moment M_m of the pier are given as

$$M_y = F_y h + PD_y = \sum_{i=1}^{N} \left| x_i f_{i,y} \right| \tag{4.32}$$

$$M_m = F_m h + PD_m = \sum_{i=1}^{N} \left| x_i f_{i,m} \right| \tag{4.33}$$

where F_y and F_m are the yield force and the maximum lateral force of the pier due to cyclic loading test; P is the vertical load; $f_{i,y}$ and $f_{i,m}$ are the corresponding forces of the i-th spring when the lateral force of pier reaches F_y and F_m, respectively, and they are given by

$$f_{i,y} = c_3 {d_{i,y}}^3 + c_2 {d_{i,y}}^2 + c_1 d_{i,y} \tag{4.34}$$

$$f_{i,m} = c_3 {d_{i,m}}^3 + c_2 {d_{i,m}}^2 + c_1 d_{i,m} \tag{4.35}$$

where

$$d_{i,y} = \frac{|x_i|}{b} d_y, \qquad d_{i,m} = \frac{|x_i|}{b} d_m \tag{4.36}$$

Then, from Eqs. (4.29) to (4.36), a new equation can be derived as

$$\begin{Bmatrix} \eta_{10} \\ \eta_{20} \end{Bmatrix} = \begin{bmatrix} \eta_{11} & \eta_{12} \\ \eta_{21} & \eta_{22} \end{bmatrix} \begin{Bmatrix} f_y \\ f_m \end{Bmatrix} \tag{4.37}$$

where

$$\eta_{10} = M_y - \sum_{i=1}^{N} \frac{k_e d_{i,y} |x_i|}{d_y d_m} \left({d_{i,y}}^2 - (d_y + d_m) d_{i,y} + d_y d_m \right) \tag{4.38}$$

$$\eta_{11} = \sum_{i=1}^{N} \frac{{d_{i,y}}^2 |x_i|}{{d_y}^2 (d_y - d_m)} (d_{i,y} - d_m) \tag{4.39}$$

$$\eta_{12} = \sum_{i=1}^{N} \frac{{d_{i,y}}^2 |x_i|}{{d_m}^2 (d_y - d_m)} (d_y - d_{i,y}) \tag{4.40}$$

$$\eta_{20} = M_m - \sum_{i=1}^{N} \frac{k_e d_{i,m} |x_i|}{d_y d_m} ({d_{i,m}}^2 - (d_y + d_m) d_{i,m} + d_y d_m) \tag{4.41}$$

$$\eta_{21} = \sum_{i=1}^{N} \frac{{d_{i,m}}^2 |x_i|}{{d_y}^2 (d_y - d_m)} (d_{i,m} - d_m) \tag{4.42}$$

$$\eta_{22} = \sum_{i=1}^{N} \frac{{d_{i,m}}^2 |x_i|}{{d_m}^2 (d_y - d_m)} (d_y - d_{i,m}) \tag{4.43}$$

Therefore, the force coordinates of yield point $Y(d_y, f_y)$ and the initial maximum point $M(d_m, f_m)$ can be determined by the following equation,

$$f_y = \frac{\eta_{10}\eta_{22} - \eta_{12}\eta_{20}}{\eta_{11}\eta_{22} - \eta_{12}\eta_{21}} \tag{4.44}$$

$$f_m = \frac{\eta_{11}\eta_{20} - \eta_{10}\eta_{21}}{\eta_{11}\eta_{22} - \eta_{12}\eta_{21}} \tag{4.45}$$

4.2.3 Hysteretic Rule of Constitutive Model

Depending on the different occasions, the hysteretic curves for springs can be divided into three types: 1) basic curve, 2) sub curve and 3) softening curve or hardening curve.

(1) Basic Curve

As shown in Fig.4-6, the hysteretic curve starting from the origin point $O(d_o, f_o)$ to the initial maximum point $M(d_m, f_m)$ is named as the "Basic Curve". When the spring firstly unloads at the point $A(d_A, f_A)$, the following hysteretic curve aims at the maximum point $M'(-d_m, -f_m)$

on the other side, which is also determined as the basic curve. The displacement-force relation of these two basic curves are approximately expressed by a cubic curve,

$$f - f_s = \alpha_3 \Delta d^3 + \alpha_2 \Delta d^2 + \alpha_1 \Delta d \tag{4.46}$$

where $\Delta d = d - d_s$ is incremental displacement from the starting point of the curve; according to the constraint conditions of displacement-force relation for this cubic curve, that is, the tangent stiffness at the starting point and the maximum point is k_e and zero, respectively, then the coefficients α_3, α_2 and α_1 are given by

$$\alpha_1 = k_e \tag{4.47}$$

$$\alpha_2 = 3\frac{(f_d - f_s)}{\Delta d_{sd}{}^2} - 2\frac{k_e}{\Delta d_{sd}} \tag{4.48}$$

$$\alpha_3 = \frac{k_e}{\Delta d_{sd}{}^2} - 2\frac{(f_d - f_s)}{\Delta d_{sd}{}^3} \tag{4.49}$$

where $\Delta d_{sd} = d_d - d_s$ is the incremental displacement from the starting point to destination point, f_d is the force coordinate of destination point on the basic curve.

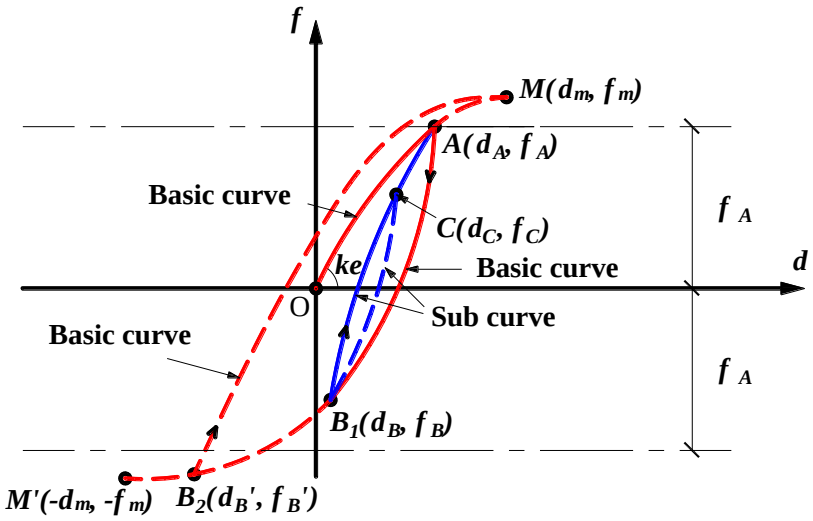

Fig. 4-6. Hysteretic curves for spring before the pier reaches the maximum horizontal load

(2) Sub Curve

When the spring unloads from the second basic curve, for example, if the spring displacement is reversed at the point $B(d_B, f_B)$, which belongs to the basic curve AM' as illustrated in Fig.4-6, the pathway forward depends on the value of spring force of the point B, i.e. f_B.

If f_B at the point *B* is less than the force value of the last unloading point *A*, f_A, the pathway forward will be an approximate quadratic curve B_1A from the point *B* to point *A*. Here, this quadratic curve is referred to as the "Sub Curve".

$$f - f_B = k_e(d - d_B) + \alpha_2(d - d_B)^2 \tag{4.50}$$

where

$$\alpha_2 = \frac{(f_A - f_B)}{(d_A - d_B)^2} - \frac{k_e}{d_A - d_B} \tag{4.51}$$

If f_B at the point *B* is larger than f_A at the last unloading point *A*, a new basic curve will be drawn from the point *B* to the maximum point *M*, like curve B_2M as shown in Fig.4-6.

On other hand, when the spring unloads from the sub curve, for instance, if the spring displacement is reversed at the point *C* on the sub curve B_1A, another new sub curve CB1 will be created. However, if the spring draws the hysteretic curve back to point *A* without unloading midway, it will go along with the original basic curve *OM* after passing through the point *A*.

(3) Softening Curve

According to the cyclic test results of specimens S-00, S-20 and U-00 as described in Chapter 2, it is found that the hysteresis curves showed a negative-slope linear trend after these specimens reached their maximum lateral load. The hysteretic curve of springs should reflect the behavior

of steel piers. Thus, the similar negative-slope linear curve is determined as "Softening Curve" with a tangent stiffness, k_d, as illustrated in Fig.4-7. The experienced displacement in softening region is defined as

$$\Delta d_D = |d_u - d_m| \tag{4.52}$$

where d_u and d_m are the displacement coordinates at unloading point U on the softening curve and the maximum point M, respectively. As shown in Fig.4-7, when the spring unloads from the softening curve, a new basic curve U^+M^- will be drawn from the unloading point U^+ on the softening curve to the maximum point M^- on the opposite side.

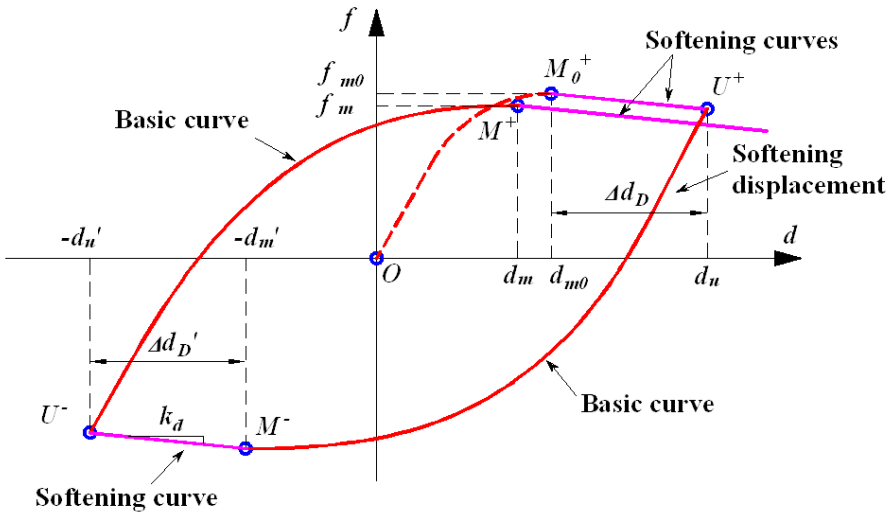

Fig. 4-7. Softening curve for spring after the pier reaches the maximum horizontal load

(4) Hardening Curve

For the specimens S-40, U-25 and U-50, in the case of partially filled with a certain height of concrete, the hysteretic behavior showed some significant differences with those of specimens S-00, S-20 and U-00, especially in the repeated large displacement region. As shown in Figs. 2-4 (c) and 2-8 (b) (c), the upward trend of lateral load of pier was once slow down due to local

buckling occurred at the base of pier after be loaded for some time. However, with continued loading, the rigidity of pier would increase since the internal concrete once again participated in transmitting the lateral load applied at the top of pier.

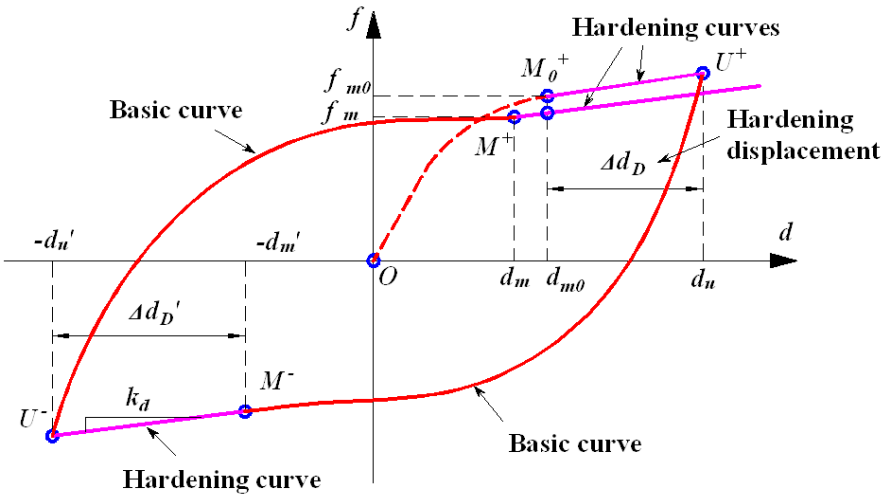

Fig. 4-8. Hardening curve for spring after the pier reaches the maximum horizontal load

Therefore, in order to represent the complex behavior of such piers, as shown in Fig.4-8, the load rising region U^+M^- of spring in the beginning is firstly defined as a basic curve, and then the hysteresis curve comes across the inflection point M^-, the point of the minimum tangent stiffness for spring. After crossing the inflection point M^-, the hysteresis curve will enter the hardening stage, which is expressed by a positive-slope linear curve named "Hardening Curve". The hardening displacement is also obtained by Eq.(4.50) like softening displacement.

(5) Variation of Maximum Load Point (Inflection Point)

As shown in Figs. 4-7 and 4-8, the maximum load point (inflection point) on the hysteresis curve moved from the original point M_0^+ to a new point M^+, which was determined by the cumulative damage caused by cyclic loading, and these coordinate changes of the maximum

load point (inflection point) can be expressed as functions of the accumulated hysteretic energy of the spring, $\sum E$,

$$\left|\frac{d_m}{d_{m0}}\right| = \gamma_2\left(\frac{\sum E}{100E_y} - \psi_0\right)^2 + \gamma_1\left(\frac{\sum E}{100E_y} - \psi_0\right) + 1 \tag{4.53}$$

$$\left|\frac{f_m}{f_{m0}}\right| = \eta_2\left(\frac{\sum E}{100E_y} - \psi_0\right)^2 + \eta_1\left(\frac{\sum E}{100E_y} - \psi_0\right) + 1 \tag{4.54}$$

where $E_y = d_y f_y/2$ is an energy unit for spring; d_{m0} and f_{m0} are respectively the initial values of displacement and force coordinates at the maximum load point (inflection point); coefficients γ_2, γ_1, η_2, η_1 and ψ_0 are obtained by the least squares method on the basis of the static cyclic loading test results of piers.

(6) Stiffness Degradation

As for the degradation rule for elastic stiffness k_e, in the softening (hardening) stage, stiffness degradation occurs whenever the spring unloads. The degraded elastic stiffness k_{ed} is assumed to be governed as follows by the accumulated hysteretic energy of the spring, $\sum E$.

$$\left|\frac{k_{ed}}{k_e}\right| = \zeta_1\left(\frac{\sum E}{100E_y} - \psi_0\right) + 1 \tag{4.55}$$

where coefficients ζ_1 is also determined by the least squares method.

4.3 Experimental Verification

On the basis of the contents stated above in Section 4.2, the calculation procedure of analysis program for developed Multiple Spring Model is shown in Fig. 4-9.

To examine the validity of the proposed multiple spring model, the analytical results obtained

by the proposed model are compared with the experimental results due to static cyclic loading, single- and bi- directional hybrid loading for the piers with different cross sectional shapes and different concrete-filled ratios.

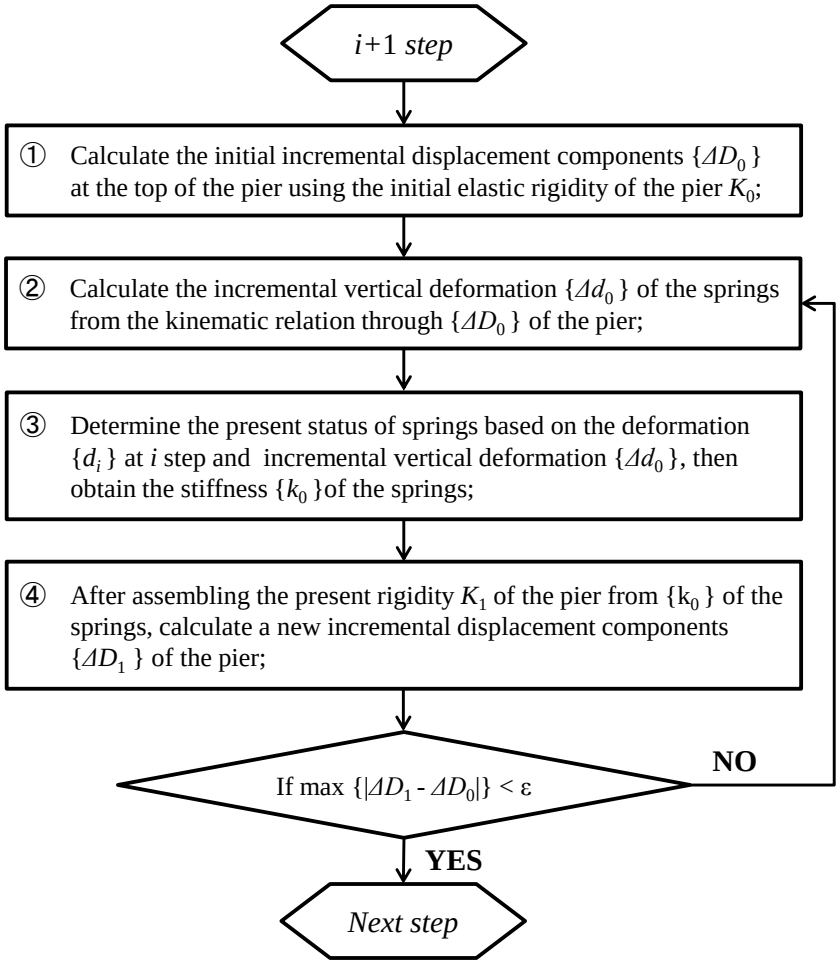

Fig. 4-9. Calculation process of analysis program

4.3.1 Comparison with Static Cyclic Loading Test

First, following the procedure introduced in Section 4.2, the parameters for the constitutive models of the springs are identified from the experimental results of static cyclic loading tests. The identified parameters of the constitutive models are summarized in Table 4-1.

Table 4-1. Identified parameters for the constitutive models of the springs

Parameter	S-00	S-20	S-40	U-00	U-25	U-50
k_e	1258	1480	1597	646	656	903
k_d	-73	58	232	-45	66	135
d_y	5.55	5.55	5.55	3.64	3.61	3.91
f_y	6920	7242	7404	2307	2368	2384
d_m	14.30	22.03	22.13	11.50	15.28	15.14
f_m	11400	13197	13861	4493	4616	5643
φ_0	0.266	0.760	0.771	0.250	0.810	0.830
γ_2	-0.388	-0.136	-0.047	-0.056	0.046	-0.005
γ_1	0.043	0.098	-0.049	-0.239	-0.322	-0.198
η_2	0.207	-0.098	-0.024	-0.183	0.048	0.029
η_1	-0.688	0.062	-0.053	-0.112	-0.301	-0.238
ζ_1	-0.196	-0.120	-0.090	-0.175	-0.047	-0.023

Note: The unit of displacement is *mm*, unit of force is *kN*, unit of stiffness is *kN / mm*.

In Fig. 4-10, the numerical analysis results obtained by multiple-spring model are compared with the static cyclic loading test results for six kinds of piers in term of the in-plane hysteretic curves. It is observed from Fig. 4-10 that the proposed model shows acceptable accuracy to express the in-plane hysteretic behavior of steel piers. However, some difference exists in the cyclic behavior in the post-peak range. This difference is more evident for pier S-40 with a sufficient concrete-filled ratio where the external steel plate cooperates fully with the internal concrete to transmit the applied load of pier. There still remains some room to improve the hysteretic rule for partially concrete-filled steel piers.

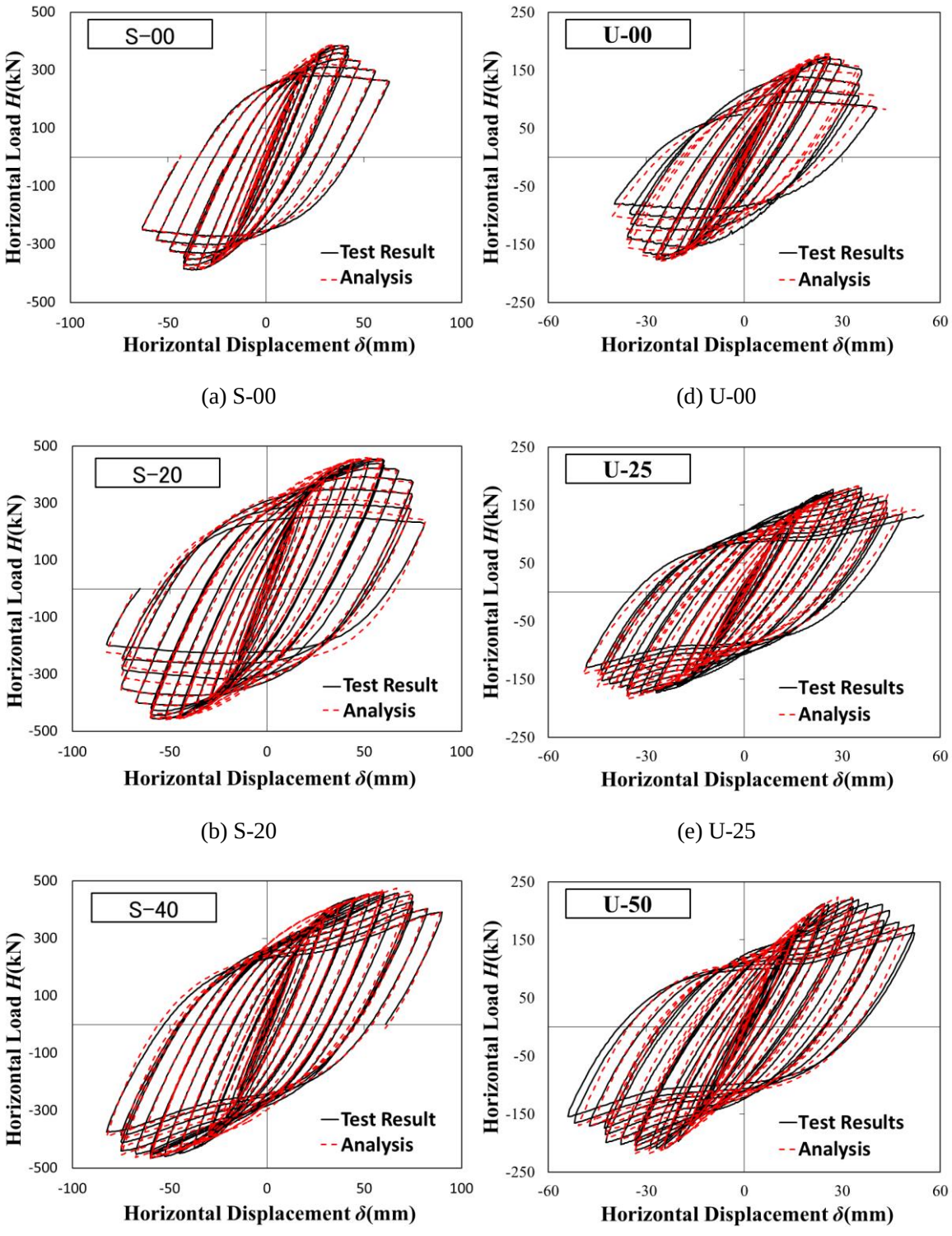

(a) S-00 (d) U-00

(b) S-20 (e) U-25

(c) S-40 (f) U-50

Fig. 4-10. Comparison between multiple-spring model and static cyclic test

4.3.2 Comparison with Single-Directional Hybrid Loading Test

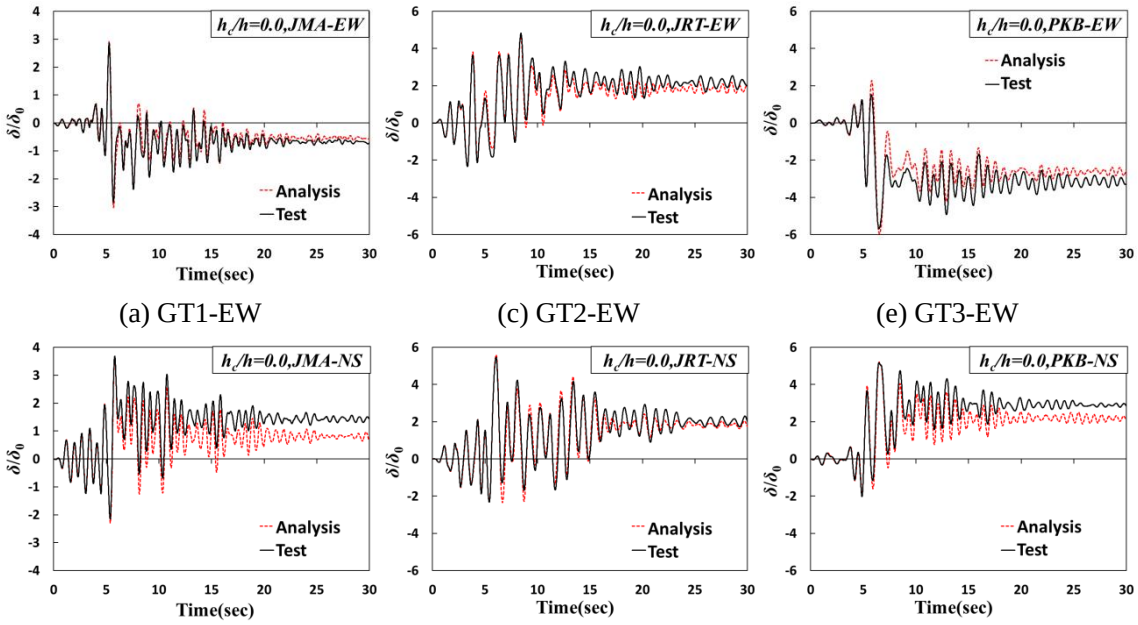

(a) GT1-EW (c) GT2-EW (e) GT3-EW

(b) GT1-NS (d) GT2-NS (f) GT3-NS

Fig. 4-11. Displacement time histories of S-00 under single-directional earthquake wave

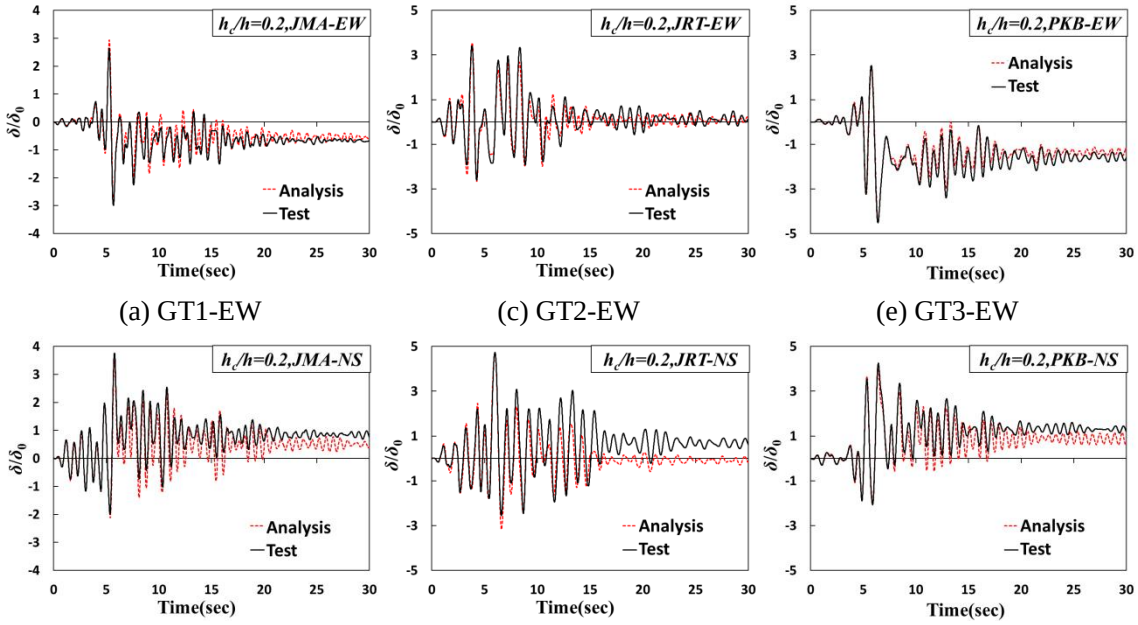

(a) GT1-EW (c) GT2-EW (e) GT3-EW

(b) GT1-NS (d) GT2-NS (f) GT3-NS

Fig. 4-12. Displacement time histories of S-20 under single-directional earthquake wave

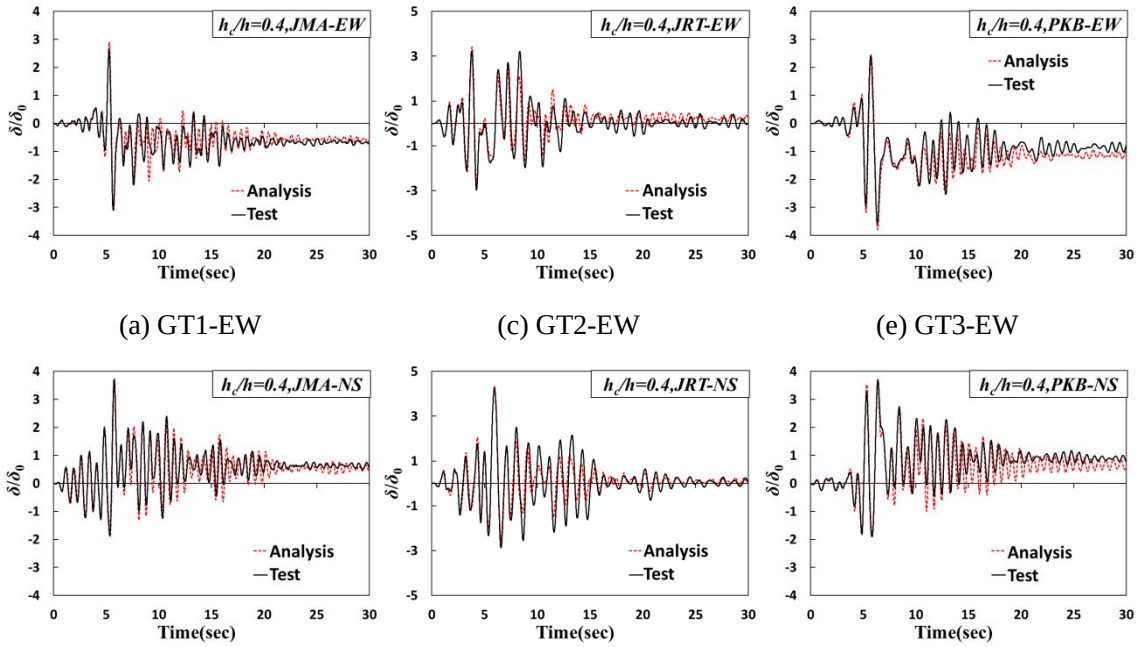

(a) GT1-EW (c) GT2-EW (e) GT3-EW

(b) GT1-NS (d) GT2-NS (f) GT3-NS

Fig. 4-13. Displacement time histories of S-40 under single-directional earthquake wave

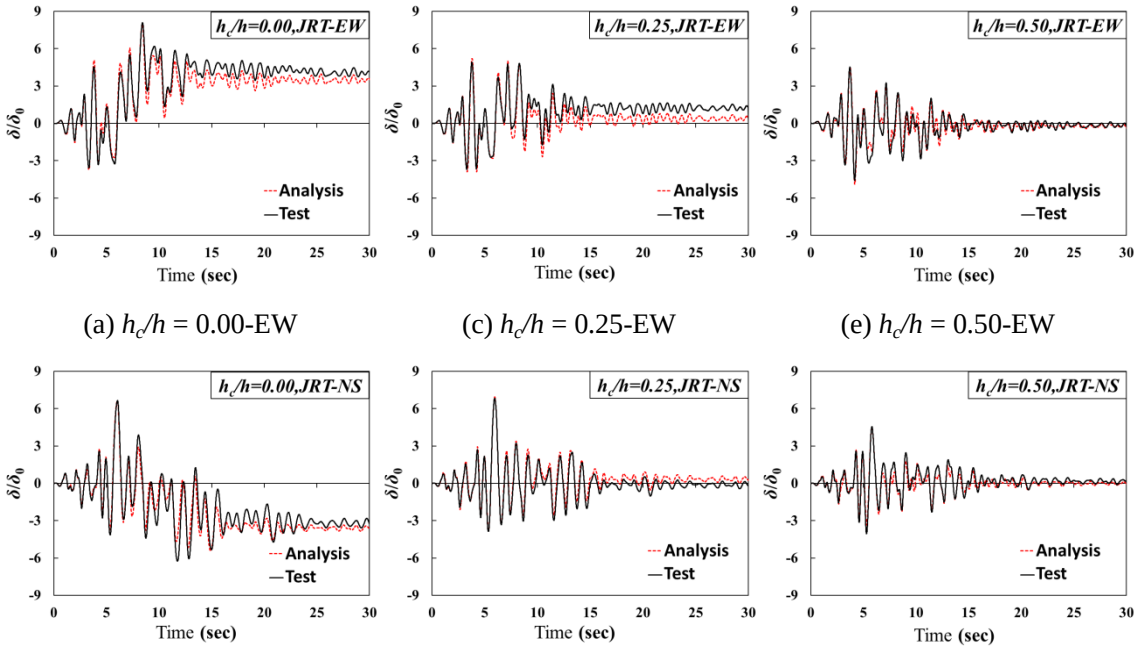

(a) h_c/h = 0.00-EW (c) h_c/h = 0.25-EW (e) h_c/h = 0.50-EW

(b) h_c/h = 0.00-NS (d) h_c/h = 0.25-NS (f) h_c/h = 0.50-NS

Fig. 4-14. Displacement time histories of circular piers under single-directional earthquake wave

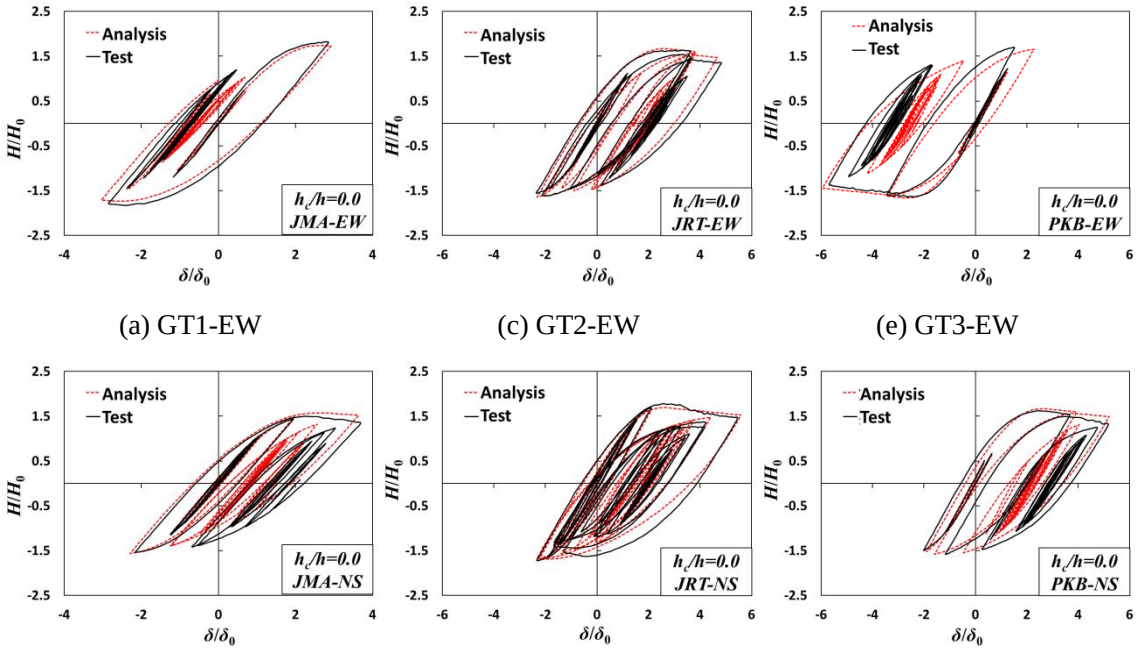

(a) GT1-EW (c) GT2-EW (e) GT3-EW

(b) GT1-NS (d) GT2-NS (f) GT3-NS

Fig. 4-15. Hysteretic curves of S-00 under single-directional earthquake wave

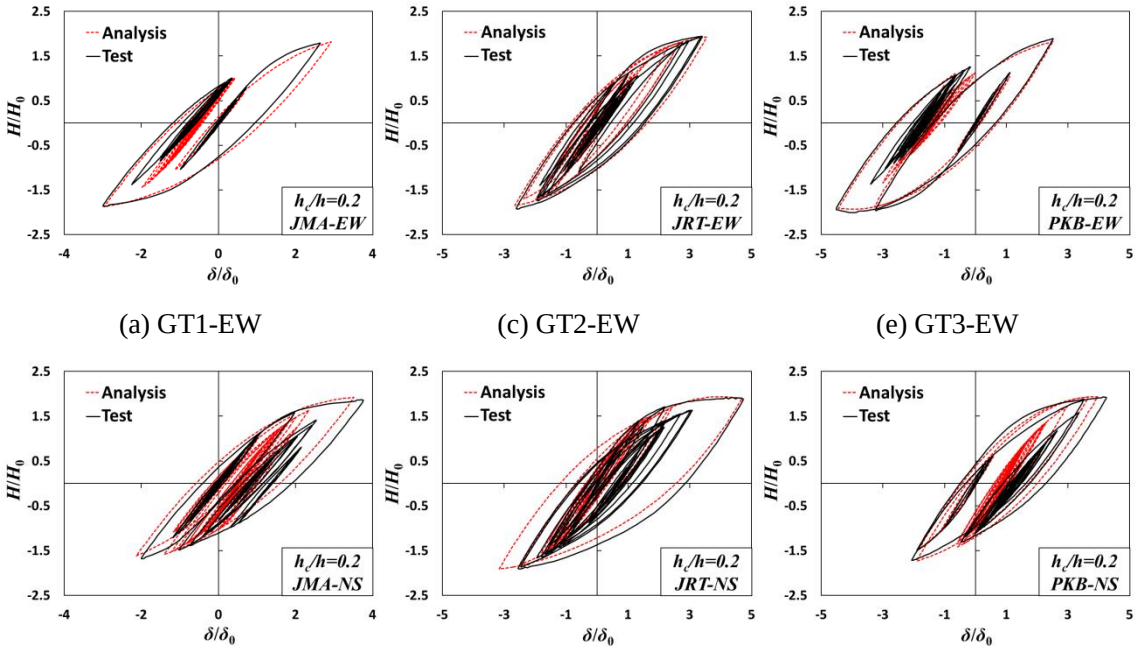

(a) GT1-EW (c) GT2-EW (e) GT3-EW

(b) GT1-NS (d) GT2-NS (f) GT3-NS

Fig. 4-16. Hysteretic curves of S-20 under single-directional earthquake wave

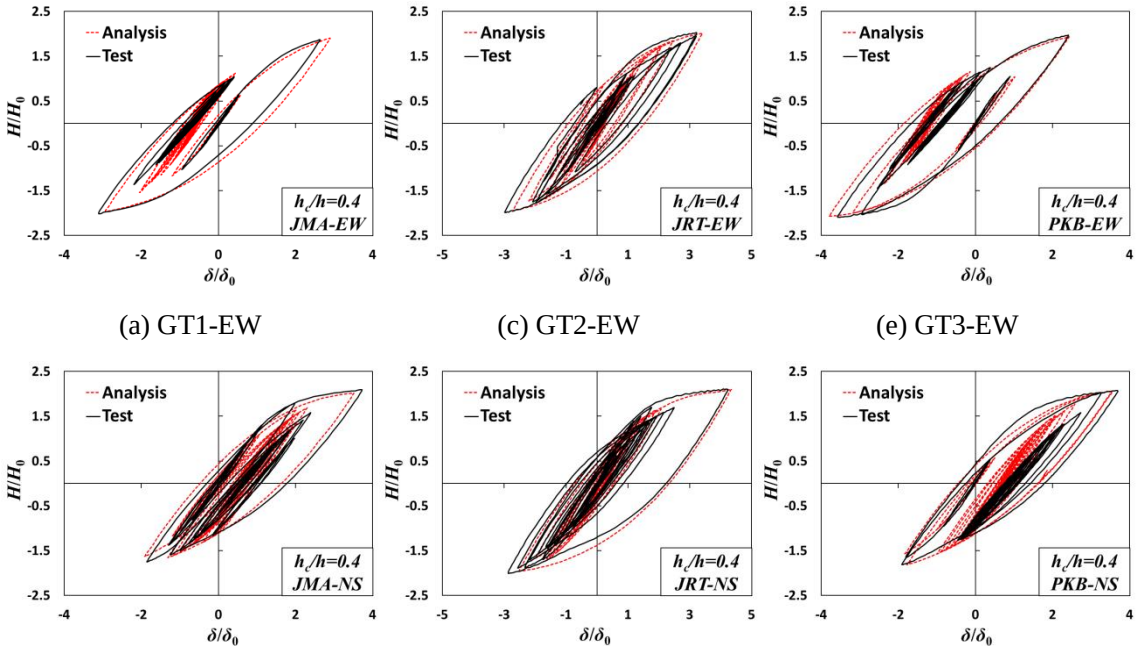

(a) GT1-EW (c) GT2-EW (e) GT3-EW

(b) GT1-NS (d) GT2-NS (f) GT3-NS

Fig. 4-17. Hysteretic curves of S-40 under single-directional earthquake wave

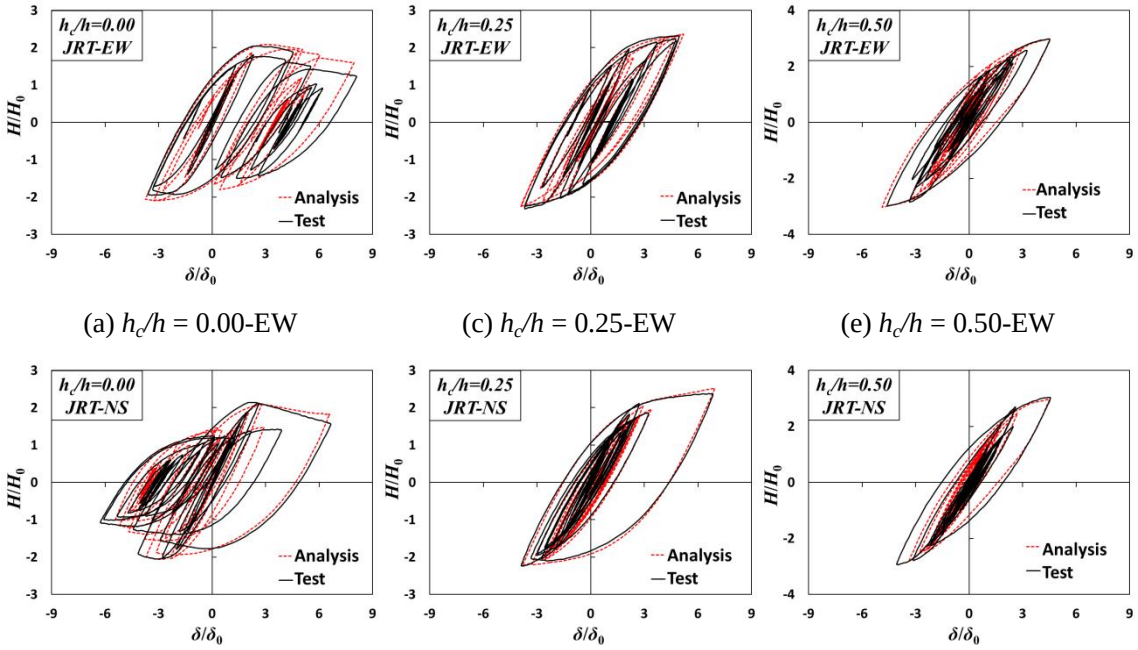

(a) h_c/h = 0.00-EW (c) h_c/h = 0.25-EW (e) h_c/h = 0.50-EW

(b) h_c/h = 0.00-NS (d) h_c/h = 0.25-NS (f) h_c/h = 0.50-NS

Fig. 4-18. Hysteretic curves of circular piers under single-directional earthquake wave

Table 4-2. Comparison between multiple-spring model and single-directional hybrid test

Specimen	*Case*	*Test Result*		*Analytical Result*		*Tolerance*	
		$\frac{\delta_m}{\delta_0}$	$\frac{H_m}{H_0}$	$\frac{\delta_m^*}{\delta_0}$	$\frac{H_m^*}{H_0}$	$\frac{\delta_m^* - \delta_m}{\delta_m}$	$\frac{H_m^* - H_m}{H_m}$
S-00	JMA-EW	2.86	1.83	3.03	1.74	6.1%	-5.2%
	JMA-NS	3.69	1.54	3.63	1.57	-1.4%	2.1%
	JRT-EW	4.82	1.63	4.67	1.67	-3.3%	2.0%
	JRT-NS	5.46	1.78	5.58	1.69	2.3%	-5.0%
	PKB-EW	5.69	1.70	5.95	1.67	4.5%	-1.9%
	PKB-NS	5.18	1.62	5.20	1.67	0.5%	2.9%
S-20	JMA-EW	2.99	1.87	2.97	1.88	-0.8%	0.1%
	JMA-NS	3.76	1.87	3.52	1.92	-6.5%	2.9%
	JRT-EW	3.40	1.94	3.55	1.92	4.3%	-1.0%
	JRT-NS	4.73	1.92	4.70	1.93	-0.7%	0.8%
	PKB-EW	4.51	2.01	4.45	1.93	-1.4%	-4.1%
	PKB-NS	4.25	1.93	3.97	1.93	-6.6%	-0.1%
S-40	JMA-EW	3.11	2.02	2.93	1.97	-5.6%	-2.5%
	JMA-NS	3.73	2.09	3.52	2.02	-5.6%	-3.5%
	JRT-EW	3.22	2.03	3.40	2.01	5.5%	-0.9%
	JRT-NS	4.24	2.11	4.35	2.10	2.7%	-0.4%
	PKB-EW	3.57	2.10	3.80	2.07	6.3%	-1.2%
	PKB-NS	3.69	2.07	3.55	2.06	-3.9%	-0.8%
U-00	JRT-EW	8.10	2.05	7.96	2.09	-1.8%	2.2%
	JRT-NS	6.66	2.14	6.59	2.11	-1.0%	-1.4%
U-25	JRT-EW	4.93	2.32	5.21	2.37	5.6%	2.0%
	JRT-NS	6.84	2.39	6.95	2.52	2.0%	5.6%
U-50	JRT-EW	4.59	2.98	4.88	3.03	6.4%	1.6%
	JRT-NS	4.56	3.04	4.52	2.97	-0.9%	-2.2%

In the single-directional dynamic response analyses, the accuracy of the proposed multiple-spring model is examined in comparison with the single-directional hybrid loading tests.

The results of the single-directional earthquake response analysis obtained by the multiple-

spring model are summarized in Figs. 4-11 to 4-18, in comparison with those obtained by the hybrid loading tests. Figs. 4-11 to 4-13 respectively show the response displacement time histories of rectangular piers, and Figs. 4-15 to 4-17 illustrate the corresponding hysteretic curves. In these figures, the test results and analytical results of rectangular piers are depicted by solid lines and dot lines, respectively, and from left column to right, the plots correspond to the results obtained under JMA, JRT and PKB earthquake waves, respectively. For the circular piers, which were loaded under JRT earthquake waves, the plots from left column to right in Figs. 4-14 and 4-18 correspond to the displacement responses and hysteretic curves of specimens U-00, U-25, and U-50, respectively.

In addition, Table 4-2 compares the maximum response displacement and maximum lateral load of the piers between the test results and analytical results, and the tolerances in the maximum lateral load and maximum displacement are about 2.2% and 3.6% on average, respectively.

It can be observed from Figs. 4-11 to 4-18 and Table 4-2 that the multiple-spring model can be an acceptable alternative to the single-directional hybrid loading test in practical design.

4.3.3 Comparison with Bi-Directional Hybrid Loading Test

In the bi-directional dynamic response analyses, the accuracy of the proposed multiple-spring model is examined in comparison with the bi-directional hybrid loading tests.

The results of the bi-directional earthquake response analysis obtained by the multiple-spring model are summarized in Figs. 4-19 to 4-27, in comparison with those obtained by the hybrid loading tests. Figs. 4-19 to 4-22 present the response displacement time histories of piers and Figs. 4-23 to 4-26 show the hysteretic curves. Fig. 4-27 illustrates the displacement trajectories.

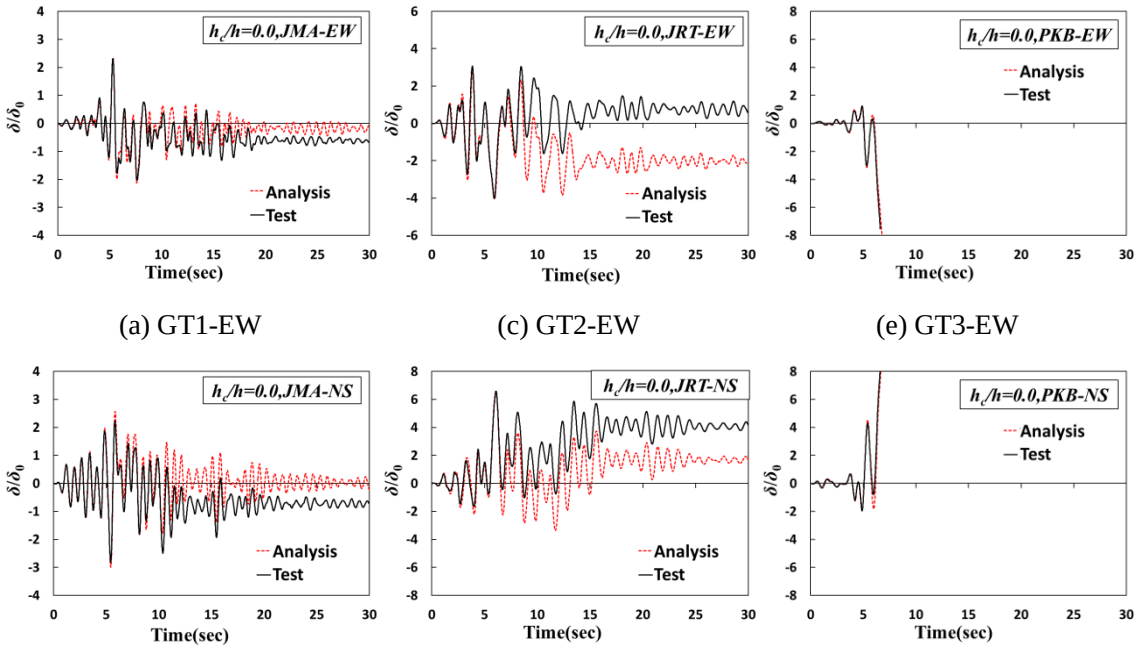

(a) GT1-EW (c) GT2-EW (e) GT3-EW

(b) GT1-NS (d) GT2-NS (f) GT3-NS

Fig. 4-19. Displacement time histories of S-00 under bi-directional earthquake waves

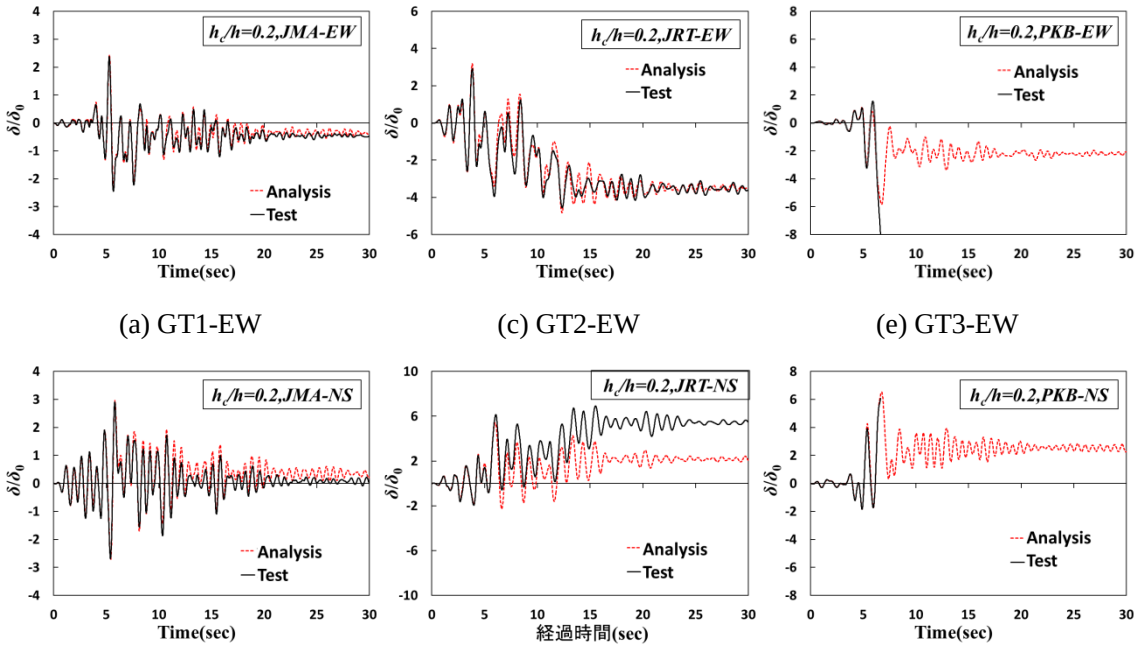

(a) GT1-EW (c) GT2-EW (e) GT3-EW

(b) GT1-NS (d) GT2-NS (f) GT3-NS

Fig. 4-20. Displacement time histories of S-20 under bi-directional earthquake waves

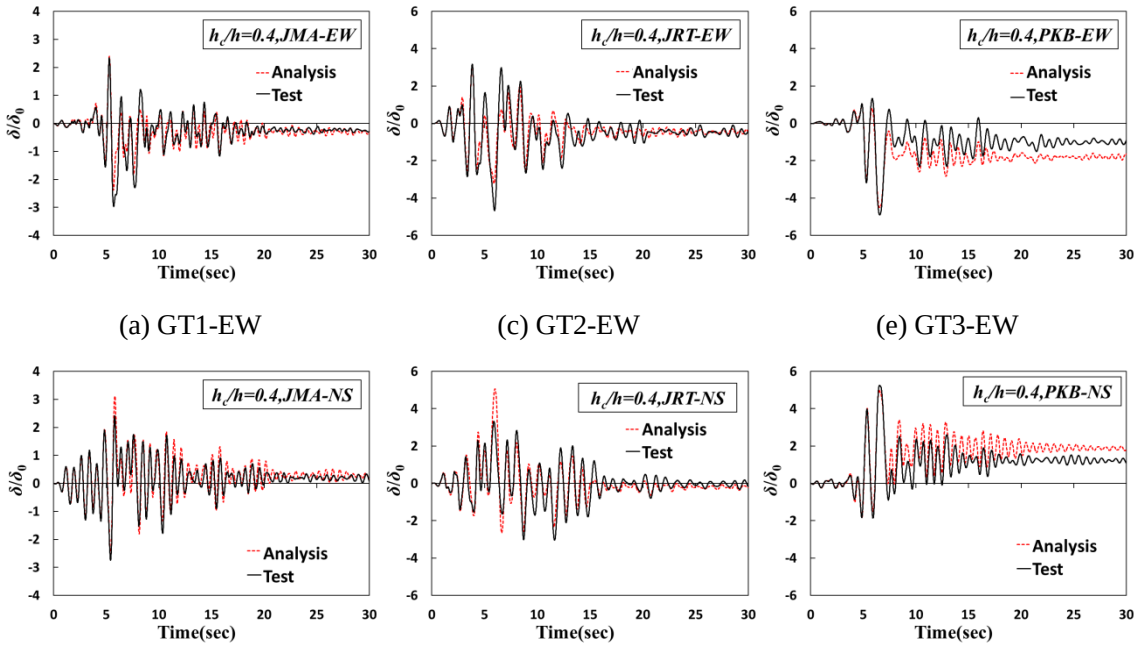

(a) GT1-EW (c) GT2-EW (e) GT3-EW

(b) GT1-NS (d) GT2-NS (f) GT3-NS

Fig. 4-21. Displacement time histories of S-40 under bi-directional earthquake waves

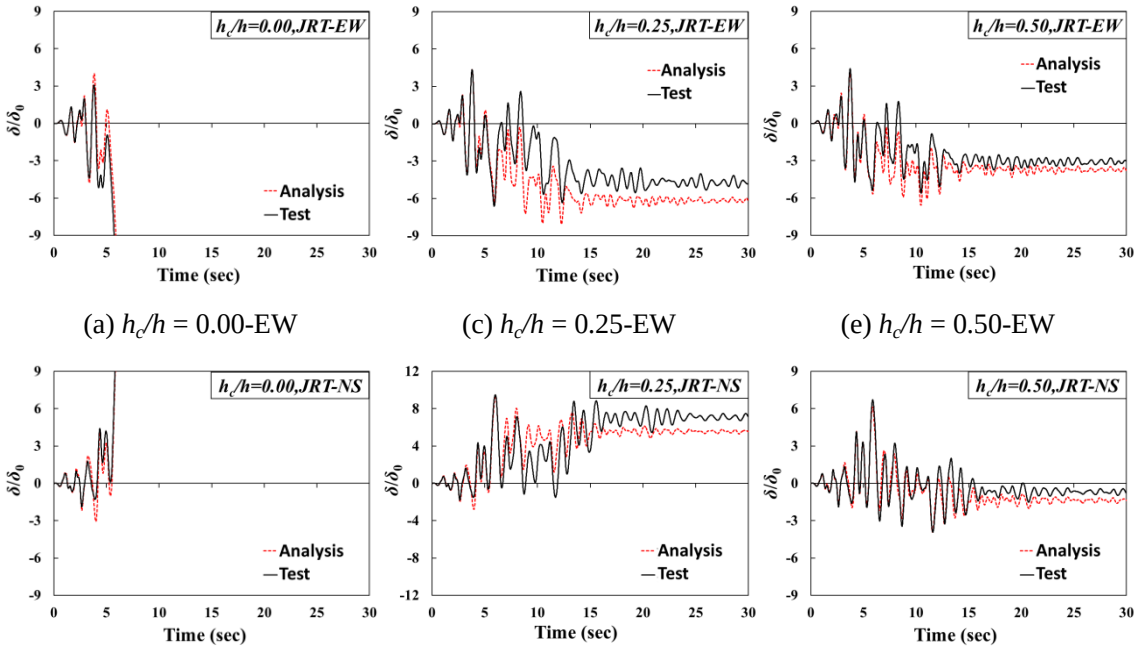

(a) h_c/h = 0.00-EW (c) h_c/h = 0.25-EW (e) h_c/h = 0.50-EW

(b) h_c/h = 0.00-NS (d) h_c/h = 0.25-NS (f) h_c/h = 0.50-NS

Fig. 4-22. Displacement time histories of circular piers under bi-directional earthquake waves

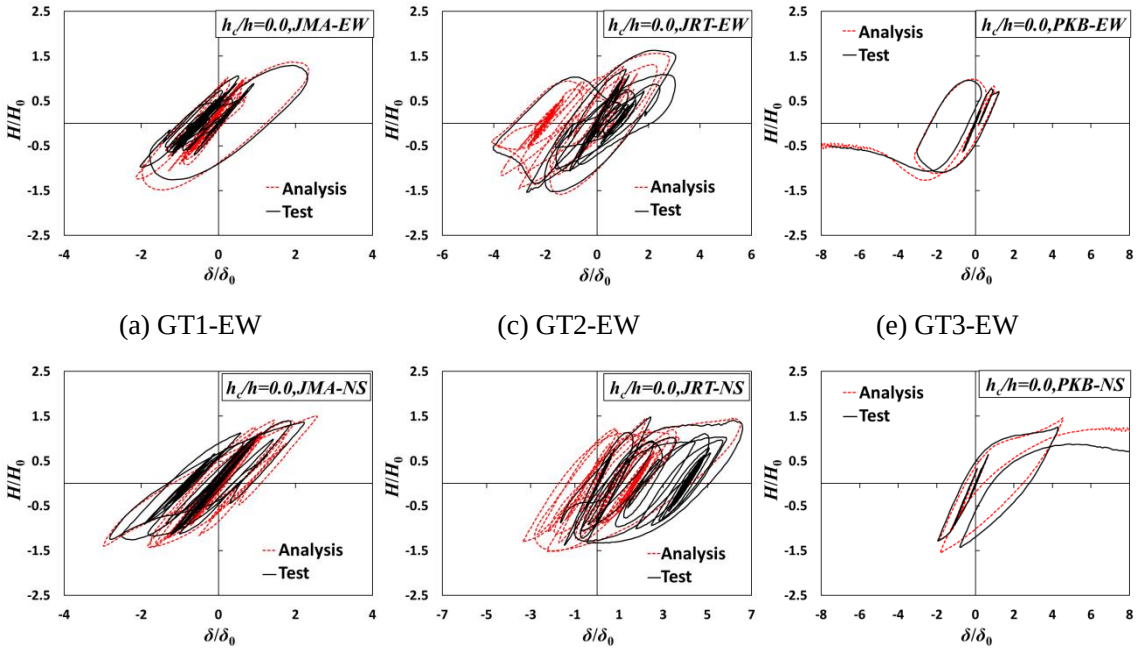

(a) GT1-EW (c) GT2-EW (e) GT3-EW

(b) GT1-NS (d) GT2-NS (f) GT3-NS

Fig. 4-23. Hysteretic curves of S-00 under bi-directional earthquake waves

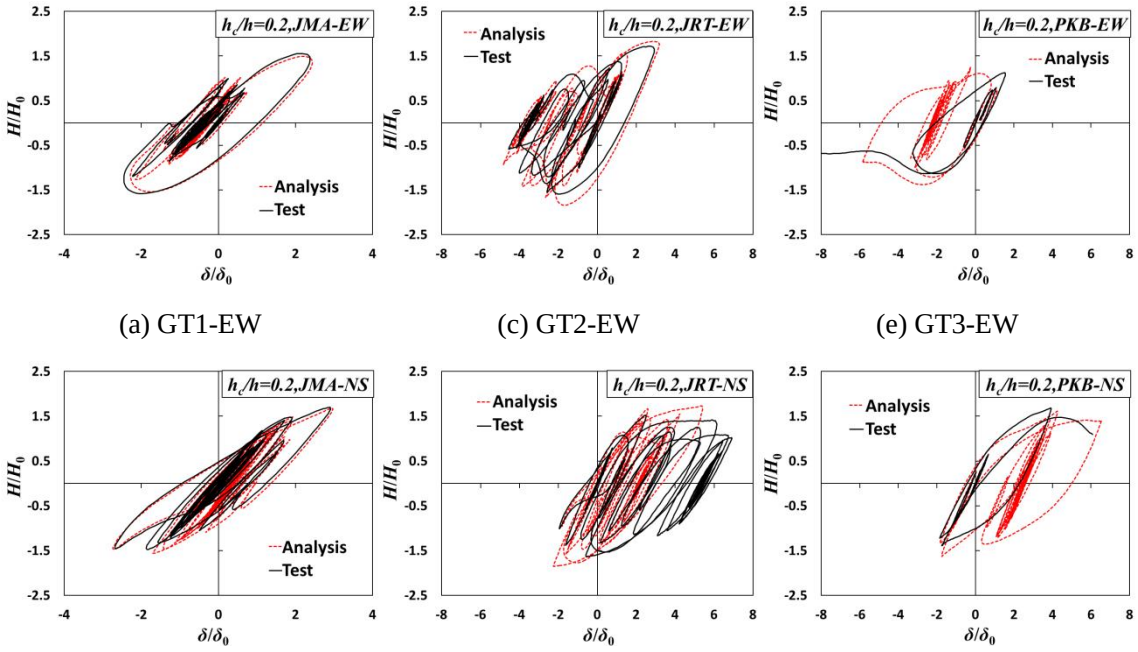

(a) GT1-EW (c) GT2-EW (e) GT3-EW

(b) GT1-NS (d) GT2-NS (f) GT3-NS

Fig. 4-24. Hysteretic curves of S-20 under bi-directional earthquake waves

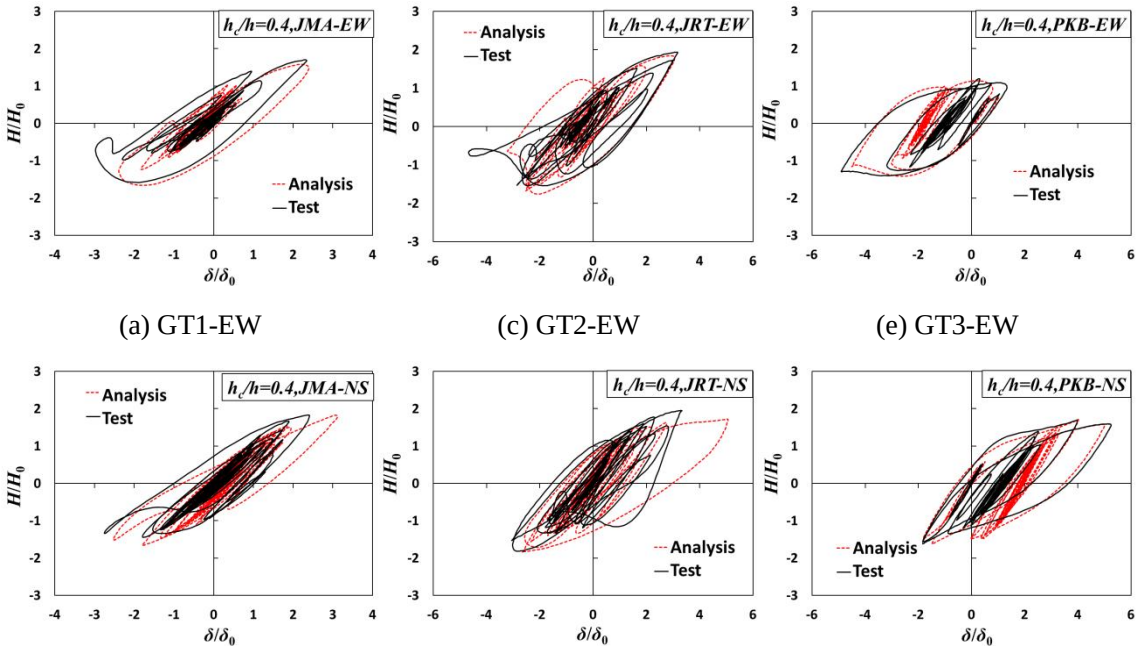

(a) GT1-EW (c) GT2-EW (e) GT3-EW

(b) GT1-NS (d) GT2-NS (f) GT3-NS

Fig. 4-25. Hysteretic curves of S-40 under bi-directional earthquake waves

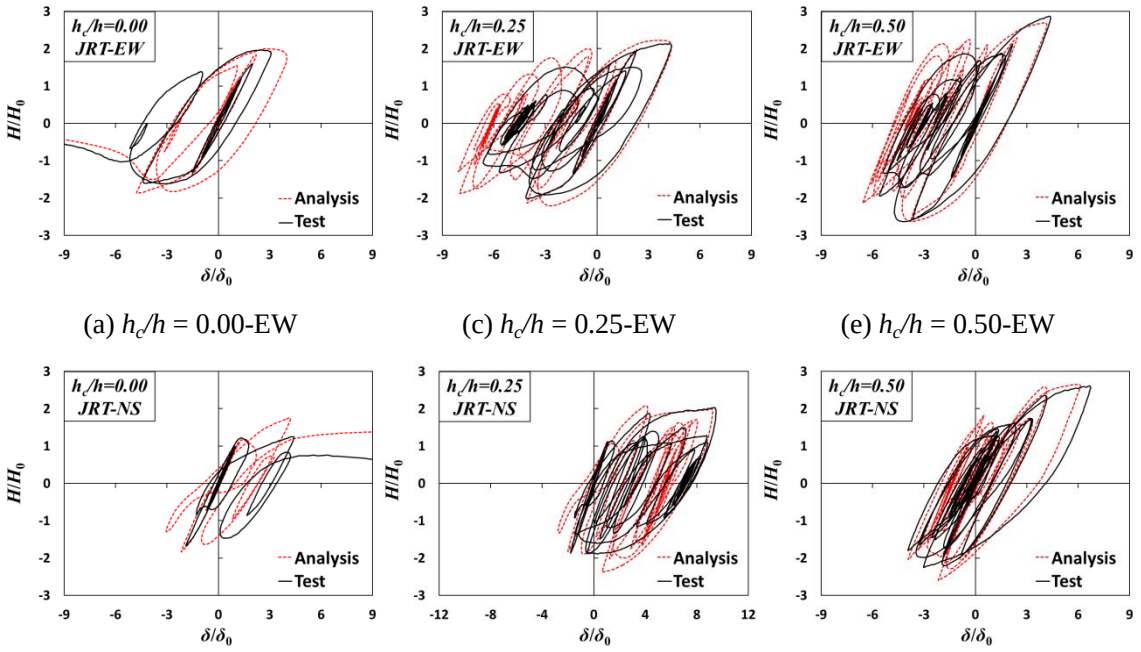

(a) h_c/h = 0.00-EW (c) h_c/h = 0.25-EW (e) h_c/h = 0.50-EW

(b) h_c/h = 0.00-NS (d) h_c/h = 0.25-NS (f) h_c/h = 0.50-NS

Fig. 4-26. Hysteretic curves of circular piers under bi-directional earthquake waves

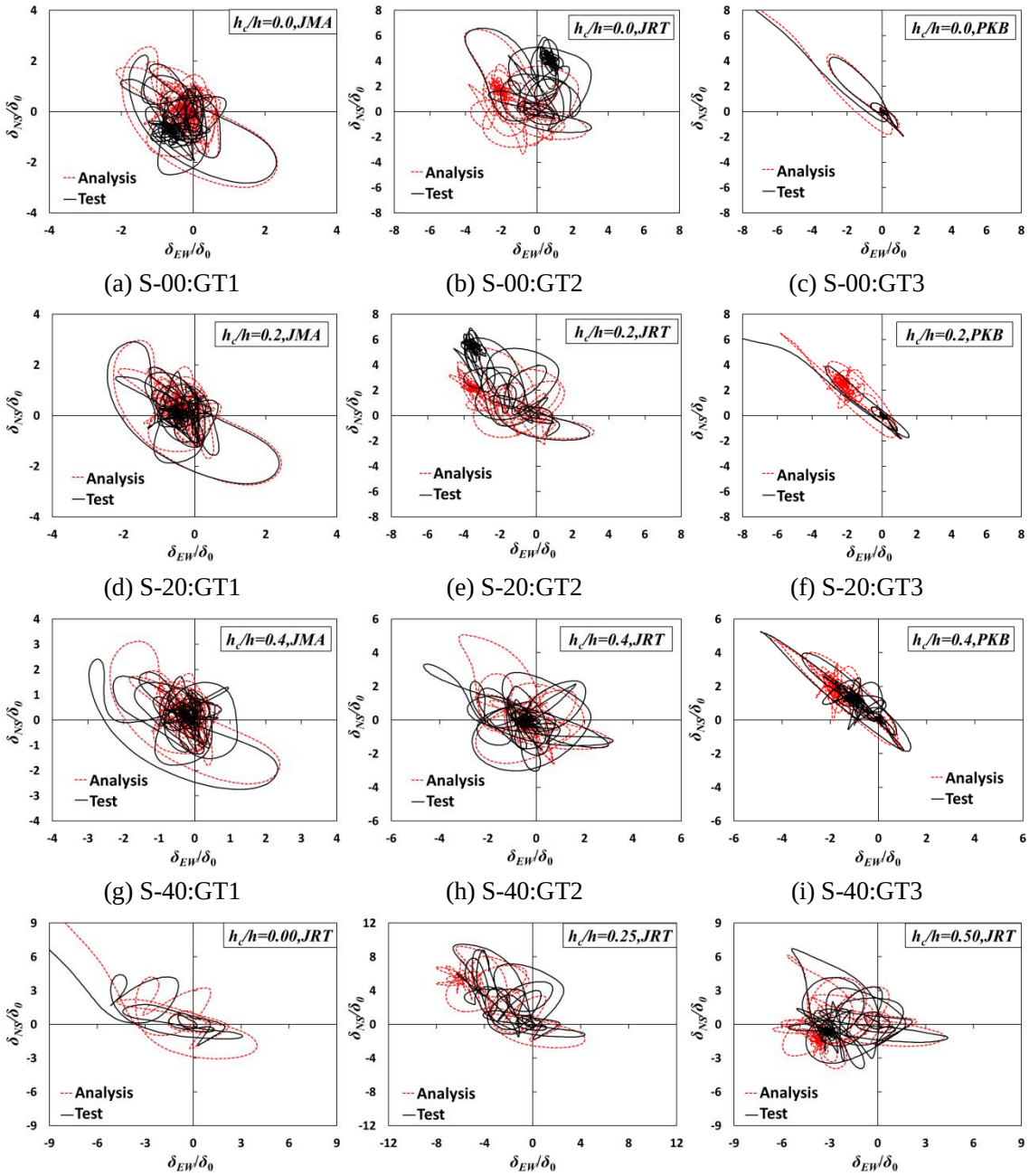

(a) S-00:GT1 (b) S-00:GT2 (c) S-00:GT3

(d) S-20:GT1 (e) S-20:GT2 (f) S-20:GT3

(g) S-40:GT1 (h) S-40:GT2 (i) S-40:GT3

(j) U-00:GT2 (k) U-25:GT2 (l) U-50:GT2

Fig. 4-27. Trajectories of response displacements under bi-directional earthquake waves

The maximum response displacement and maximum lateral load of the piers obtained by the hybrid tests and proposed analytical model are listed in Table 4-3. The tolerances in the maximum lateral load and maximum displacement are about 4.7% and 5.4% on average, respectively.

Among the three kinds of earthquake waves, the piers under JRT earthquake waves exhibit the largest difference in hysteretic behavior between the multiple-spring model and hybrid loading test. This is probably because the coupling effect of JRT bi-directional earthquake waves on large local buckling of piers are most complex and the present hysteretic rule for multiple-spring model also needs to be improved.

However, except for the error caused by large local buckling, it can be observed from Figs. 4-19 to 4-27 and Table 4-3 that the multiple-spring model can be an acceptable alternative to the bi-directional hybrid loading test in practical design as long as the local buckling is moderate and not extremely large.

Table 4-3. Comparison between multiple-spring model and bi-directional hybrid test

Specimen	*Case*	*Test Result*		*Analytical Result*		*Tolerance*	
		$\frac{\delta_m}{\delta_0}$	$\frac{H_m}{H_0}$	$\frac{\delta_m^*}{\delta_0}$	$\frac{H_m^*}{H_0}$	$\frac{\delta_m^* - \delta_m}{\delta_m}$	$\frac{H_m^* - H_m}{H_m}$
S-00	JMA-2D	3.33	1.47	3.45	1.56	3.5%	5.5%
	JRT-2D	7.40	1.69	7.42	1.60	0.3%	-5.1%
	PKB-2D	collapse	collapse	collapse	collapse	—	—
S-20	JMA-2D	3.44	1.82	3.39	1.76	-1.5%	-3.2%
	JRT-2D	7.82	1.78	6.34	1.94	-18.9%	8.8%
	PKB-2D	collapse	collapse	8.32	1.79	—	—
S-40	JMA-2D	3.68	1.89	3.57	1.95	-3.0%	3.3%
	JRT-2D	5.69	2.04	5.93	1.91	4.2%	-6.3%
	PKB-2D	7.18	2.05	6.73	1.95	-6.3%	-4.9%
U-00	JRT-2D	collapse	collapse	collapse	collapse	—	—
U-25	JRT-2D	11.37	2.28	11.13	2.48	-2.1%	8.4%
U-50	JRT-2D	8.59	2.94	8.34	2.84	-2.9%	-3.4%

4.4 Conclusions

In view of the application to the practical design, a multiple-spring model is proposed to express the complex bi-directional hysteretic behavior of thin-walled steel piers. The model consists of a rigid bar and multiple nonlinear springs located at the pier base. These multiple springs can present not only the interaction between the axial force and the biaxial bending but also the local buckling effect and $P-\Delta$ effect. The constitutive relation for each spring is expressed by the multi-curve model and the parameters of this model are calibrated on the basis of the in-plane hysteretic behavior of piers subjected to static cyclic loading.

In comparison with static cyclic test results, it was observed that the proposed model showed acceptable accuracy to express the in-plane hysteretic behavior of steel piers. However, some difference existed in the cyclic behavior in the post-peak range. There still remains some room to improve the hysteretic rule for partially concrete-filled steel piers.

To verify the validity of proposed model under dynamic loading, single- and bi- directional earthquake dynamic response analyses are carried out. We compared the maximum response displacement and maximum lateral load of the piers between the test results and analytical results. When the pier was loaded by single-directional ground motion, it was observed that the tolerances in the maximum lateral load and maximum displacement were about 2.2% and 3.6% on average, respectively. For bi-directional loading, the corresponding tolerances changed to approximately 4.7% and 5.4% on average, respectively.

It can be said that the multiple-spring model can be an acceptable alternative to the costly hybrid loading test in practical design as long as the local buckling is moderate and not extremely large.

CHAPTER 5
CONCLUSIONS

The thin-walled bridge piers are required to be able to withstand severe earthquake without collapsing due to their important role in the total life-line system. The appropriate seismic design and keep the function of steel piers is significant for safe and serviceability in big cities especially in post-earthquake periods. The current seismic design specifications allow applying independent single-directional transverse forces in the design of bridge piers.

However, the actual seismic waves consist of three-directional components and the seismic response of bridge piers is affected by the two horizontal components simultaneously, even if the effect of vertical component is negligible. Therefore, it is very important to study bi-directional loading effect on the steel bridge piers. During the past decade, a lot of effort was concentrated on investigating the basic characteristics of the seismic response of steel bridge piers through bi-directional cyclic loading tests or finite element analysis. However, there are still lacks of dynamic test results on steel piers with a rectangular or circular section under coupled ground motions in two horizontal directions.

At the same time, the partially concrete-filled steel bridge piers demonstrated their excellent structural performance in the 1995 Kobe Earthquake. Thus, a lot of experimental and analytical studies on the inelastic cyclic behavior of partially concrete-filled steel bridge piers under single-directional loading have been conducted in order to develop a reliable earthquake-resistant design method in the last ten years. Therefore, further experimental investigations on the behavior of such piers under actual severe earthquakes are required to make a supplement to the current seismic design method.

For this purpose, a series of static cyclic loading tests and single- and bi- directional hybrid loading tests have been conducted by the author on steel bridge piers with different cross sectional shapes and various concrete-filled ratios, and the related experimental results are discussed in the Chapter 2 and Chapter 3.

From the Chapter 2, following conclusions are obtained,

(1) Both strength and ductility of steel piers under static cyclic loading can be significantly increased by adequate filled-in concrete;

(2) For the stiffened rectangular piers, in the case of low concrete-filled ratio ($h_c/h = 0.20$), the hollow steel section just above the diaphragm buckled severely, while in the case of sufficiently filled with concrete ($h_c/h = 0.40$), slight local buckling occurred only in the flange and web plates at the pier base.

(3) For the circular piers without diaphragm, the local buckling of plates was observed at the column base regardless of the length of the filled-in concrete.

The acceleration data recorded on the three kinds of grounds in the 1995 Kobe Earthquake are used in the hybrid loading tests. And the conclusions of Chapter 3 are summarized as follows:

(1) For the steel piers with low concrete-filled ratio or even without concrete infill, which may have an ability to withstand damage caused by single-directional loading, will probably suffer severe damage or even collapse due to actual bi-directional earthquake actions, especially in the medium and soft grounds.

(2) For the piers of adequate concrete-filled ratio, they showed excellent earthquake resistant performances under either single- or bi-directional loading.

(3) The maximum horizontal load caused by bi-directional loading was only about 2%~7% lower on an average than that of single-directional loading tests, and it is possible to

predict the maximum horizontal load of the steel piers in actual bi-directional loading conditions from the single-directional test results.

(4) The maximum and residual displacements caused by the bi-directional loading, especially in the medium and soft grounds, showed much larger values than those due to single-directional loading. Accordingly, it is pointed that the displacement response during an actual earthquake cannot be correctly estimated by single-directional loading test results, and the conventional seismic design specification based only on single-directional loading test or analysis results may lead to safety issues.

(5) A modified admissible displacement method, considering the bi-directional loading effect, was proposed for the seismic design.

(6) For the steel piers on the soft ground, the complex seismic behavior caused by actual bi-directional earthquake loading can be approximately simulated by the results of proposed new single-directional loading test method which was developed on the basis of principal component analysis (PCA).The validity of this method was verified by the hybrid test results of circular piers.

In the Chapter 4, the following analytical studies were carried out:

(1) A multiple-spring model, consisting of a rigid bar and multiple nonlinear springs located at the pier base, was proposed to express the complex hysteretic behavior of thin-walled steel piers subjected to biaxial bending and axial force.

(2) A multi-curve constitutive model for nonlinear spring was developed to faithfully reproduce the hysteretic behavior of steel piers and the parameters of this model were calibrated on the basis of the in-plane hysteretic behavior of the piers subjected to static cyclic loading.

(3) In comparison with the single-directional loading test results, it is pointed that the proposed model is able to accurately predict the seismic response of steel piers under single-directional strong earthquake.

(4) It is noted that the proposed model also can be an acceptable alternative to the bi-directional hybrid loading test in practical design as long as the local buckling is moderate and not extremely large.

Needless to say, there are limitations pertaining to the current experimental study and proposed analytical model, which offer several opportunities for future studies:

(1) As indicated previously, the present study is aimed at laying emphasis on the effects of bi-directional loading. Then, the width-thickness ratio parameter of the flange plate for stiffened rectangular piers, R_R, the radius-thickness ratio parameter for circular piers, R_t, and the slenderness ratio parameter, λ, were taken as specific values though these values are selected as the representatives of average values commonly used in actual structures.. Thus, further experimental investigations on the seismic behavior of steel piers with various values of parameters under bi- directional loading are necessary to carry out.

(2) The present experimental work was conducted by using only the acceleration data recorded on the three kinds of grounds in the 1995 Kobe Earthquake. In light of these experimental observations, adequate inclusion of the effects of bi-directional loading in seismic design would seem prudent. In order to clarify the seismic behavior of steel piers under actual earthquake loading, it is required to conduct much more experimental studies of steel piers subjected to various strong seismic motions.

(3) The proposed new single-directional loading test method, which was developed on the

basis of principal component analysis (PCA), is limited to the steel piers on the soft ground. Its implementation in other different seismic waves should be explored.

(4) The proposed multiple-spring model is generally applicable. However, some difference existed in the hysteretic behavior in the post-peak range when piers were under bi-directional loading. There still remains some room to improve the hysteretic rule for nonlinear springs.

REFERENCES

Aoki, T., Ohnishi, A. and Suzuki, M. (2007). "Experimental Study on The Seismic Resistance Performance of Rectangular Cross Section Steel Bridge Piers Subjected to Bi-Directional Horizontal Loads." *Structural Eng./Earthquake Eng. & Applied Mech.,* JSCE, 63(4), pp. 717-726 (in Japanese).

Dang, J., Nakamura, T., Aoki, T. and Suzuki, M. (2010). "Bi-Directional Loading Hybrid Tests of Square Section Steel Piers." *J. Structural Eng.,* JSCE, 56A, pp. 367-380 (in Japanese).

Ge, H. and Usami, T. (1992). "Strength of Concrete-Filled Thin-Walled Steel Box Columns: Experiment." *J. Struct Eng.,* ASCE, 118(11), pp. 3036-3054.

Ge, H. and Usami, T. (1995). "Analytical Study on Ultimate Strength and Deformation of Partially Concrete-Filled Steel Beam-Columns of Box Sections." *Structural Eng./Earthquake Eng.,* JSCE, I-31(513), pp. 77-88 (in Japanese).

Ge, H. and Usami, T. (1996). "Cyclic Tests of Concrete-Filled Steel Box Columns." *J. Struct Eng.,* ASCE, 122(10), pp. 1169-1177.

Ge, H., Asada, H., Susantha, K.A.S. and Usami, T. (2001). "Unified Earthquake Resistance Verification Procedure for Partially Concrete-Filled Steel Piers with Thin- and Thick-Walled Sections." *J. Struct Eng.,* JSCE, 47A, pp. 783-792(in Japanese).

Ge, H., Susantha, K.A.S., Satake, Y. and Usami, T. (2002). "Comparative Study of Demand Prediction Procedures for Partially Concrete-Filled Steel Bridge Piers." *J. Struct Eng.,* JSCE, 48A, pp. 675-682(in Japanese).

Ge, H., Susantha, K.A.S., Satake, Y. and Usami, T. (2003). "Seismic Demand Predictions of Concrete-Filled Steel Box Columns." *Eng. Struct.,* 25, pp. 337-345.

Goto, Y., Jiang, K. and Obata, M. (2006). "Stability and Ductility of Thin-Walled Circular Steel Columns under Cyclic Bidirectional Loading." *J. Structural Eng.,* ASCE, 132(10), pp. 1621-1631.

Goto, Y., Jiang, K. and Obata, M. (2007). "Hysteretic Behavior of Thin-Walled Stiffened Rectangular Steel Columns under Cyclic Bi-Directional Loading." *Structural Eng./Earthquake Eng. & Applied Mech.,* JSCE, 63(1), pp. 122-141 (in Japanese).

Goto.Y, Koyama.R, Fujii.Y and Obata.M. (2009). "Ultimate State of Thin-Walled Stiffened Rectangular Steel Columns under Bi-Directional Seismic Excitations." *Structural Eng./Earthquake Eng. & Applied Mech.,* JSCE, 65(1), pp. 61-80 (in Japanese).

Goto, Y., Kumar, G.P. and Obata, M. (2009). "FEM Analysis for Hysteretic Behavior of CFT Bridge Piers

Considering Interaction between Steel Tube and Infilled Concrete." *Structural Eng./Earthquake Eng. & Applied Mech.*, JSCE, 65(2), pp. 487-504 (in Japanese).

Goto, Y., Wang, Q., Takahashi, N. and Obata, M. (1998). "Three Surfaces Cyclic Plasticity Model for Fem Analysis of Steel Bridge Piers Subjected to Seismic Loading." *Structural Eng./Earthquake Eng.*, JSCE, I-43(591), pp. 189-206 (in Japanese).

Hayakawa, R., Kawashima, K. and Watanabe, G. (2004). "Effect of Bilateral Loadings on the Flexural Strength and Ductility of Reinforced Concrete Bridge Columns." *Structural Eng. /Earthquake Eng.*, JSCE, I-67(759), pp.79-98 (in Japanese).

Japan Society of Civil Engineering. (2002). *Report on the Hanshin-Awaji earthquake disaster - Part I Damage to civil engineering structures bridge structures*. Tokyo: Maruzen (in Japanese).

Japan Road Association. (2012). *Specification for highway bridges - Part V Seismic design*. Tokyo: Maruzen (in Japanese).

Jiang, L., Goto, Y. and Obata, M. (2001). "Multiple Spring Model for 3d-Hysteretic Behavior of Thin-Walled Circular Steel Piers." *Structural Eng. /Earthquake Eng.*, JSCE, 18(2), pp. 111s-127s.

Kitada, T. (1998). "Ultimate Strength and Ductility of State-of-The-Art Concrete-Filled Steel Bridge Piers in Japan." *Eng. Struct.*, 20(4-6), pp. 347-354.

Kobayashi, M., Usami, T. and Suzuki, M. (1997). "A Hysteresis Model for Concrete-Filled Steel Bridge Piers and Its Application to Elasto-Plastic Seismic Response Analysis." *J. Struct Eng.*, JSCE, 43A, pp. 859-868 (in Japanese).

Kulkarni, N.G., Kasai, A. and Tsuboi, H. (2009). "Displacement Based Seismic Verification Method for Thin-Walled Circular Steel Columns Subjected to Bi-Directional Cyclic Loading." *Eng. Struct.*, 31, pp. 2779-2786.

Lai, S., Will, G. and Otani, S. (1984). "Model for Inelastic Biaxial Bending of Concrete Members." *J. Struct Eng.*, ASCE, 110(ST11), pp. 2563-2584.

Maeno, H., Morishita, N., Ge, H., Aoki, T., Takano, K. and Yoshimitsu, T. (2002). "Proposal for Check of Ultimate Earthquake Resistance of Partially Concrete-Filled Steel Bridge Piers with Rectangular Box Sections." *J. Struct Eng.*, JSCE, 48A, pp. 667-674 (in Japanese).

Morishita, M., Aoki, T. and Suzuki, M. (2000). "Experimental Study on The Seismic Resistance Performance of Concrete-Filled Steel Tubular Columns." *J. Struct Eng.*, JSCE, 46A, pp. 73-83 (in Japanese).

Nagata, K., Watanabe, E. and Sugiura, K. (2004). "Elasto-Plastic Response of Box Steel Piers Subjected to Strong Ground Motions in Horizontal 2 Directions." *J. Structural Eng.*, JSCE, 50A, pp. 1427-1436 (in Japanese).

Nishida, H. and Unjoh, S. (2004). "Dynamic Response Characteristic of Reinforced Concrete Column Subjected to Bilateral Earthquake Ground Motions." *13th World Conf. on Earthquake Eng.*, Vancouver, B.C., Canada, 576.

Oide, K., Nakajima, A. and Saiki, I. (2000). "Three Dimensional Dynamic Response Analysis of Bridge Piers by Rigid-Body-Spring Model." *Structural Eng./Earthquake Eng.*, JSCE, I-52(654), pp. 259-270 (in Japanese).

Ogimoto, H., Kawashima, K., Watanabe, G. and Nagata, S. (2005). "Effect of Bilateral Excitation on The Seismic Performance of Reinforced Concrete Bridge Columns Based on Hybrid Loading Test." *Structural Eng. / Earthquake Eng.*, JSCE, I-73(801), pp. 33-50 (in Japanese).

Saizuka, K., Usami, T., Kiso, E. and Itoh, Y. (1995). "Pseudo-Dynamic Tests of Concrete-Filled Steel Bridge Piers." *J. Structural Eng.*, JSCE, 41A, pp. 277-288 (in Japanese).

Saizuka, K. and Usami, T. (1997). "Verification of Proposed Method for Check of Ultimate Earthquake Resistance on The Basis of Hybrid Test Results Concrete-Filled." *Structural Eng. / Earthquake Eng.*, JSCE, I-40(570), pp. 287-296 (in Japanese).

Usami, T. and Ge, H. (1994). "Ductility of Concrete-Filled Steel Box Columns under Cyclic Loading." *J. Struct. Eng.*, ASCE, 120(7), pp. 2021-2040.

Usami, T., Ge, H. and Saizuka, K. (1997). "Behavior of Partially Concrete-Filled Steel Bridge Piers under Cyclic and Dynamic Loading." *J. Construct. Steel Res.*, 41(2/3), pp. 121-136.

Usami, T., Suzuki, M., Mamaghani, I. and Ge, H. (1995). "A Proposal for Check of Ultimate Earthquake Resistance of Partially Concrete Filled Steel Bridge Piers." *Structural Eng. / Earthquake Eng.*, JSCE, I-33(525), pp. 69-82 (in Japanese).

Usami, T., Suzuki, T. and Itoh, Y. (1995). "Pseudo-Dynamic Tests of Concrete-Filled Steel Columns with Prototype Details." *Structural Eng. / Earthquake Eng.*, JSCE, I-33(525), pp. 55-67 (in Japanese).

Watanabe, E., Sugiura, K. and Oyawa, W. (2000). "Effects of Multi-Directional Displacement Paths on the Cyclic Behavior of Rectangular Hollow Steel Columns." *Structural Eng./Earthquake Eng.*, JSCE, 17(1), pp. 69s-85s.

LIST OF PUBLICATIONS

1. "Experimental Study of the Seismic Behavior of Partially Concrete Filled Steel Bridge Piers under Bidirectional Dynamic Loading",

   Huihui Yuan, Ji Dang, and Tetsuhiko Aoki, *Earthquake Engineering & Structural Dynamics*, Article first published online: 30 MAY 2013, DOI: 10.1002/eqe.2320 (Accepted).

2. "鋼製橋脚の水平２方向地震応答解析のための曲線近似 MS モデル",

   党　紀, 袁　輝輝, 五十嵐晃, 青木徹彦, *土木学会論文集 A2 (応用力学)*, Vol.69, 2013 年 8 月 (Accepted).